University of Alberta

Laboratory Study on the Generation and Characterisation of CO_2 Colloidal Gas Aphrons

by

Mousumi Ghosh

A thesis submitted to the Faculty of Graduate Studies and Research
in partial fulfillment of the requirements for the degree of

Master of Science

in

Petroleum Engineering

Civil and Environmental Engineering

© **Mousumi Ghosh**
Fall 2013
Edmonton, Alberta

Abstract

This research focuses on determining an optimum formulation of generating aqueous-based CO_2 Colloidal Gas Aphrons (CGAs) than can be used for CO_2 sequestration and enhanced oil recovery project.

Different pairs of polymers and surfactants were tested, with varying concentrations, to determine the best polymer – surfactant pair that can provide stable, viscous CO_2 CGAs. The screening criteria used were: low shear rate viscosity (LSRV), viscosity profile, change in median diameter (d50), and frequency-time distribution.

To simulate reservoir conditions, viscometry tests and dynamic oscillation tests were conducted on CO_2 CGAs, along with the base fluid solution, under high pressures and high temperatures to determine the rheology, stability, and viscoelastic properties of CO_2 CGAs and associated base fluid.

Results of the experimental investigations have shown that stable CO_2 colloidal gas aphrons can be generated under high pressure and high temperature conditions.

Acknowledgement

Table of Contents

List of Tables:

List of Figures:

List of Abbreviations:

CGAs	Colloidal Gas Aphrons

Polymers

CMC	Carboxymethyl cellulose
XG	Xanthan Gum
HEC	Hydroxyethyl cellulose

Surfactants

DDBS	Dodecylbenzene sulfonate, sodium salt
N85	Nonylphenol ethoxylate (trade name: Surfonic N85)

Charge on Polymer or Surfactant

An	Anionic (negative charge)
Non	Nonionic (no charge)

Terms involving CGA Characterisation

LSRV	Low Shear Rate Viscosity
d50	Median outer diameter of the colloidal gas aphrons
HLB	hydrophilic-lipophillic balance
HCB	hydrophilic-CO_2-phillic balance

Terms involving Viscoelastic behavior of CGAs

G'	Elastic Modulus
G"	Viscous Modulus
LVE	Linear Viscoelastic region

1. Introduction

1.1. Overview and Background of the Problem

Climate control is one of the biggest concerns today when it comes to growing demands of energy. One big factor that causes climate changes is the rising emission of greenhouse gases from industrial settlements. In order to deal with the greenhouse gas emission problem, CO_2 sequestration, so far, has been the most effective solution to reducing greenhouse gas levels in the atmosphere. On the other hand, the cost of producing energy increases day-by-day due to the need for extracting increasing amounts of lower quality resources and conducting enhanced oil recovery (EOR) on residual conventional resources. EOR methods have been applied in many reservoirs, across the world, to access the remaining oil that has not been recovered through primary and secondary recovery methods. CO_2 EOR, in gaseous form, has been implemented in various fields that have managed to produce 8 to 20% of original oil in place (OOIP).

CO_2 sequestration projects, injected in gaseous state, have its potential risks. Few such risks entail leakage of CO_2 gas from injection wells, abandoned wells, cracks in the upper seal that leads to surface, and seismic activity from inadequate storage capacity in the formation for the intended injected volume of CO_2. CO_2 storage is made more secure by either dissolving the CO_2 gas in water or converted to minerals such as calcium carbonate, rather than leaving it inside the formation in gaseous or supercritical fluid state.

1.2. Statement of the Problem

CO_2 CGAs can be used for various applications in the petroleum industry, such as CO_2 sequestration, EOR, drilling operations (due to the unique bridging ability of CGAs that block the pores in the formation), and hydraulic fracturing (due to their enhanced stability at low shear and static conditions).

Therefore, it is important to understand how to successfully generate stable CO_2 CGAs and determine the rheological characteristics under high pressure and high temperature conditions.

Colloidal Gas Aphrons (CGAs), introduced by Sebba, are micro-foams that have additional encapsulation of viscous water layer and surfactant layers that help prevent diffusion of the trapped gas from the core of the CGA to outside. CGAs have been characterised as shear thinning fluid and used as drilling fluids due to their effectiveness in pore blocking. Unlike foams, the additional encapsulation of the CGAs prevents gas diffusion. The resistance of the CGAs to flow in porous media enables the CGAs to recover hydrocarbons at more favourable mobility ratios and sweep efficiencies.

Numerous work have been conducted on understanding the air CGAs, based on rheology, stability, flow properties and other physico-chemical properties. However, to this date, there has been no published work shown on generation and characterisation of CGAs that has CO_2 gas trapped in their core, instead of air. This study introduces a new alternative to air-based CGAs, termed CO_2 CGAs (aqueous based CO_2 Colloidal Gas Aphrons), that can help achieve safe and secure disposal of CO_2, along with conducting CO_2 EOR with more favorable sweep efficiencies.

1.3. Objectives of the Research

The objectives of this research work are:

- Design and construct appropriate set-up that can be used for development of CO_2 colloidal gas aphrons (CO_2 CGAs).
- Develop a test protocol for characterizing the CO_2 CGAs, generated using various combinations of polymer and surfactant types and investigating the rheology, yield, and stability of CO_2 CGAs.
- Determine the optimum formulation (i.e., determine the type and concentration of polymer and surfactant) that would create stable CO_2 CGAs.

- Determine the rheological characteristics of CO_2 CGAs under high pressure and temperature conditions.

1.4. Scope of the Research

There are three main sections of this research. The first section focuses on literature studies on understanding the structure and characterisation of CGAs, as well as investigating the types of surfactant and polymer needed to generate stable CO_2 CGAs. The second section involves on figuring out the best polymer-surfactant duo that provides desirable CO_2 CGAs, based on rheology, yield, and stability. The third section deals with testing CO_2 CGAs, generated from the best polymer-surfactant duo, under high pressure-high temperature conditions, based on rheological and yield characteristics.

The major tasks can be listed as follows:

1. Literature studies

   – Literature review on CGAs and their characterisation and industrial applications

   – Review on suitable polymer and surfactant types for generation of CO_2 CGAs

2. Generating CO_2 CGAs

   – Preparing safe lab procedures for generating CO_2 CGAs

   – Using the chosen polymer and surfactant types to see whether stable CO_2 CGAs are generated or not

3. Characterisation of CO_2 CGAs

   – Determine optimum polymer type and concentration on generating high yield, stable CO_2 CGAs

   – Investigate the type of surfactant on rheology and stability of CO_2 CGAs

- Identifying the best polymer-surfactant duo for generating viscous, stable CO_2 CGAs of high yield

- Comparing the CO_2 CGAs, of best polymer-surfactant duo, to the air CGAs, of its best polymer-surfactant duo in terms of rheology, yield, and stability

4. High pressure-high temperature tests on CO_2 CGAs

- With optimum formulation of generating CO_2 CGAs figure, conduct rheology and stability tests on CO_2 CGAs

1.5.   Methodology of the Research

This study begins with in-depth literature review on preparation and characterisation of air CGAs, surfactants used for CO_2 foam generation, and shear thinning polymers used in drilling fluids and chemical flooding. This detailed analysis lead to identifying possible pairs of polymer and surfactants that were capable of generating CO_2 CGAs. Comparison was made to air CGAs, generated from the same pairs of polymer and surfactant. Based on rheology and stability characteristics, the best polymer-surfactant pair was chosen, leading to optimum formulation of generating stable CO_2 CGAs. Rheological characteristics of CO_2 CGAs, generated from the best polymer-surfactant pair, were further analysed under elevated pressures and temperatures to simulate and predict their behaviour under reservoir conditions.

1.6.   Expected Contributions of the Research

In this study, a thorough analysis of the characteristics of CO_2 CGAs, generated from various polymer-surfactant pairs, has been conducted, in terms of rheology and stability. From this analysis, the optimum formulation of stable CO_2 CGAs has been provided. Rheological results of CO_2 CGAs, under ambient conditions, displayed shear thinning non-Newtonian fluid. Under increasing pressures and low

temperatures, rheological tests of CO_2 CGAs, consisting of viscosity profile, amplitude sweep and frequency sweep, show favourable results, indicating strongly associated, stable dispersions.

1.7.   Structure of the Thesis

In chapter 1, the introduction to the thesis study is provided. It contains the problem statement, research objective, and scope of the research.

Chapter 2 states the literature review of work done on air CGAs with regards to their structure, application, generation, stability, rheology, and EOR agents.

Chapter 3 provides details on experimental programs and procedures in order to generate CO_2 CGAs.

In chapter 4, results and discussions on stability and rheology of CO_2 CGAs are being presented.

In chapter 5, the comparison is shown of CO_2 CGAs to air CGAs, both generated from same pair of polymers and surfactants, based on rheology and stability.

Chapter 6 presents rheological results on CO_2 CGAs, generated from the best pair of polymer and surfactant, at high pressure – high temperature conditions.

Chapter 7 concludes the thesis.

Chapter 8 contains references.

2. Literature Studies

2.1. Structure of CGA

CGAs, introduced by Sebba (1987), are double layered, nearly perfect spherical microbubbles with surfactant tri-layers that inhibit coalescence and trap the gas at the core of the microbubble. Figure 2-1 shows the structure of a CGA proposed by Sebba (1987). The inner layer is the surfactant monolayer. The outer layer is the surfactant double layer. In between the inner surfactant monolayer and the outer surfactant bilayer, there exists viscous water lamella that provides additional stability to the CGAs. Presence of water soluble, viscosifying polymer molecules enhances the viscosity of this layer, and thus in turn, the stability of CGAs. Because of this enhanced stability, CGAs can be compressed and pumped downhole to be used as drilling fluid (and possibly for EOR in the future), all the while retaining their structure.

Amiri and Woodburn (1990) conducted a study of the liquid drainage rate in CGA dispersions and estimated the CGA shell thickness. Their experimental results support the postulate of CGA dispersions having a finite shell thickness of 0.75μm. Bredwell and Worden (1998) estimated the thickness of the surfactant-laden CGA shell to be in the range of 200nm to 300nm. Jauregi et. al (2000) investigated the structural features of CGAs and measured the CGA diameter using theoretical models and experimental methods. Their results supported Sebba's hypothesis of the existence of multilayers of surfactants oriented around the gas bubbles.

Taking a close look at Sebba's CGA structure, it is seen that the outer bilayer of surfactant closely resembles a bilayered vesicle. Figure 2-2 shows an example of a bilayered vesicle. From surface science literature (or surfactant literature), it is well known that above critical micelle concentration, the orientation of surfactant molecules inside the bulk phase is dictated by their critical packing parameter and hydrophobicity (Berg (2010)). Surfactant molecules form bilayered vesicles when, for a certain tail

length, the effective head group area is too small, leading to critical packing parameter values of the surfactant molecules to be within ranges of 0.5 to 1. Thus, the hydrophobicity of the surfactant molecules should be higher than their hydrophilicity (low hydrophilic-lipophilic balance (HLB) values).

Beside surfactant molecules comprising of double tails, it is thermodynamically possible for cationic amphiphiles (mixture of single tailed cationic and anionic surfactants) to form spontaneous bilayered vesicles (Kunjappu and Somasundaran (1996)). Another way to form bilayered vesicles is to introduce a rigid segment into the alkyl chain length of the surfactant molecule, thus restricting the conformational mobility of the surfactant molecule (Kunjappu and Somasundaran (1996)).

The common surfactants used, so far, for generating aqueous-based CGAs have been water soluble single tailed surfactants with high HLB, indicating the orientation of surfactants, in the bulk phase above critical micelle concentration, being not bilayered vesicles. Thus, the outer surfactant bilayer of the CGAs is clearly not meant to be bilayered vesicle.

Sebba probably suggested that the outermost surfactant layer was merely attached to the second surfactant monolayer through hydrophobic and steric interactions. The visual depiction of these interactions, provided by Sebba, is not accurate and produces confusion. Zheng et. al (2009) addressed this discrepancy of the CGA structure by providing his own proposed structure of the CGA drilling fluids which is shown in Figure 2-3. He agreed with Sebba's CGA structure up until the second outermost layer of surfactants. The outermost surfactant monolayer, according to Zheng, does not exist in neat spherical form; instead, mixtures of polymer, surfactant, and perhaps other solid particles attach themselves to the outer surfactant monolayer through steric or charge stabilization. According to figure 2-3, high concentration of mixture of polymer, surfactant, and solid particles exists close to the outer surfactant monolayer, and as the distance from this outer layer of surfactant increases towards the bulk, the

concentration decreases gradually due to lower van Der Waals forces. Eventually, the mixture concentration becomes equivalent to the bulk base fluid concentration.

Nonetheless, the presence of the viscous water layer and the added outer surfactant monolayer with polymer-surfactant molecules sterically attached (or, in Sebba's case, additional outer surfactant bilayer), prolonging the duration of the microbubbles, makes CO_2 CGAs much more morphologically suitable alternative to its gaseous form for proposing CO_2 sequestration and enhanced oil recovery projects.
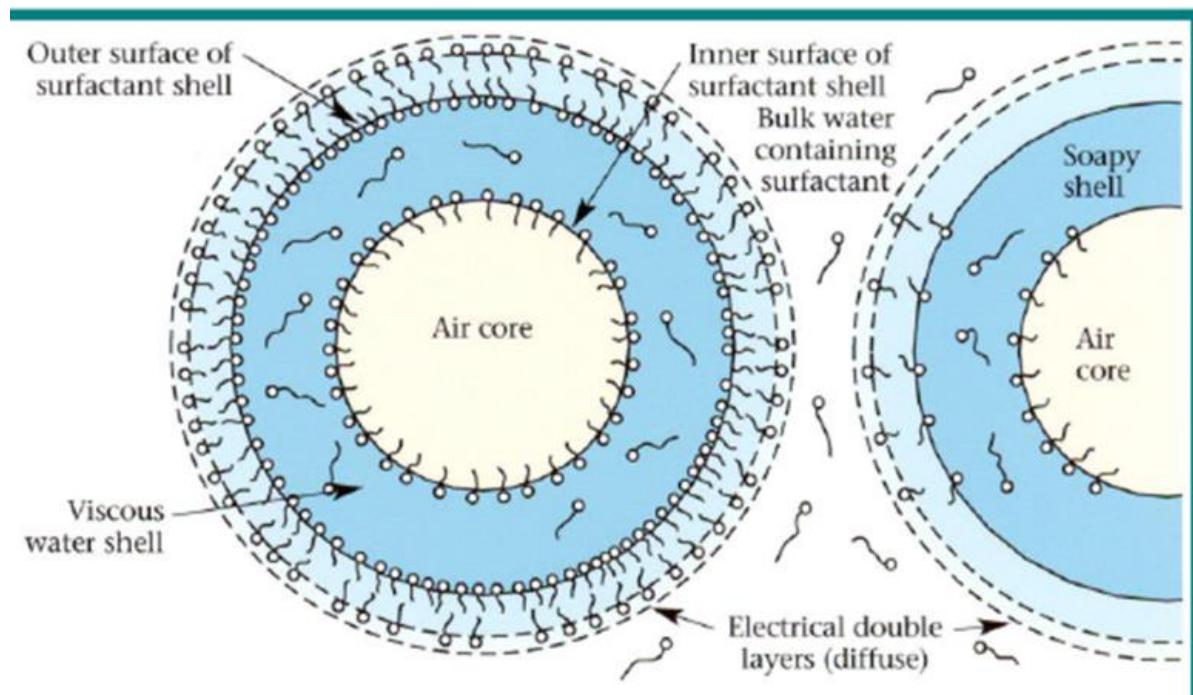
Figure 2-1: Sebba's CGA Structure (Sebba (1987))

Spherical Bilayer Vesicle
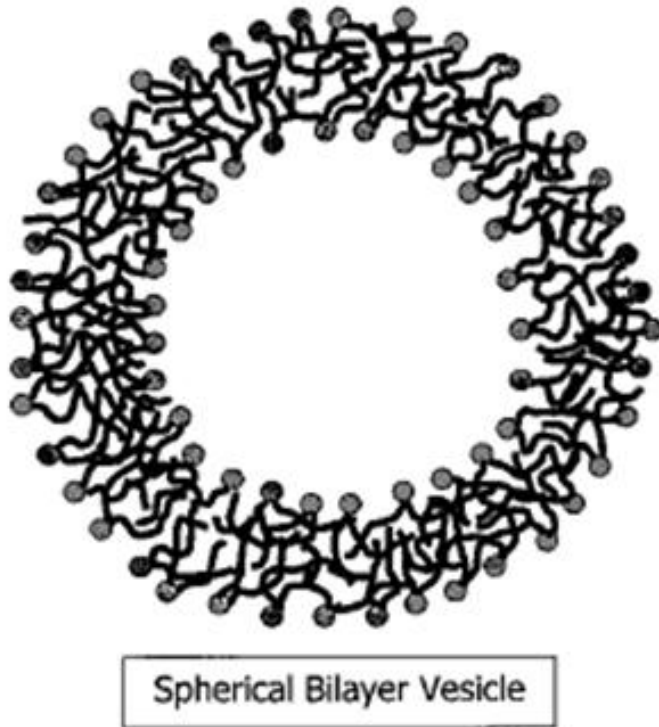
Figure 2-2: Example of a bilayered vesicle (Nagarajan (2002))

solids

gas core

surface tension
reducing membrane

high viscosity
layer

Air

high viscosity
fixing membrane

compatibility
enhancing membrane

concentration transition layer
of polymer & surfactants
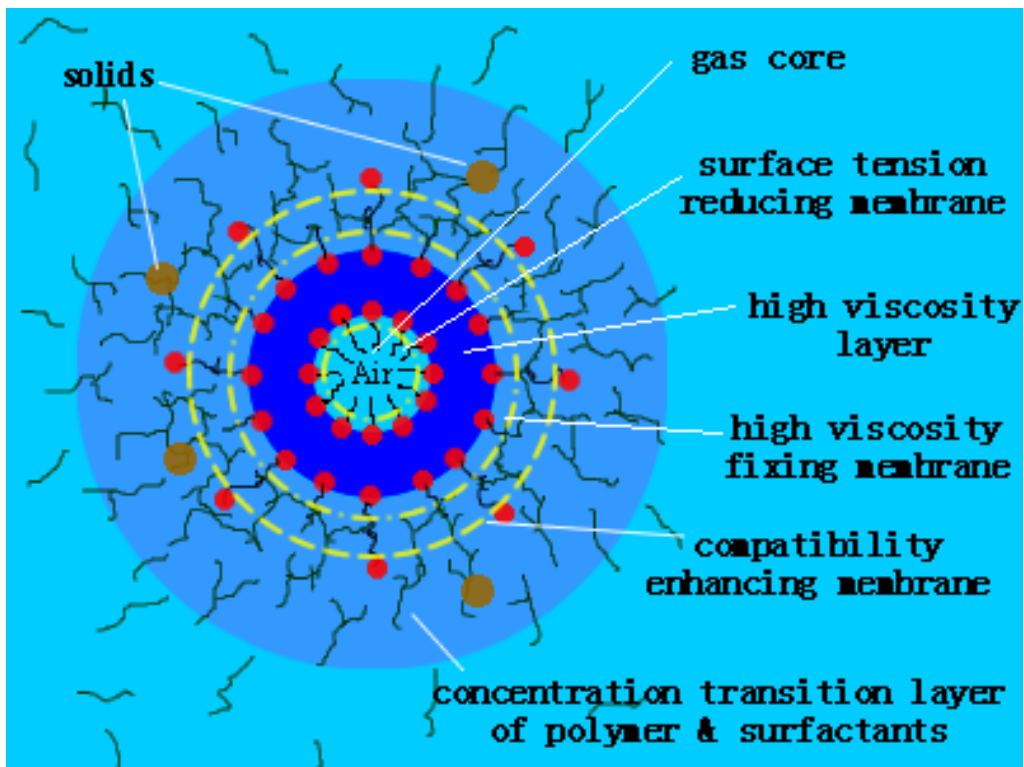
Figure 2-3: Proposed Structure of water-based micro-bubble drilling fluid by Zheng et. al (2009)

2.1.1. Comparison of CGA Structure to Foam Structure

Foams have been well known to mankind from the earliest days. Foams have been widely applied in various industrial branches such as foam fractionation for enriching solution of proteins and enzymes and waste water treatment (Stevenson (2011)), firefighting (Exerowa and Kruglyakov (1997), Manzello and Yang (2002)), and thermal insulation (Exerowa and Kruglyakov (1997)).

In the petroleum industry, foams have found numerous EOR applications. CO_2 foams have been mainly used, in the petroleum industry, as EOR displacing fluid (Enick and Olsen (2012), Heller (1994), Kuehne et. al (1992)) and hydraulic fracturing fluids (Phillips et. al (1987), Harris et. al (1984)). Despite both CGAs and foams being disperse systems consisting of gas bubbles separated by soapy-liquid films, there exists some structural differences between them.

Figure 2-4 below show the structure of a foam with air trapped inside. Instead of surfactant trilayers (in case of CGAs in figure 2-1), the gas is trapped within a surfactant monolayer. The viscous water shell is absent as well. Thus, the electrical barrier to coalescence of bubbles, in case of foams, is lower than in case of CGAs. Furthermore, the diffusion rate of the trapped gas through the surfactant monolayer, in case of foams, will be higher than the diffusion rate of gas through multiple alternating layers of surfactant and polymer, in case of CGAs. Thus, with regards to structural stability, stability of foams is much lower than stability of CGAs.

Foams can be classified as either dry foams with polyhedral shapes (gas fraction will be 90% or higher), or wet foams with spherical shapes (gas fraction is usually within 60%) (Sebba (1987)).

Nonetheless, since generation of both stable CO_2 CGAs and stable CO_2 foams require the ideal surfactant type and concentration. Thus, the surfactant molecules providing stable CO_2 foams are assumed to provide stable CO_2 CGAs as well.
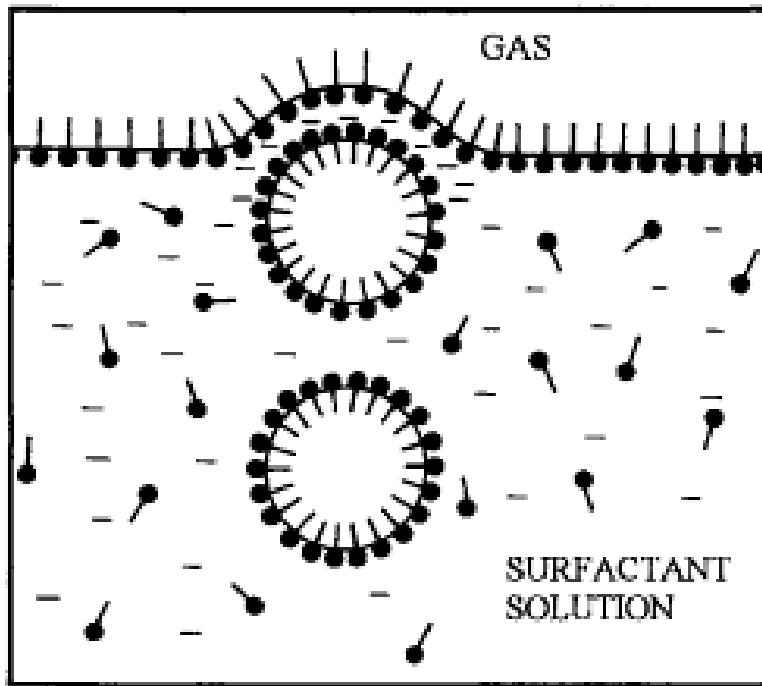
Figure 2-4: Structure of aqueous foams (Exerowa and Kruglyakov (1997))

2.2. CGA Application

Besides being used as drilling fluid, CGAs have found numerous industrial applications, involving high mass transfer rates in separation of metals and other impurities by CGA floatation process (Ciriello et. al (1982), Caballero et. al (1989)), extraction of enzymes (Save et. al (1993)), protein recovery (Wallis et. al (1985), Save et. al (1993), Jauregi and Varley (1998)), and so on. CGAs have also been used as ultrasound contrast agents for enhancement of ultrasound images (Talu et. al (2006)).

2.3. CGA Generation

There are various methods to generate CGAs, such as mechanical agitation, sonication, microchannel emulsification, fluidic oscillation, and so on. While stirring the polymer-surfactant aqueous solution, high energy input is essential because this high energy creates a localized high shear zone that breaks apart

large bubbles (possibly bubbles greater than 100 microns) into smaller bubbles, termed microbubbles, which in turn, increases the surface area per unit volume, making the CGAs ideal for numerous applications involving mass transfer rates (Bredwell, Telgenhoff, Worden, 1995).

Sebba (1985) first generated CGAs using the Venturi throat generator, where the surfactant solution passed through the Venturi throat at very high speeds, while allowing air through very small opening. This method successfully produced very small microbubbles in the range of 25 to 50 microns. However, due to the need of high flowrates of water and the recycling of solution to increase the microbubble concentration, this process was proved impractical.

Sebba (1987) introduced a new method of generating CGAs, called the spinning disc generator, where two vertical baffles were attached to either side of the disc. By rotating the discs at speeds greater than 4000rpm, waves are formed at the surface which hit the baffles and must then re-enter the solution, thus in turn, trapped an unstable thin layer of gas between the baffles and the liquid breaking up into aphrons. This method was shown to produce large volumes of CGAs in a short time period.

Longe (1989) and several other authors (Jauregi et. Al (1997), Zhao (2009), Dai and Deng (2003), Tseng et. al (2006), Bjorndalen and Kuru (2010)) used the baffle system, in addition to stirring the base solution at high speeds exceeding 4000rpm, to produce CGAs. Save and Pangarkar (1994) used a propeller for stirring the surfactant solution instead of spinning disc. Spinelli (2010) prepared the CGAs using a high pressure-high temperature filter press without the filtering element under pressure differential of 200psi.

Xu et. al (2008) demonstrated that CGAs, generated by sonication, were of smaller diameter, higher gas holdup and larger interfacial area than the CGAs, generated by mechanical agitation. Recently, Samuel (2012) prepared CGAs using high speed homogenizer, POLYTRON PT6100, at 8000rpm, thus eliminating the need for baffles.

2.4. CGA Stability

The ability of CGAs to trap the gas at its core over longer duration is indicative of CGA stability with time. Taking a close look at Sebba's CGA structure (Figure 2-1), there are three barriers that inhibit the outward diffusion of the gas from its core: the inner surfactant monolayer, the viscous water layer, and the additional surfactant bilayer. On colloidal level, there are various factors weakening the three barriers mentioned above, which in turn, affects the stability of CGAs. These factors are:

- Pressure differential and concentration gradient of the gas between the CGA core and the outer bulk
- Thickness of the double layer
- Diffusion rate of gas through the aphron shell
- Drainage rate of the viscous water layer
- Type and concentration of surfactant used
- Surfactant solubility and affinity

CGAs destabilize over time in mainly two methods: liquid drainage followed by coalescence and creaming, and Ostwald bubble ripening.

The viscosified water layer, in the CGAs, drains in two major steps. Initially, the viscosified water drains out of the shell under the effect of gravity. Once majority of the liquid is drained, further drainage occurs due to surface tension gradient. The CGAs lose their spherical shape and become polyhedral. Once critical thickness is reached, the film separating the two bubbles ruptures, and coalescence of the bubbles take place. Since the gas holdup of these foam-like bubbles increases, the density of the bubbles decreases, and due to buoyancy effects, the bubbles cream towards the top of the container.

In Ostwald bubble ripening method, larger microbubbles continue to grow at the expense of smaller microbubbles due to gradient in internal pressure of the microbubbles having different radii. Bubble ripening depends on various factors such as diffusivity of the gas through the film, surface tension of the film, elasticity of the film, and pressure gradient of gas inside the core of microbubbles which depends on the radii of the microbubbles.

Sebba (1987) observed "bubble ripening" phenomena on CGAs. He calculated out the rate of shrinking of CGAs to be inversely proportional to the radius of the CGAs. He stated that CGAs with diameter smaller than 25 microns shrank quickly and disappeared. Bredwell and Worden (1998) devised a method to compute the mass transfer coefficient using CGAs and estimated the shell thickness of non-ionic surfactant, Tween 20, to be in the range of 200 to 300nm. They attributed the destabilization of CGAs to both liquid drainage followed by coalescence and Ostwald bubble ripening.

Dai and Deng (2003) proposed an effective way to enhance the CGA stability by adding silica sol solution (which dissociates into negative charges in water) to the CGA solution prepared from hexadecyltrimethyl ammonium chloride (HTAC) (cationic surfactant). The size of the CGAs did not change for over 12 hours indicating that the outer surfactant layer (with positive charge from HTAC) came in contact with the negatively charged silica sol, and formed a tight stable encapsulation.

Feng et. al (2009) described the phenomenon of liquid drainage in CGAs to be occurring in three stages: liquid drainage by gravity, followed by microbubbles losing their colloidal properties and transforming into foams, and further drainage taking place under the influence of plateau border suction. Save and Pangarkar (1994) investigated on the effect of the type of surfactants and their concentrations, stirring time, surface tension and pH of liquid on the stability of CGA. It was found that with increasing alkyl chain length, stability and yield of CGAs are enhanced. Chaphalkar et. al (1993) studied the size

distribution and stability of CGA generated from cationic, anionic, and non-ionic surfactants using particle size analyzer, and found that increase in ionic strength decreases microbubble diameter.

Bjorndalen and Kuru (2008) performed experiments to investigate the effect of surfactant concentration (with respect to the critical micelle concentration), polymer concentration, and viscosity of base fluid on CGA stability. It was observed that the stability of CGAs is enhanced with surfactant concentrations at or above critical micelle concentration, increasing polymer concentrations, and increasing base fluid viscosity. Samuel (2012) generated CGAs and studied the effect of various types of surfactants on the stability of the CGAs. The pair of anionic polymer, Xanthan Gum, and anionic surfactant, dodecyl benzene sulfonate, sodium salt, provided the most stable CGAs.

2.5. CGA Rheology

As it has been mentioned in the previous section, thickness and drainage rate of the double layer affect the CGA stability. The stability of CGAs depends to a great extent on their rheological characteristics. The rheology of CGAs is generally discussed with two characteristics in mind: the viscosity profile over a broad range of shear rate, and the viscosity at a low shear rate (LSRV).

Diffusion of gases through the encapsulation of the microbubble depends on the concentration and pressure gradient of the gas, permeability and diffusivity of the gas through the encapsulation, and thickness of the encapsulation itself. Katiyar and Sarkar (2010) developed a model of gas permeation through an encapsulated microbubble:

$$-k_g \left.\frac{\partial C}{\partial r}\right|_R = h_g [C_w - C(R)] \ (Equation \ 2-1)$$

where $\frac{\partial C}{\partial r}\Big|_R$ is the concentration gradient of the gas, C_w is gas concentration inside the microbubble, $C(R)$ is the gas concentration at a distance R, k_g is the diffusivity in the surrounding liquid, and $h_g \approx k_g^e/\delta$, where k_g^e is the diffusivity of the gas through the film, and δ is the thickness of the film.

Clunie et. al (1967) stated that the range of thickness of the CGA shell, in order for the CGAs to be stable, should be somewhere in between the range of 4 microns and 10 microns, and alteration of this critical thickness will result in rupturing of the water layer in the shell. Ivan et. al (2002) states that in order to prevent diffusion of water molecules from lamellae to the bulk, increasing the viscosity of water will help prevent diffusion. This is done by addition of a viscosifier, like polymer, which inhibits the transfer of water molecules and stabilizes the CGAs.

Yang et. al (2012) performed experimental study on microbubble coalescence in a T-junction microfluidic device to see the effect of liquid viscosities and two phase superficial velocities on coalescence behaviour. It was found that drainage rate of liquid film, in between two microbubbles, is significantly reduced, and coalescence can be prevented by increasing the bulk liquid phase viscosity.

Brookey (1998) states that the stability of the CGAs can be enhanced by addition of high yield, shear thinning polymer that will viscosify the water lamellae, resulting in strengthening of the CGA shell. Growcock et. al (2005) characterised the rheological properties of CGAs to follow the power law model. Larmignat et. al (2008) and Zhao et. al (2008) both described the CGAs to be shear thinning fluids.

2.6.   CGA Core Flooding Experiments

Numerous core flooding experiments have been performed in labs with CGAs as injection fluid. Most of the CGA core flooding tests have been performed to test the ability of CGAs, as drilling fluids, to form a

bridge across the formation, limiting fluid invasion into formation, and examine the degree of formation damage caused by CGAs.

Growcock et. al (2005) worked on understanding formation sealing and damage under simulated downhole conditions, by conducting flow visualization tests. These tests indicated that the CGAs move through the porous media in "Bubbly Flow" regime, resulting in the ability of CGAs to move at a velocity greater than the liquid phase and inhibit movement of the drilling fluid into the formation.

Bjorndalen et. al (2011) conducted sandpack tests with radial and linear core holders and measured the maximum pressure drop per unit distance to determine the ability of CGAs bridging mechanism, while changing the permeability, CGA composition, injection flow rates, and wettability. It was shown that water-wet reservoirs with high permeability are ideal for effective CGA blocking.

Shivhare (2011) investigated the ability of oil based CGAs to form bridge-like structure and block the formation pores. The core flow tests were conducted with a radial sand packed core and the maximum pressure drop attained by the CGAs was measured. The oil based CGAs were found to establish an effective seal, thereby inhibiting fluid loss and minimizing formation damage.

Samuel (2012) devised experimental procedure to test the effectiveness of aqueous based CGAs as chemical enhanced recovery agents in both visual and radial cells. The oil recovery performance of CGAs was compared to polymer flooding, surfactant-polymer solution flooding, water flooding, water followed by CGA flooding, and water followed by polymer flooding. The CGAs performed very well with recovery being between 75% (for radial cell experiments) to 90% (for visual cell experiments) at lower injection pressure than required for other viscous chemical recovery agents, such as polymer flooding.

3. Experimental Program and Procedure

3.1. Materials Used for CO_2 CGA Generation

3.1.1. Screening Criteria for Polymer-Surfactant Systems

3.1.1.1. Surfactant Chosen

Surfactants are used in various applications, such as detergents, emulsions, paints, adhesives, etc., to reduce the interfacial tension between two otherwise immiscible phases. The molecular structure of any surfactant basically is divided into two parts: the head (hydrophilic portion) and the tail (hydrophobic portion). There are mainly three types of surfactants: anionic (with negative charged head), cationic (with positive charged head), and nonionic (with no charge on head). The solubility and affinity of a surfactant is determined through its hydrophilic-lipophilic balance (HLB) measure. The HLB of a surfactant depends largely on the ratio of the length of the tail to the degree of hydrophilicity of the functional group at the head.

Xing et. al (2010) designed the selection criteria of surfactants for producing stable CO_2-in-brine foams in the reservoir. Some of these criteria, pertaining to generating CO_2 CGAs, were as follows:

- Nonionic surfactants are preferred over ionic surfactants, because the pressure required to dissolve small amounts of ionic surfactants is well above minimum miscible pressure values

- The tails of these surfactants should contain CO_2-phillic functional groups with hydrocarbon alkyl chains

- These surfactants should contain ethylene oxide units that has been proven to be more suitable hydrophiles than propylene oxides

- According to Bancroft's rule, surfactants should be more soluble in the continuous aqueous phase to generate stable CO_2-in-brine emulsions

Rocha et. al (2001) conducted experiments on generating highly stable CO_2-in-water emulsions with surfactants containing alkylene oxide-, siloxane-, and fluorocarbon-based tails, and studied the effect of temperature, hydrophilic-CO_2-philic balance (HCB), and salinity on CO_2-in-water emulsion stability. While stable CO_2-in-water emulsions were formed from all three types of surfactants stated above, the alkylene oxide-based surfactants were preferred because these types of surfactant are less expensive and less toxic than the siloxane and fluorocarbon-based surfactants.

Usually, the types of surfactant, used for generating CO_2 foams, have belonged to either anionic or non-ionic groups. Table 3-1 below lists a number of surfactants that have been used successfully in the past to generate stable CO_2 foams.

Table 3-1: List of Surfactants used to Generate CO_2 Foams in the past

Reference	Surfactants	Type of surfactant
Xing et. al (2010)	- Triton X100 - Tergitol NP 4, 6, 9, 12, 15 - Surfonic N85 - Cedepal CO 630 and 710 - Tergitol TMN 6, 9 - PEG monolaurate 600	Non-ionic
Zeng et. al (2006), Chang and Grigg (1999)	Chevron Chaser CD 1045	Anionic & Non-ionic
Yaghoobi and Heller (1994)	- Ethoxylated Alcohol Glyceryl Sulfonate (Shell Enordet X 2001) - Alpha Olefin Sulfonate (Chevron Chaser CD 1040)	Anionic
	Alkyl phenol ethoxylate (Chevron Chaser CD 1050)	Non-ionic
	Chevron Chaser CD 1045	Anionic & Non-ionic
Lescure and Claridge (1986)	- Igepal 610, 710 - X 2001, 2002, 2003 - EMULPHOGENE 720BC	Non-ionic
	AES 1215-3S, 911-2.5S	Anionic

Kuehne et. al (1992)	• Alpha Olefin Sulfonate (AOS) • Alcohol ethoxysulfate (AEOSO4) – (also known as Alipal CD-128) • Alcohol ethoxysulfonate (AEOS30) – (also known as Avanel S-30)	Anionic
	• Alkyl phenol ethoxylate (APEO) • Ethoxy Alcohol (EOA)	Non-ionic

In order to generate stable CO_2 CGAs that provide good electric barriers to coalescence, the HCB of the surfactant, which is strongly influenced by the presence of CO_2-philic alkylphenol, fluoralkyl, or fluoroether tails, plays an important role. The two surfactants, used in this study, to generate stable CO_2 CGAs are: Surfonic N85 (non-ionic) and dodecyl benzene sulfonate, sodium salt (anionic). The properties of these two surfactants are listed in Table 3-2 below:

Table 3-2: Properties of Surfactants chosen for Generating CO_2 CGAs

Properties	Surfonic N85 (nonionic) [Chemical name: Nonylphenol, ethoxylated]	Dodecyl benzene sulfonate, sodium salt (anionic)
Denoted in this study as	N85	DDBS
Chemical Formula	$C_{15}H_{23}(OCH_2CH_2)_nOH$; n = # of ethylene oxide units ≈ 8 - 9	$C_{18}H_{29}NaO_3S$
Appearance	Colourless liquid	Off white powder
Molecular Weight	594.0 g/mol	348.49 g/mol
HLB	12.6	11.7
Supplier	Huntsman Corporation	ACROS

3.1.1.2. Polymer Chosen

Polymers are essential component of CGAs that enhances the stability of the aphrons by increasing the viscosity of the water lamellae in the aphron shell. Brookey et al (1998) characterises the ideal polymer to high yield stress, shear thinning polymer that will allow the aphrons to be stable under cyclic compression and expansion, all the while keeping the aphron morphology same.

Keeping Sebba's aphron structure in mind, the polymer, in addition imparting viscosity, must not react with the surfactant that is being used to generate CO_2 CGAs. Oppositely charged polymer-surfactant systems tend to strongly associate and associative phase separation takes place, thus preventing both the polymer and the surfactant to fulfill their role of providing structural stability to CGAs (Holmberg et. al (2002)). Since surfactants of non-ionic and anionic nature have been chosen to generate CO_2 CGAs, cationic polymers are eliminated.

In order to trap the CO_2 gas successfully in the bubble as long as possible, the polymer-laden viscous water lamellae in the shell must have low diffusivity to CO_2 gas. Xanthan Gum, an anionic biopolymer, has been used extensively by several authors (Growcock et. al (2005), Cardoso et. al (2010), Bjorndalen and Kuru (2008), Samuel (2012)) in the petroleum industry to generate stable air CGAs. Other water soluble polymers that have been tested by several authors to be shown to have low diffusivity to CO_2 gas are listed in Table 3-3 below:

Table 3-3: Summary of Research Pertaining to CO_2 Gas Diffusion through Polymer Solutions (Ju and Ho (1986))

Reference	Technique Used	Polymer Systems Used	Gas Used	Polymer concentration range (wt.%)	Influence of Polymer addition on Diffusion
Astarita et. al (1964)	Laminar jet	Carboxymethyl cellulose, Carbopol, Polyacrylamide	CO_2 gas	$0 - 3$	Increased diffusion
Dim et. al (1971)	Laminar jet	Methocel	CO_2 gas	$0 - 0.3$	Increased diffusion
Mashelkar and Soylu (1974)	Falling films (wetted wall, wetted sphere, and wetted cone)	Hydroxyethyl cellulose, Polyacrylamide, Polyox, Carboxymethyl cellulose	CO_2 gas	$0 - 1$	Increased and Decreased
Perez and	Falling films	Carbopol	CO_2 gas	$0 - 1$	Increased and

Sandall (1973)	(wetted wall, wetted sphere, and wetted cone)				Decreased
Mashelkar and Soylu (1982)	Falling films (wetted wall, wetted sphere, and wetted cone)	Polyox, Polyacrylamide	CO_2 gas	$0 - 0.1$	Increased diffusion
Srinivasan (1967)	Falling films (wetted wall, wetted sphere, and wetted cone)	Carboxymethyl cellulose	CO_2 gas	$0 - 0.13$	Increased diffusion
Quinn and Blair (1967)	Stagnant medium	Carboxymethyl cellulose, Polyethylene glycol	CO_2, SO_2 gas	$0 - 4$	Decreased diffusion
Aiba and Someya (1965)	Membrane method	Carboxymethyl cellulose	CO_2 gas	$0 - 1.5$	Decreased diffusion

From table 3-3 above, it is seen that depending on the experiment type, the answer to the effect of polymer concentration on CO_2 diffusivity through polymer solution came out contradictory. The two methods, membrane method and the stagnant medium method, are two techniques where there is no case of hydrodynamic boundary layers, and are of interest to this study, since the diffusion of CO_2 gas will be from inside a stationary aphron core to the outer atmosphere while the aphron solution is sitting still. Conducting CO_2 gas diffusion experiments through these two methods showed that an increase in concentration of carboxymethyl cellulose (CMC) and polyethylene glycol (PEG) will decrease the diffusion of CO_2 gas through the polymer solution.

In this study, the following three polymers have been chosen to generate CO_2 CGAs:

a) Carboxymethyl cellulose (anionic)

b) Xanthan Gum (XG) (anionic)

c) Hydroxyethyl cellulose (HEC) (non-ionic)

Table 3-4: Properties of Polymers chosen for Generating CO_2 CGAs

	Carboxymethyl cellulose (CMC)	Hydroxyethyl cellulose (HEC)	Xanthan Gum (XG)
Trade Name	-	Natrosol HiVis	Barazan D
Supplier	-	Diversity Technical Corporation	Baroid Industrial Drilling Productions
Appearance	Off white to light beige powder	White, free-flowing granular powder	Yellow – white powder
Category	Derivative of cellulose	Hydroxyethyl ether of cellulose	Polysaccharides

3.1.2. Surfactant-Polymer Pair Chosen with Optimum Concentrations

3.1.2.1. Optimum Polymer Concentration

Samuel (2012), in her study, determined the optimum concentration of Xanthan Gum (XG), in order to provide the desired rheological and stability characteristics to the CGAs, is to be 2 lb/bbl (0.55 wt%). This is the concentration of XG used in this study as well in order to generate stable CO_2 CGAs. The concentration of the other two polymers, hydroxyethyl cellulose (HEC) and CMC, was also chosen to start with 2 lb/bbl (0.55 wt%). The LSRV of the base fluid solution was measured and is plotted on Figure 3-1.
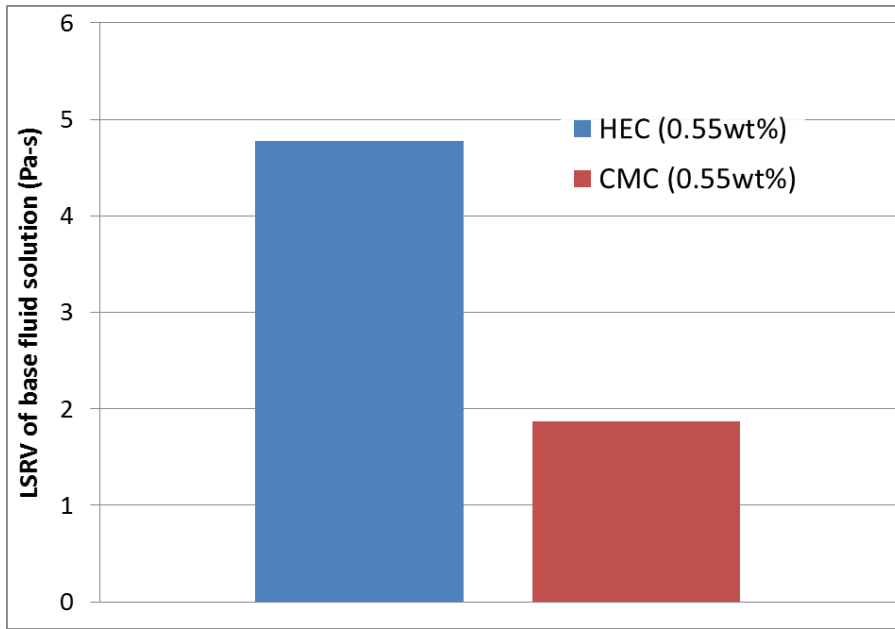
Figure 3-1: LSRV of Base fluid of HEC and CMC at 2 lb/bbl (0.55 wt%)

According to MacPhail et. al (2008), the minimum viscosity of the base fluid, in order to prevent the water molecules from diffusing into the bulk solution, has to be greater than 40,000cp (40 Pa-s). Figure 3-1 clearly indicates that the concentration of 2 lb/bbl (0.55 wt%), in case of both HEC and CMC, does not provide enough viscosity to keep the CGAs stable. Thus, the range of concentration, for these two polymers, was increased at increments of 1.5 lb/bbl till the base fluid LSRV value surpasses 40,000cp. Figure 3-2 shows the LSRV value of base fluid solution with varied concentration of HEC and CMC.
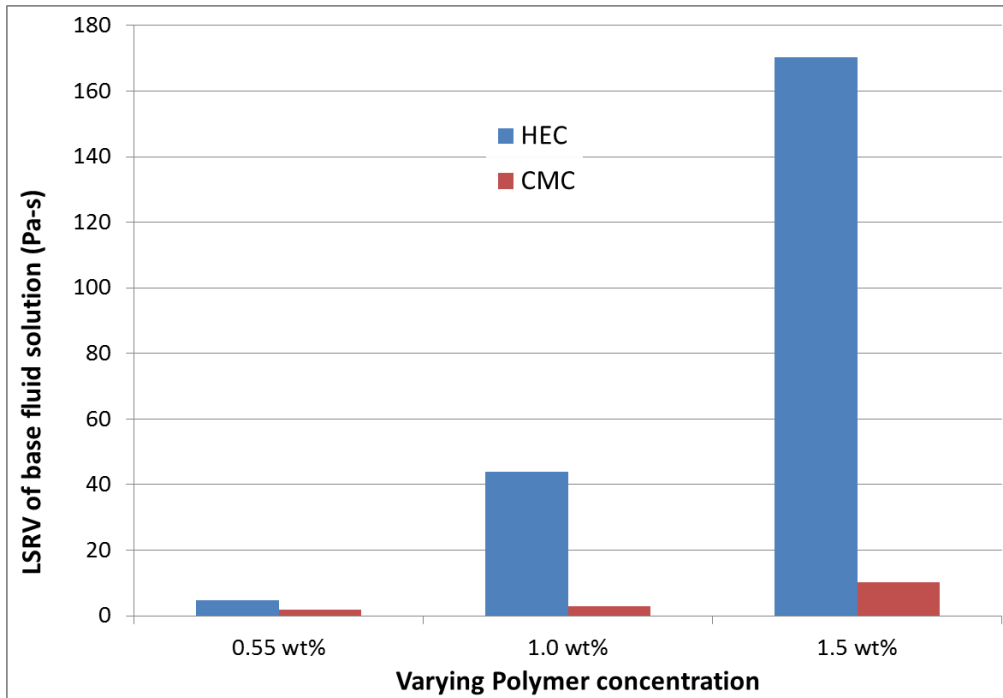
Figure 3-2: LSRV of Base fluid of HEC and CMC at varied concentrations

It is seen from figure 3-2 above that even at high concentrations of 5 lb/bbl (1.5 wt%), CMC failed to impart any significant additional viscosity to the base fluid solution. Thus, CMC is eliminated. In the concentration range of 3.5 to 5 lb/bbl (1.0 to 1.5 wt%), the LSRV of base fluid solution containing HEC is high enough to provide stability to the CO_2 CGAs. To decide the optimum concentration of HEC, CO_2 CGAs were generated with 1 lb/bbl (0.29 wt%) DDBS, and both concentration values (3.5 lb/bbl (1.0 wt%) and 5 lb/bbl (1.5 wt%)) of HEC were used. The stability of CO_2 CGAs from both HEC concentrations was compared. Figure 3-3 plots the time stability plot of CO_2 CGAs, generated using both concentrations of HEC.
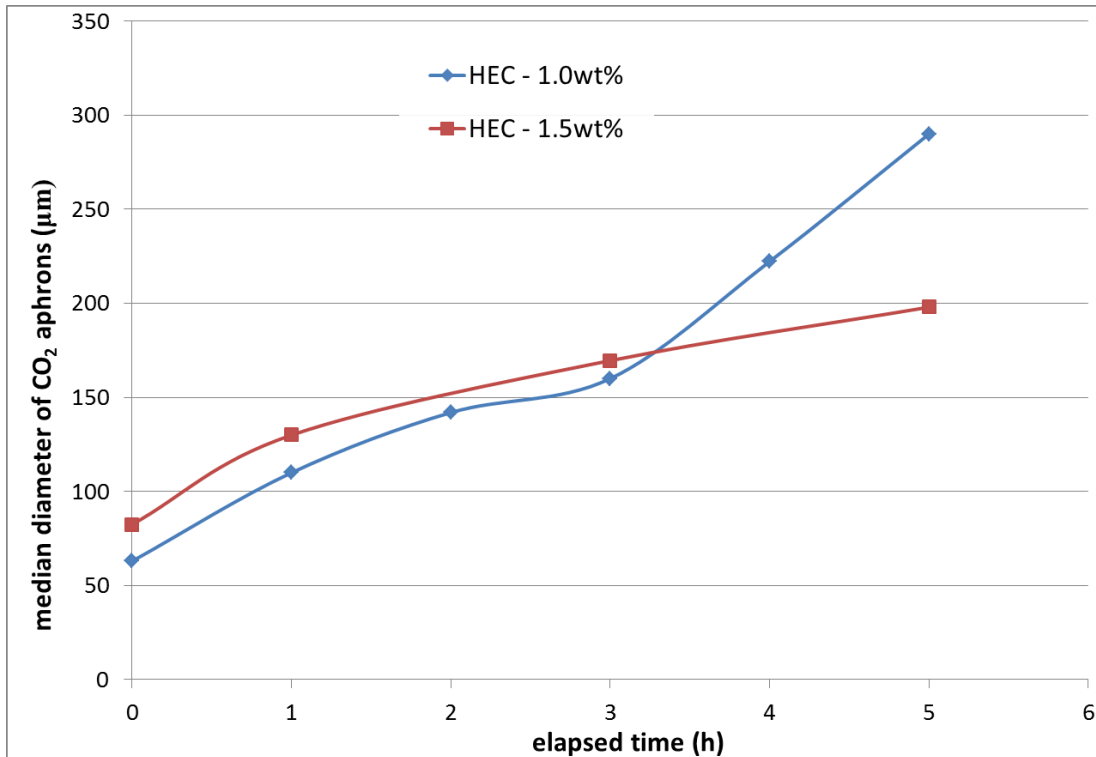
Figure 3-3: Time-stability plot of CO_2 CGAs from 3.5 lb/bbl (1.0 wt%) and 5 lb/bbl (1.5 wt%) HEC (with 1lb/bbl DDBS)

From figure 3-3 above, the desired concentration, that provides the most stable CO_2 CGAs, for HEC is 5 lb/bbl (1.5 wt%). Thus, XG (at 2 lb/bbl concentration) and HEC (at 5 lb/bbl concentration) are the two polymers that will be used throughout the rest of this study.

3.1.2.2.   Optimum Surfactant Concentration

As mentioned previously, two surfactants, one anionic and other non-ionic, were chosen to provide stable CO_2 CGAs: DDBS and N85. According to Bjorndalen and Kuru (2008), the stability of CGAs was enhanced with increasing concentrations of surfactants till the critical micelle concentration point; at or above critical micelle concentration, the stability of CGAs was not greatly affected with increasing

concentrations of surfactants used. Thus, in this study, the concentration range of surfactants used is well above their critical micelle concentration.

Samuel (2012) used DDBS to generate stable air CGAs, and found out the optimum concentration of DDBS, providing the smallest median diameter over a longer duration, to be 1 lb/bbl (0.29 wt%). In this study, 1 lb/bbl is the concentration used for DDBS. The concentrations chosen for N85 were 1 lb/bbl (0.29 wt%) and 2 lb/bbl (0.55 wt%). With optimum concentrations for the polymer decided, CO_2 CGAs were generated with following polymers- N85 pairs at stated concentrations:

- XG (at 2 lb/bbl) & N85 (at 1 lb/bbl)

- XG (at 2 lb/bbl) & N85 (at 2 lb/bbl)

- HEC (at 5 lb/bbl) and N85 (at 1 lb/bbl)

- HEC (at 5 lb/bbl) and N85 (at 2 lb/bbl)

The time-stability plot of CO_2 CGAs, generated from the four pairs of polymer-surfactant stated above, is shown in Figure 3-4 below:
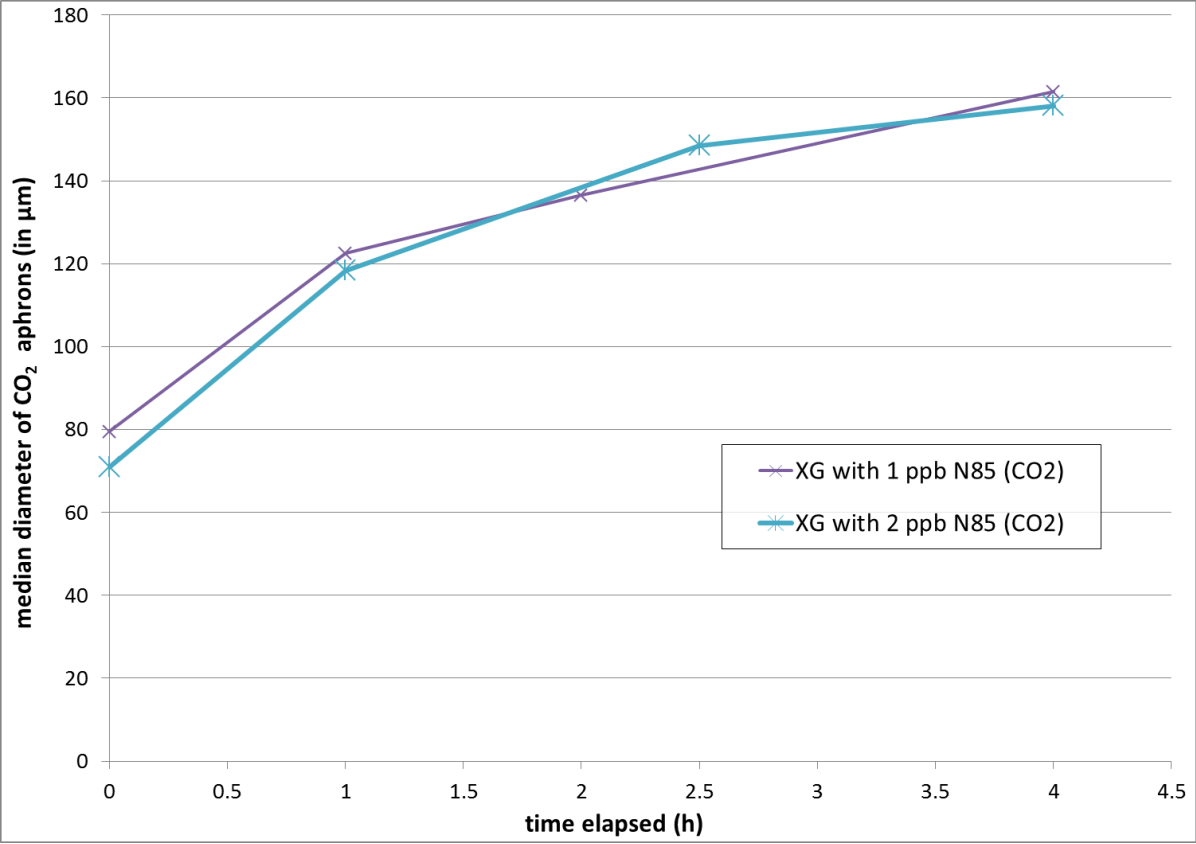
Figure 3-4 (a): Time-stability plot comparison of CO_2 CGAs generated from two different concentrations of Surfonic N85: 1 lb/bbl and 2 lb/bbl (with Xanthan Gum as polymer)
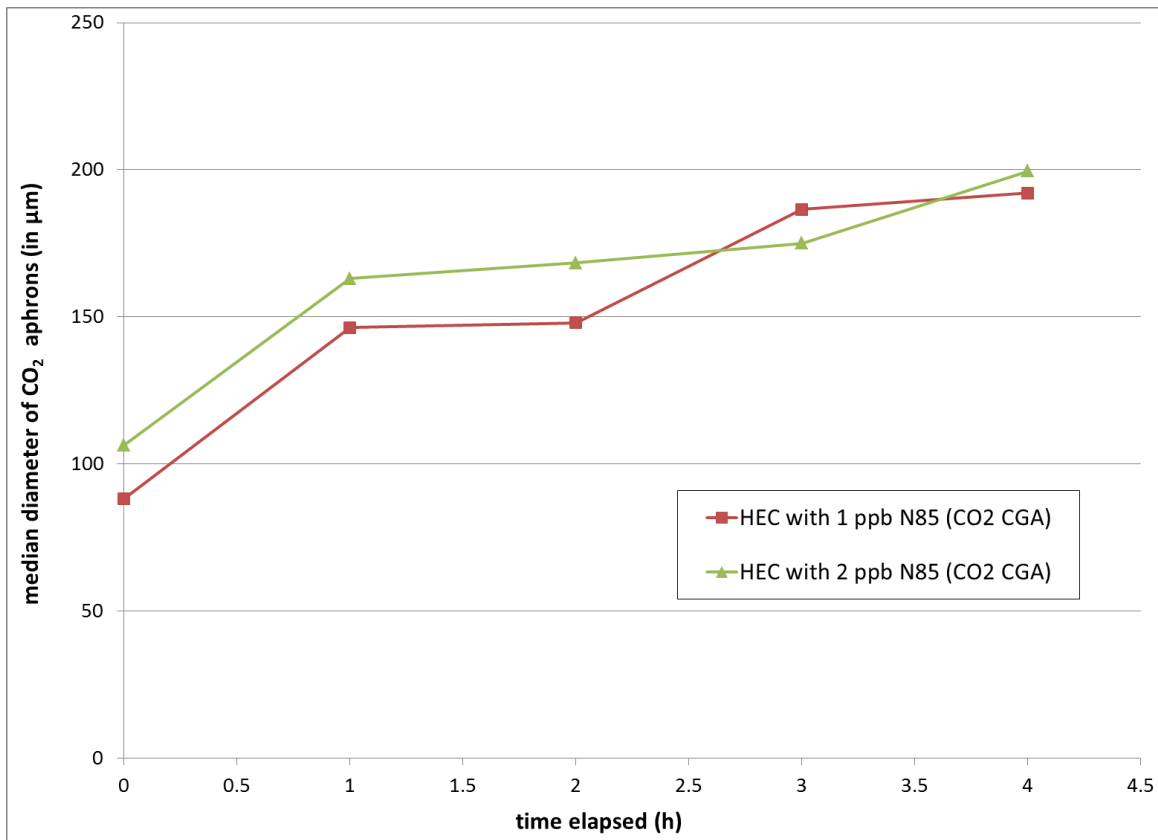
Figure 3-4 (b): Time-stability plot comparison of CO_2 CGAs generated from two different concentrations of Surfonic N85: 1 lb/bbl and 2 lb/bbl (with Hydroxyethyl cellulose as polymer)

From figures 3-4 (a) and (b), it turns out there is no significant change in CGA stability using either concentration values of N85. Thus, the lower of the two concentration values, 1 lb/bbl, is chosen as the optimum concentration for N85.

3.1.2.3.   Chosen Polymer-Surfactant Pairs with Optimum Concentrations

The pairs of polymer-surfactant system used in this study are listed below in Table 3-5:

Table 3-5: List of Polymer-Surfactant pairs used in this study

Surfactant conc. / Polymer conc.		Surfonic N85	Dodecyl benzene sulfonate, sodium salt
		(1 lb/bbl)	(1 lb/bbl)
Hydroxyethyl cellulose (HEC)	(5 lb/bbl)	Denotes as: **HEC/N85 (Non-Non)**	Denotes as: **HEC/DDBS (Non-An)**
Xanthan Gum (XG)	(2 lb/bbl)	Denotes as: **XG/N85 (An-Non)**	Denoted as: **XG/DDBS (An-An)**

3.1.3.   Water

Bjorndalen and Kuru (2008) prepared CGAs using both tap water and de-ionized water, and did not find any significant effect on stability of CGAs. CO_2 CGAs were generated using both tap water and de-ionized water, with XG/DDBS (An-An) polymer-surfactant pair. The time-stability plot of these CGAs is plotted on Figure 3-5 below:
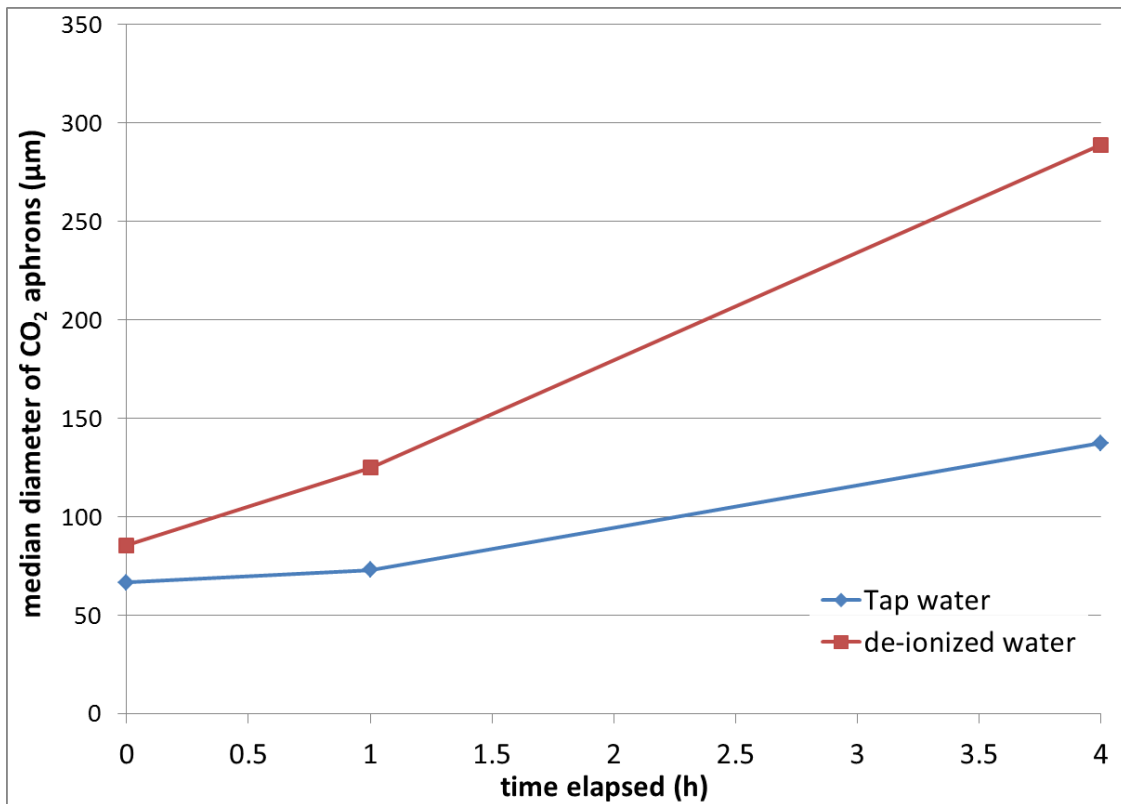
Figure 3-5: Median Diameter comparison of CO_2 CGAs (prepared from tap water & de-ionized water)

Figure 3-5 shows that tap water provides CO_2 CGAs of smaller diameter with time, making tap water preferable over de-ionized water.

3.2.   Equipments Used

3.2.1. Digital Scale

In order to weigh the chemicals, the precision balance Ohaus EP 2012 Explorer Pro was used. Figure 3-6 shows the picture of the digital scale used in the following experiments.

Figure 3-6: Picture of the Digital scale

3.2.2. Magnetic Stirrer

To prepare the base fluid and ensure its homogeneity, the digital magnetic stirrer ISOTEMP, from Fisher

Scientific, was used. Figure 3-7 shows the picture of the magnetic stirrer.

Figure 3-7: Picture of the Magnetic Stirrer

3.2.3. Homogenizer with CO_2 Cylinder

The POLYTRON PT6100 digital homogenizer, in conjunction with CO_2 cylinder, was used in order to generate CO_2 CGAs. The maximum allowed rotating speed is 26,000rpm. The experimental setup is shown in Figure 3-8 below.

Figure 3-8: Picture of the Homogenizer with CO_2 Cylinder

3.2.4. The Test Cell

The test cell, shown in figure 3-9 (a) below, is made of stainless steel which allows for samples inside the cell to be mixed at high pressures in excess of 100psi. The black seal around the stirrer, in figure 3-9 (b), isolates the contents inside the test cell from the outer atmosphere.

| Figure 3-9 (a): The Test Cell | Figure 3-9 (b): The Seal to isolate the contents inside from the outer atmosphere |
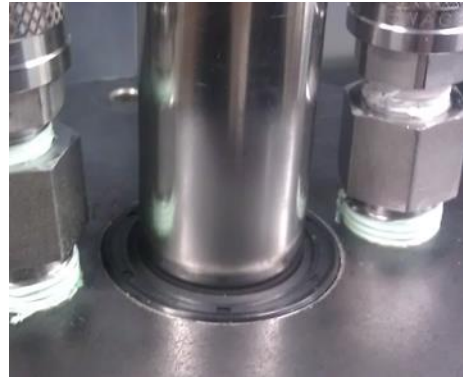
3.2.5. Rheometer

The rheometer used in this study is the Bohlin C-VOR 150, from Malvern Instruments. The device has shear rates that ranges from $0.0001s^{-1}$ to $10,000s^{-1}$. This rheometer can be used for multiple purposes, such as viscometry, oscillation, creep test, and so on. It can be used at either ambient conditions (Peltier mode) or high pressure-high temperature conditions (HPC mode).

The rheometer, when used at ambient mode, has a cone and plate measuring system with separating gap of 0.15mm. When used at high pressure mode, this rheometer has a stator-rotor system with fluid placed in the concentric annulus. Figures 3-10 (a) and (b) show the Bohlin rheometer at low pressure mode and high pressure mode, respectively.

Figure 3-10 (a): The Bohlin Rheometer at Ambient conditions;

Figure 3-10 (b): Rheometer with Elevated Pressure condition

3.2.6. Microscope System

Measurements of the outer diameter of the CO_2 CGAs with time and bubble size frequency distributions were conducted using the Leica DM 6000M microscope. A camera (Leica DFC280) is attached at the top of the device for taking the images. Figure 3-11 below shows the digital microscope.
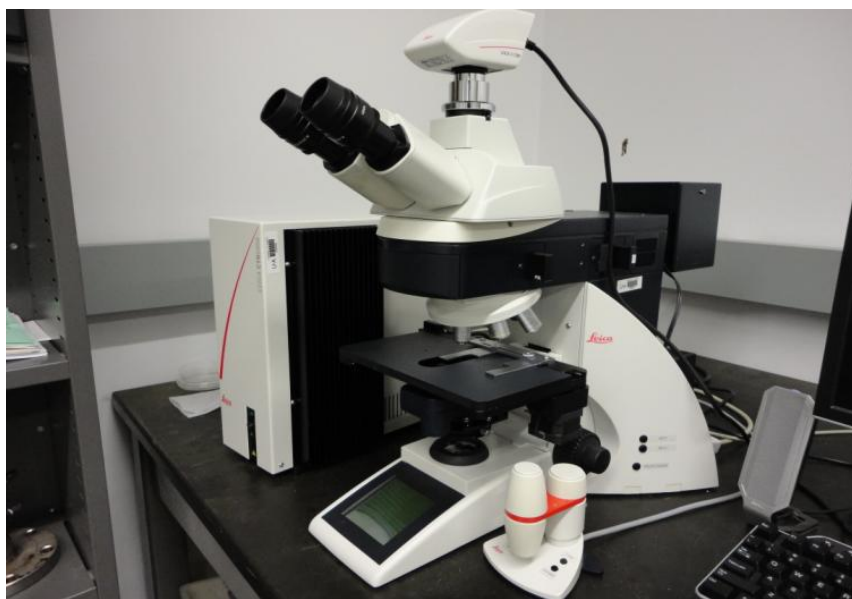
Figure 3-11: Picture of the Digital Microscope

3.3. Experimental Procedure for Generating CO_2 CGAs

3.3.1. Preparation of Base fluid

In order to generate aqueous based CO_2 CGAs, the first step is to prepare the base fluid. In this study, the base fluid comprises of polymer, surfactant, and tap water. The base fluid was prepared using ISOTEMP magnetic stirrer. The aqueous solution of polymer and surfactant was gently stirred at 400 rpm for approximately 20 minutes at 22.5 ± 0.5°C temperature. This was to ensure homogeneity of base fluid.

3.3.2. Preparation of CO_2 CGAs

A sketch of the experimental setup, for preparation of CO_2 CGAs, is shown in figure 3-12. The CGAs were created using the POLYTRON PT6100 homogenizer. The gel-like, viscous, homogeneous base fluid was poured into the reactor vessel. Vacuum was applied to ensure no air was present. CO_2 gas was constantly supplied to the vessel under 5psi pressure so that no air could leak in. The base fluid solution was agitated for 5 minutes at 8000rpm. The high energy, generated from the stirring, aided in creating the added encapsulation consisting of polymer induced viscous solution layer and multiple surfactant layers.
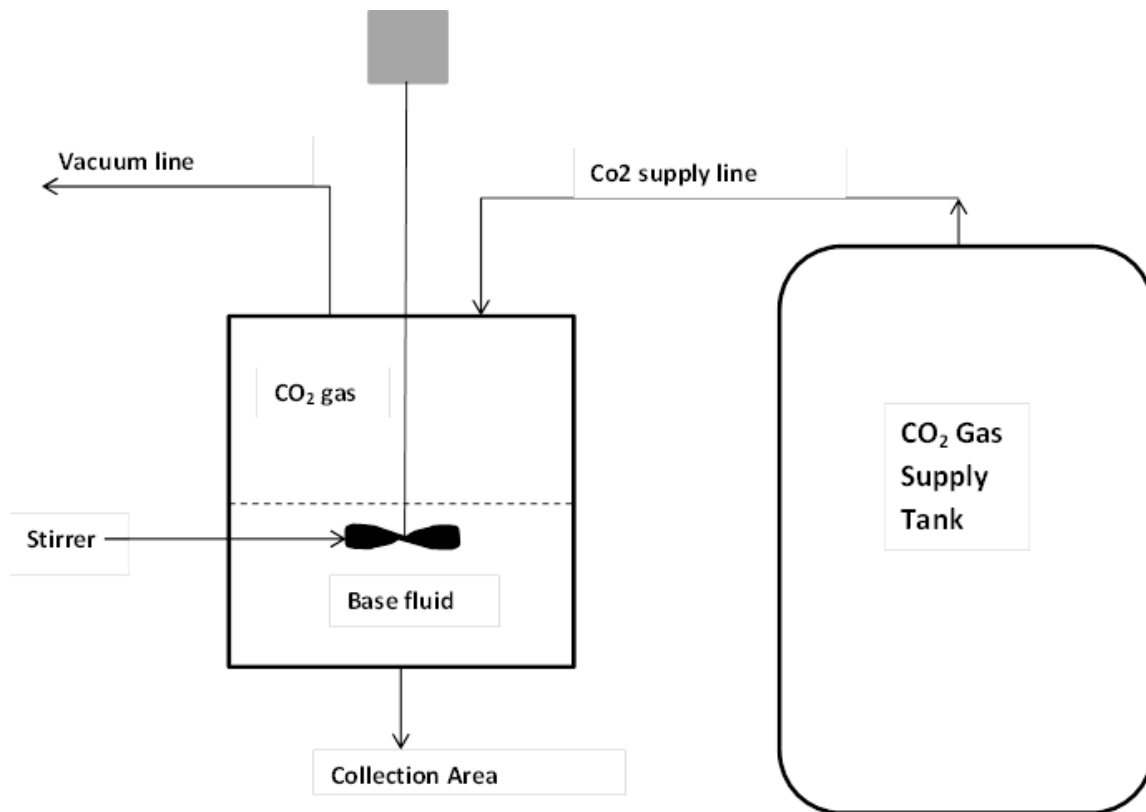
Figure 3-12: Experimental Setup for Generating CO_2 CGAs

3.4. CO_2 CGA Characterisation

3.4.1. Rheology

Rheological characteristics of the base fluid solution and the newly prepared CO_2 CGA sample were measured using a cone and plate type rheometer (4°/40mm geometry) (Bohlin C-VOR150 rheometer). For each test run, new samples were used. The LSRV and the viscosity profile data were collected using the Bohlin software (version 6.50.5.7). The LSRV value of both base fluid solution and CO_2 CGAs were measured at constant shear rate of $0.01s^{-1}$. The increase (or decrease) in LSRV, after aphronization, is caused due to Laplace pressure, indicating high yield and aggregation of CO_2 CGAs (Ivan et. al (2002)). Viscosity profiles of both base fluid and the corresponding CO_2 CGAs were measured in the shear rate ranges of $0.01s^{-1}$ to $100s^{-1}$.

3.4.2. Stability

The change in outer diameter of CO_2 CGAs with time is indicative of CO_2 CGA stability. If the increase in the size of CO_2 CGAs is gradual with time, the CGAs are more stable. Outer diameter measurements of CO_2 CGAs were conducted with the help of Leica Image Analysis CTR6000 microscope. The magnification used was 10 times. The CO_2 CGA sample was taken out of the reactor vessel at specific time intervals (increments of 1 hour) to minimize the exposure of the sample to air. Using the Leica Application software (version 3.3.0, Build: 2872), multiple pictures of the CGAs in the petridish were taken. The outer diameters of all the CGAs were measured using Leica MW (version V3.6.2) software and exported to MS Excel. The median diameter of CO_2 CGAs, referred to as d50, was plotted against time to represent the time-stability of CO_2 CGAs.

The frequency distribution of CO_2 CGAs is a good representation of total yield and stability of CGAs with time. The time intervals used in this study are initial time, after 1 hour, and after 5 hours. At each

desired time interval, the outer diameter of the CGAs fell into six categories: 0-50μm, 50-100μm, 100-150μm, 150-200μm, 200-250μm, and >250μm. The percentage of CO_2 CGAs, falling into each of these categories, provides a frequency distribution of the outer diameter of CGA at each time interval. The position of the peak denotes the median diameter of the CGAs, and the more towards left the peak is, the smaller the median CGA diameter is at the specified time interval. In this study, the CO_2 CGA sample, in the petridish, adequately represents the concentration of CO_2 CGAs throughout the whole bulk inside the reactor vessel.

Table 3-6: List of the Criteria for deciding the Best Polymer-Surfactant Composition

Rheology	Change in Low Shear Rate Viscosity (LSRV) after microbubble generation	The increase in viscosity, after microbubble generation, indicates stable and "energized" encapsulation, which helps prevent outward diffusion of gases and outward diffusion of viscous water molecules into the bulk
	Change in viscosity profile (from shear rate values between 0.01 s^{-1} to 100 s^{-1}) after microbubble generation	
Stability	Change in median microbubble diameter with time (over a range of approx. 20 to 25 hours)	The more gradual increase in outer diameter indicates more stable encapsulation surrounding the gas at the core of the microbubble, which in turn, lowers the diffusion rate of the gas
	Frequency distribution of CGAs at three different time intervals: initial time, after 1 hour, after 5 hours	The position and height of the maximum point on the distribution plot determines the yield and median diameter of the microbubble sample. The more the position of the maximum point is towards the left at all time intervals, the smaller the median diameter is at all time intervals. Narrow distribution indicates less polydispersity.

3.4.3. HP-HT Rheology

After the best polymer-surfactant combination for generating stable CO_2 CGAs was determined, further analysis was carried out on both the base fluid and the corresponding CO_2 CGAs, in terms of rheology and viscoelastic behaviour. In order to predict the physical state and flow behaviour of CO_2 CGAs at

typical reservoir conditions, these tests were conducted under elevated pressures and temperatures, using the same rheometer (Bohlin CVOR150 rheometer). Instead of a cone and plate type, there is concentric cylinder measuring system, allowing for Couette flow of fluids inside the annular space. The rheometer comprises a cup and bob measuring system assembly in a completely closed environment. Supported with low friction, precision jewel bearings, the bob is driven by the rheometer through an external magnetic coupling. The entire cell is pressurized by CO_2 gas in a pressurized cylinder that acts as an external pressure source.

Both the viscometry tests, (which included the LSRV and the viscosity profile) and the dynamic oscillation tests (consisting of amplitude sweep and frequency sweep) were measured at elevated temperatures of 25°C and 75°C, and elevated pressures of 100psi, 500psi, and 800psi.

3.4.3.1. Viscoelastic Behavior

Viscoelastic materials display both elastic and viscous behavior. Thus, while conducting dynamic oscillation tests (amplitude sweep and frequency sweep) on viscoelastic materials, two important parameters that are measured throughout the test are: elastic modulus (G') and viscous modulus (G").

Elastic modulus represents the elastic behavior of the test sample. When finite stress is applied on a viscoelastic test sample and removed thereafter, the sample does not come back to its original form entirely. The energy that drives the reformation process of the sample is known as elastic modulus (or storage modulus). It is denoted in this study as G'. Viscous modulus displays the viscous behavior of the test sample. On applying and then removing the stress on a viscoelastic test sample, the energy consumed during the process of changing the sample's structure is known as viscous modulus (or loss modulus). It is denoted in this study as G".

For a viscoelastic sample, elastic modulus being higher than viscous modulus indicates structural rigidity and stability. The viscoelastic behavior of the test sample exhibit rigid, gel character, analogous to

elasticity of a solid. Viscous modulus dominating elastic modulus indicates structural mobility. The viscoelastic response of the test sample exhibit mobile, liquid character, depicting flow behavior of liquids.

The amplitude sweep was measured at varied shear stress range of 1.42Pa to 10.0Pa in order to determine the linear viscoelastic (LVE) region, keeping the frequency value constant at 0.1Hz. In the LVE region, the test sample shows reversible structural deformation. Other oscillation tests, conducted within the LVE region of the test sample, ensures that sample's structure remain undestroyed.

From the amplitude sweep plot, the linear viscoelastic regions of base fluid and CO_2 CGAs were determined. Following the amplitude sweep, the frequency sweep was conducted at one constant stress point (in the linear viscoelastic region) in order to determine the time-dependant shear behavior of the base fluid and CO_2 CGAs. From frequency sweep results, elastic and viscous moduli were plotted against varying frequencies (range: 0.01Hz to 2.0Hz). Plot of elastic modulus and viscous modulus against frequency provided the viscoelastic spectra of both base fluid and CO_2 CGAs.

3.4.3.2. Viscoelastic Behavior of Dispersions

Several experiments have been conducted (Marze et. al (2005), Cohen-Addad et. al (1998), Herzhaft et. al (2005)) and several simulations and mathematical models (Vincent-Bonnieu et. al (2006), Rioual et al (2005), Koehler et. al (1998), Höhler and Cohen-Addad (2005)) have been constructed to predict and determine the viscoelastic response of dispersed systems, such as foams and emulsions, at micron scale. Foams, concentrated emulsions, gels, micro-gels, pastes, and other such materials belong to a class of "soft glassy materials" that exhibit similar rheological behavior. Three main rheological properties observed in these materials are:

- They display non-Newtonian, shear thinning behavior (Herzhaft et. al (2005), Khan et. al (1988))

- When subjected to small stresses (within the LVE region of the disperse systems where the structure and arrangement of bubbles do not change permanently), they behave as viscoelastic solids showing high elasticity (Weaire and Hutzler (2001), Khan et. al (1988)). Generally, elastic modulus dominates over viscous modulus for these soft glassy materials.

- When the applied stress to the dispersed systems go beyond the yield stress (outside the LVE region of the dispersed system), they flow irreversibly like liquids and permanent droplet rearrangements take place (Saint-Jalmes and Durian (1999)). In this case, usually, viscous modulus exceeds elastic modulus and the droplets are sheared in the direction parallel to the flow direction, as depicted in figure 3-13.

Since CGAs are gas-in-liquid dispersions with higher liquid fraction in the encapsulation than wet foams, CGAs can be grouped with other gas-in-liquid or liquid-in-liquid dispersed systems. Thus, the viscoelastic behavior of CO_2 CGAs, determined from amplitude sweep and frequency sweep tests, could be correlated to the viscoelastic behavior of soft glassy materials.
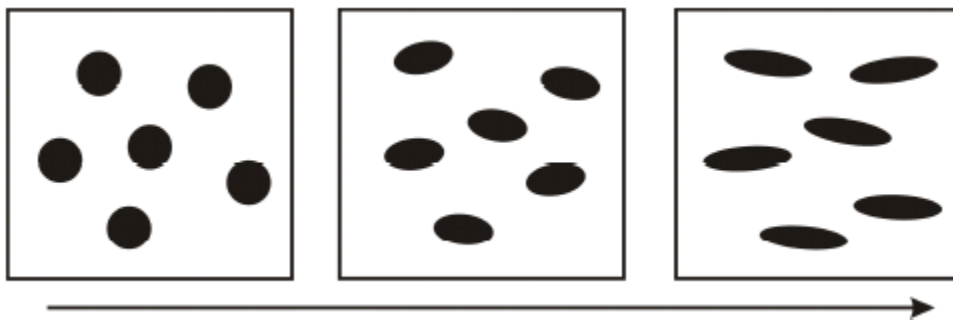

Figure 3-13: Deformation and the orientation of droplets (the arrow shows the direction of flow) (Derkach (2010))

Viscometry test results will provide the answer to the effectiveness of CO_2 CGAs, under simulated reservoirs conditions, in sweeping the reservoir without viscous fingering at varied shear rates. Oscillation test results, on the other hand, will determine the viscoelastic character of the CO_2 CGAs, and is an indication of the stability of the colloidal dispersions (in this case, CO_2 aphrons) in a gelled base fluid system under reservoir conditions.

4. Experimental Results & Discussions at Ambient Pressure and Temperature

As mentioned before, aqueous-based CO_2 CGAs have been generated from four pairs of polymer-surfactant, stated in Table 3-5. Figures 4-1 (a) to (d) show the CO_2 CGAs being generated from the four pairs of polymer-surfactant systems. A quick visual analysis of the four figures leads to a few conclusions:

- It seems CO_2 CGAs, generated with DDBS as surfactant, exist in higher numbers per unit area than CO_2 CGAs, generated from N85 surfactant.

- The average outer diameter of CO_2 CGAs that are generated from N85 surfactant looks smaller than that of CO_2 CGAs, generated from DDBS surfactant.
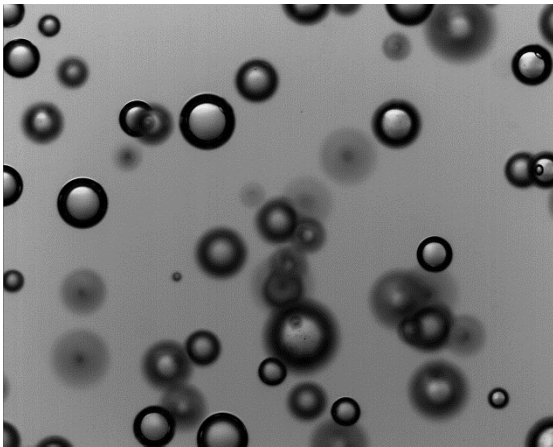

(a) XG/DDBS (An-An) CO_2 CGAs
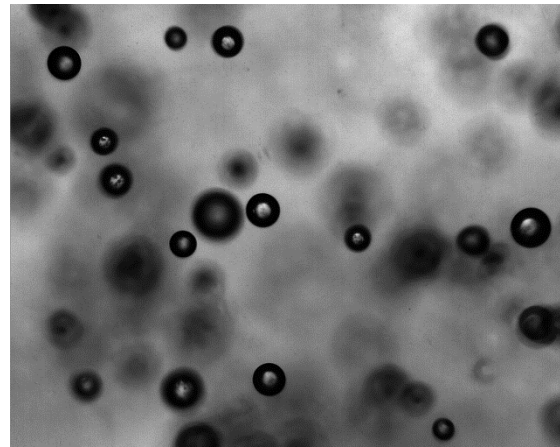
(b) XG/N85 (An-Non) CO_2 CGAs
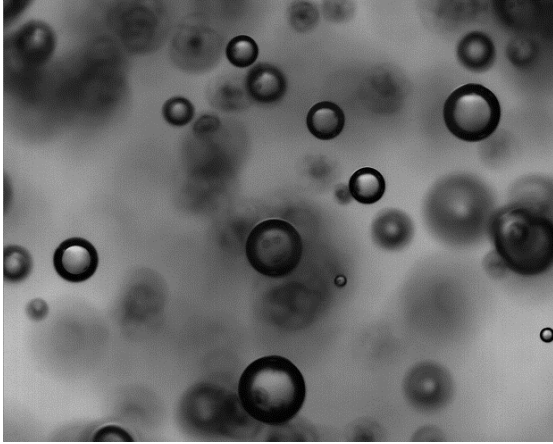
(c) HEC/DDBS (Non-An) CO_2 CGAs   (d) HEC/N85 (Non-Non) CO_2 CGAs
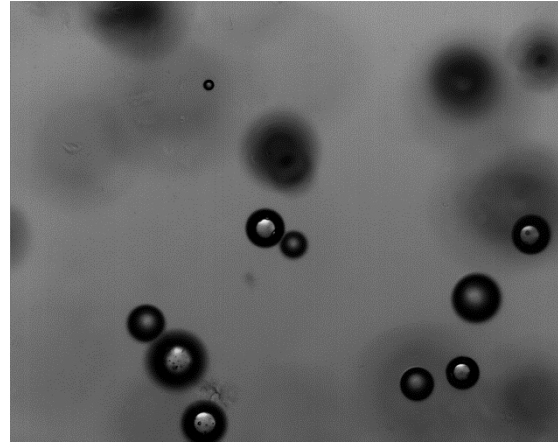
Figure 4-1: Microscopic pictures of CO_2 CGAs initially for four Polymer-Surfactant Base fluid solutions

Further comparison and analysis has been conducted based on rheological and stability characteristics of CO_2 CGAs to determine the optimum formulation of producing CO_2 CGAs.

4.1. Rheological Results

4.1.1. Low Shear Rate Viscosity (LSRV)

From figures 4-2 (a) & (b), it is seen that HEC imparts more viscosity to the base fluid solutions than XG does. This makes sense since the optimum concentration of HEC (5 lb/bbl), used in this study, was found to be much higher than that of XG (2.0 lb/bbl). Addition of N85 surfactant to the base fluid solution (prepared by either XG or HEC) generates more viscous base fluid than adding DDBS surfactant.

Figure 4-2 (b) shows that the highest increase in LSRV, on aphronizing, occurs in XG/DDBS (An-An) pair. Interestingly enough, the LSRV of CO_2 CGAs, from HEC/N85 (Non-Non) solution, decreases after

aphronizing the base fluid. The general trend of Figures 4-2 (a) & (b) show that the base fluid which has

the lowest LSRV (XG/DDBS pair in this case) yields the highest LSRV value after generating CO_2 CGAs
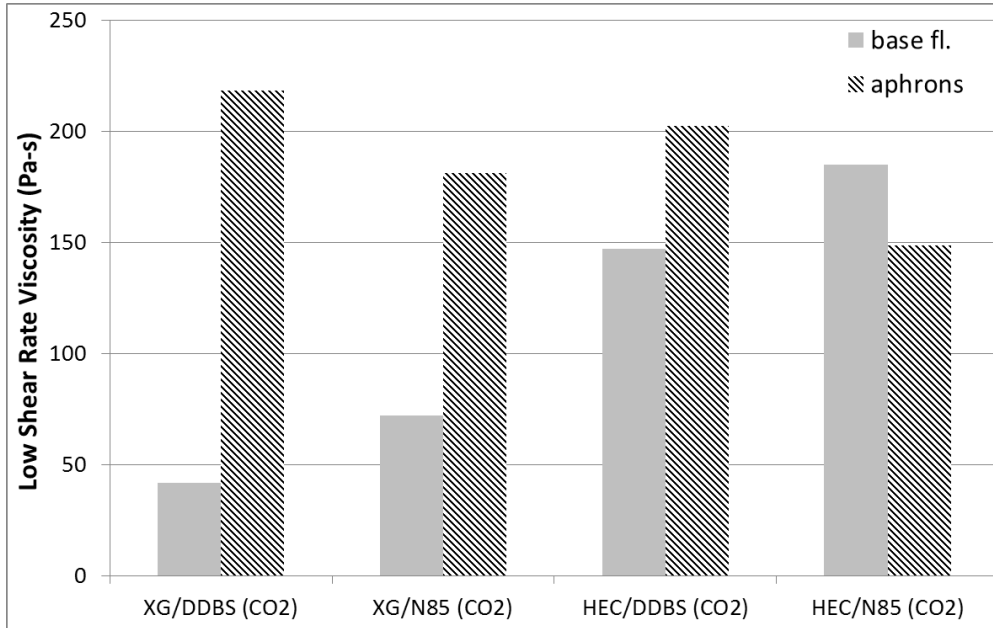
Figure 4-2 (a): Low Shear Rate Viscosity (LSRV) of four Base fluid solutions and their corresponding CO_2 CGAs
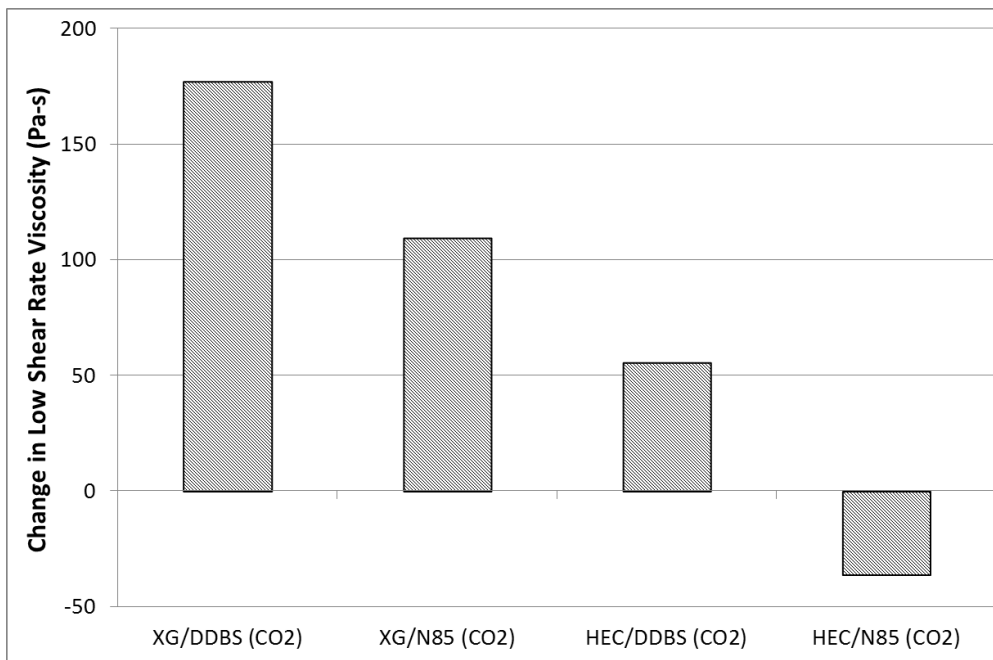

Figure 4-2 (b): Change in LSRV of CO_2 CGAs on aphronizing the Base fluid solutions

4.1.2. Viscosity Profile

Figures 4-3 (a) to (d) show the viscosity profile of four base fluid solutions and their corresponding CO_2 CGAs, generated from the four pairs of polymer-surfactant, at shear rates varying from $0.01s^{-1}$ to $100s^{-1}$. Both the base fluid and the corresponding CO_2 CGAs, from all four fluid pairs, show non-Newtonian, shear thinning rheological behavior.
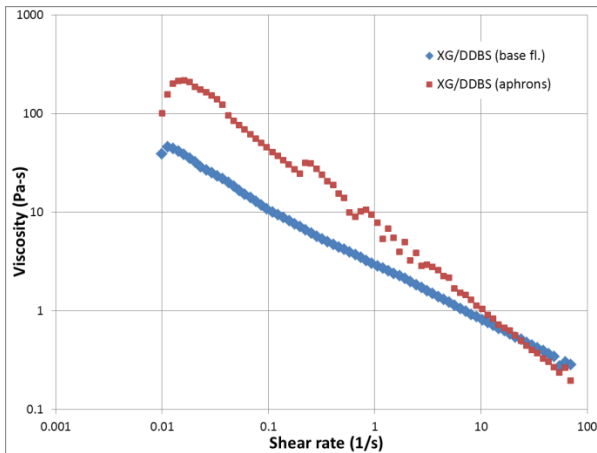

(a)
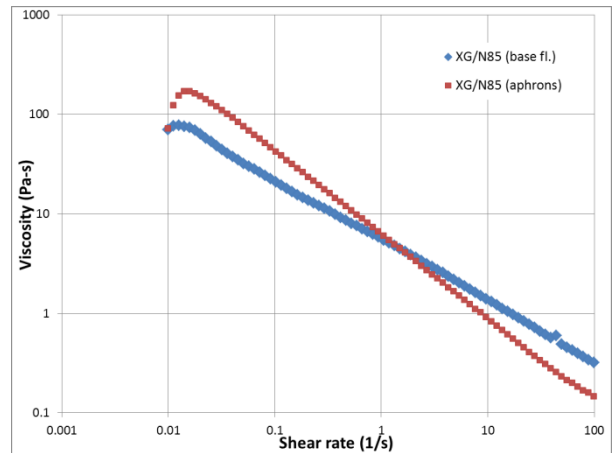
(b)
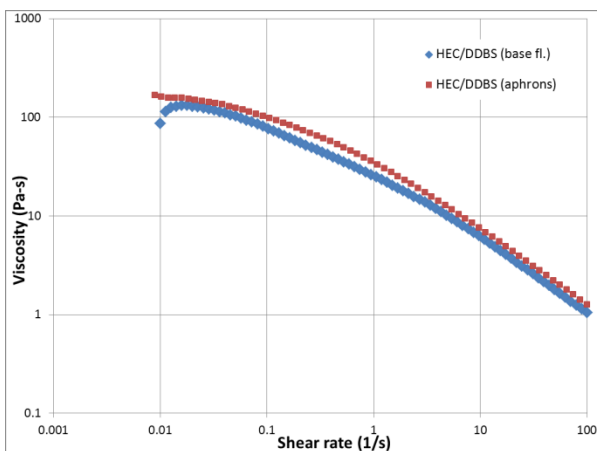
(c)
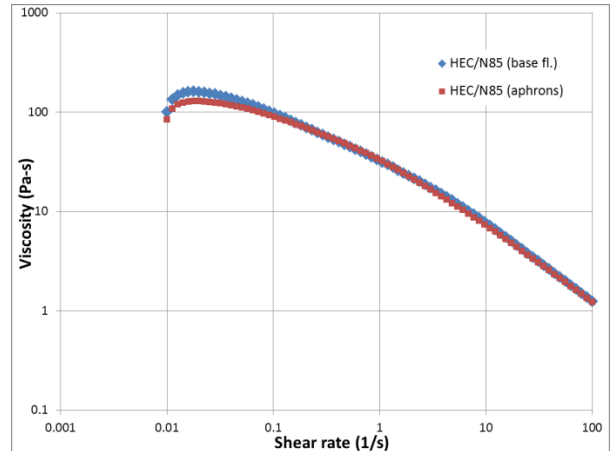
(d)

Figure 4-3: Viscosity Profile of CO_2 CGAs generated from (a) XG/DDBS (An-An); (b) XG/N85 (An-Non); (c) HEC/DDBS (Non-An); (d) HEC/N85 (Non-Non)

From figures 4-3 (c) & (d), it is seen that there is a negligible difference in viscosity at all shear rates between the base fluid and corresponding CO_2 CGAs, when HEC is used as the viscosifier. Addition of XG, on the other hand, increases the viscosity of the CO_2 CGAs considerably, after the base fluid is sheared at high speeds. Taking a close look at figures 4-3 (a) & (b) however, the viscosity of base fluid exceeds the viscosity of the corresponding CO_2 CGAs at shear rate values greater than $10s^{-1}$.

4.1.3. Discussion of Rheological Results

The increase in viscosity, at all shear rates, upon high shearing of base fluid is attributed to Laplace pressure (Ivan et al (2002)). At high shear rates, the energy transferred to base fluid into creating new interfacial area results in increasing the bulk viscosity of the resulting aphron solution. However, if the number of bubbles/microbubbles produced are small and are further apart, then the there is little change in any rheological properties (Chàvez-Montes et al (2007)). Therefore, no or very slight change in viscosity is indicative of low yield unstable aphrons. From the LSRV and the viscosity profile plots, it is established that high shearing of the base fluid solutions, containing XG, enables the transferred energy to efficiently generate high volumes of small microbubbles that increases the overall viscosity of the aphron solution upto the shear rate value of $10s^{-1}$.

Noticeable increase in viscosity is observed in CO_2 CGAs when XG is used. This difference in rheological behavior most likely arises due to variation in the molecular weight and the Mark-Houwink-Sakurada equation (MHS equation) 'a' parameter of XG and HEC. MHS equation provides an empirical relationship between the intrinsic viscosity of the polymer solution and the molecular weight of the polymer as follows:

$$[\eta] = K(MW)^a \ (Equation \ 4-1)$$

In equation 4-1 above, $[\eta]$ is the intrinsic viscosity, MW is the molecular weight of the polymer, and 'K' and 'a' are constants. Polymers having higher values of 'a' indicate more swelling of the polymer molecules in the solvent. For two polymers having same molecular weights, the polymer, with the higher 'a' parameter value, has higher molecular expansion in aqueous solution than the other polymer.

As per the Polymer Handbook, the 'a' parameter value of XG is 1.14 compared to that of HEC ('a' value = 0.7). This indicates better solubility and expansion of the XG molecules in the water.

Thus, rheological results dictate XG, combined with either of the surfactants, to be the better choice of polymer for contributing additional viscosity to the water lamellae in the aphron encapsulation and provide high yield stable CO_2 CGAs.

4.2.   Stability Results

4.2.1.   Time-Stability

The time stability plot, that records the change in outer diameter of CO_2 CGAs with time, is shown in Figure 4-4. The median diameter, indicated as d50, of CO_2 CGAs is plotted against time.
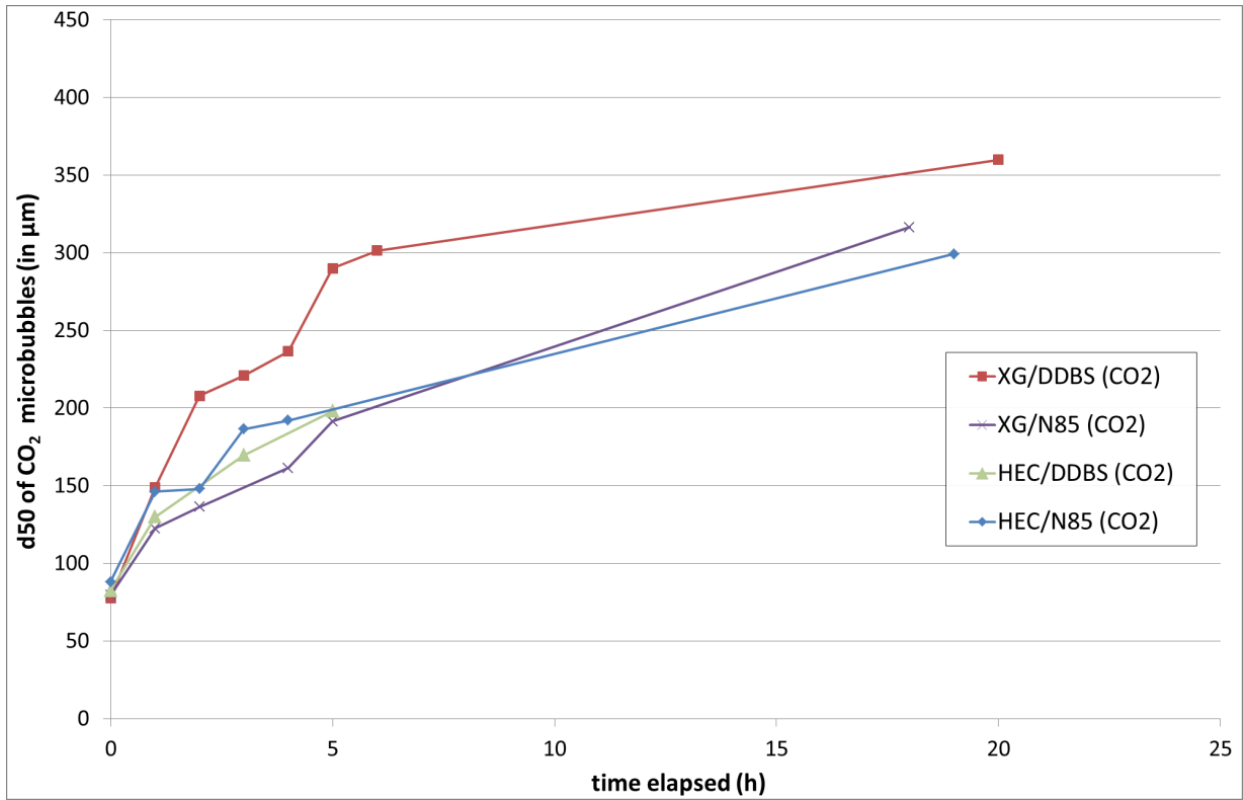
Figure 4-4: Time-Stability plot of CO_2 CGAs: Change of d50 Diameter over time

Initially, the d50 of CO_2 CGAs, of all four base fluid pairs, were close to each other in the range of 75µm to 90µm. With time, d50 of the CO_2 CGAs increased. Eventually, the rate of increase in d50 was different for CO_2 CGAs, generated from the different polymer-surfactant pair. In general, rapid growth of CO_2 CGAs was observed in the first five to six hours, followed by slower growth rate after until the end of the experiment. CO_2 CGAs, from XG/N85, showed the lowest rate of change in d50, whereas, CO_2 CGAs, from XG/DDBS, showed highest rate of increase in d50 value.

### 4.2.2. Frequency-Distribution

Figures 4-5 (a) to (c) below show the frequency distribution of CO_2 CGAs, for all four fluid pairs, at three different time intervals of initial time, after 1 hour, and after 5 hours, respectively.
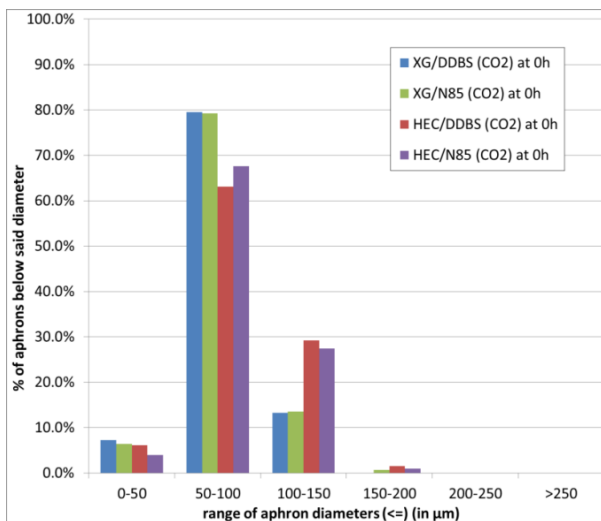
(a)
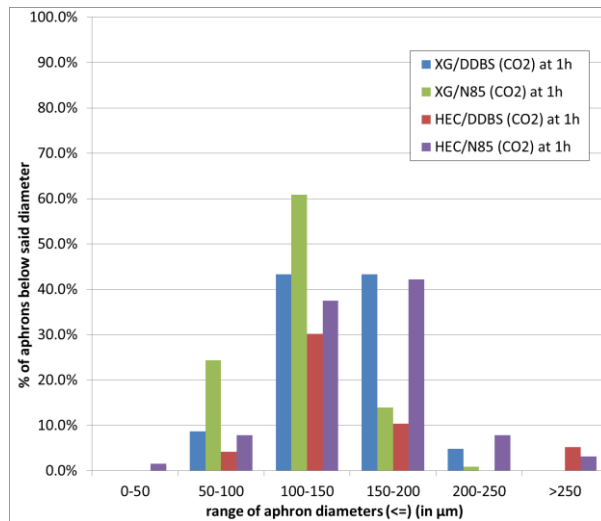
(b)
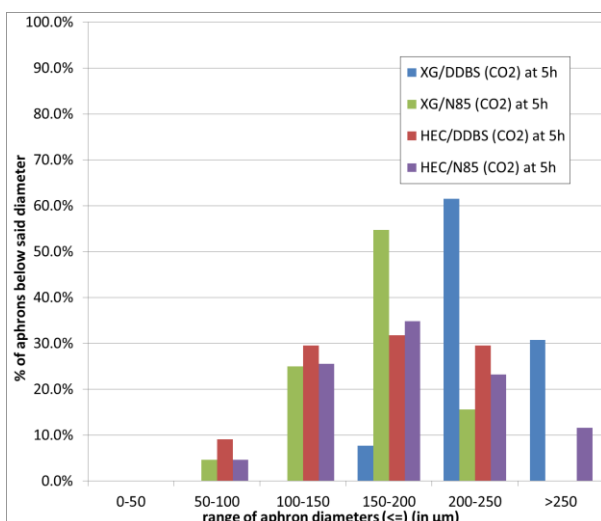
(c)

Figure 4-5: Frequency-Time plot of CO_2 CGAs from all four Polymer-Surfactant solutions at (a) initially; (b) after 1 hour; (c) after 5 hours

Initially, from figure 4-5 (a), the outer diameters of CO_2 CGAs, for all four pairs, fall mostly in between 50-100µm range. The highest yield of aphrons, that fall in the 50-100µm range, are from the pairs of XG/DDBS and XG/N85. It is seen from figure 4-5 (b) that after 1 hour, XG/N85 pair provides the highest yield of CO_2 aphrons that fall in the ranges of 50-100µm and 100-150µm. Further on, after 5 hours (figure 4-5 (c)), XG/N85 pair, once again, provides the highest yield of CO_2 aphrons in the ranges of 100-

150µm and 150-200µm. There are no CO_2 CGAs, from XG/N85 pair, in the >250µm range at the 5 hour interval.

4.2.3. Discussion of Stability Results

From stability point of view, XG/N85 pair solution provided the most stable CO_2 CGAs. From the previous section of the discussion on rheological results of CO_2 CGAs, it was found that XG polymer is the better viscosifying agent for stable aphron encapsulation. Another reason for the enhanced stability of CO_2 CGAs (from XG/N85 pair) might be due to the non-ionic surfactant, N85 that contains nonylphenol tails (that are strongly CO_2-phillic) and ethylene oxides (that is mildly CO_2-phillic) (Adkins et. al (2010)). As per Xing et al (2010), it was found that the most stable CO_2-in-brine emulsions were generated using surfactant class belonging to branched or linear alkylphenol ethoxylates.

4.3. Summary - Best Polymer-Surfactant Pair for Stable CO_2 CGAs

Table 4-1 below summarizes the best polymer-surfactant pair that provides the desired characteristics to CO_2 CGAs.

Table 4-1: Best Polymer-Surfactant pair providing most stable CO_2 CGAs in terms of the characteristics stated below

Characteristics		Best pair for CO_2 CGAs
Rheology	LSRV	XG/DDBS (An-An)
	Viscosity profile	XG/DDBS (An-An)
Stability	Time stability	XG/N85 (An-Non)
	Frequency-distribution	XG/N85 (An-Non)

5. Experimental Results - Comparison to Corresponding Air Aphrons

Keeping all the experimental procedures and other factors such as, pressure, temperature, concentration of chemicals used, constant, air CGAs were produced using the same four solutions of polymer and surfactants that were used for generating CO_2 CGAs. Furthermore, air CGAs, from the best polymer-surfactant pair, were compared to CO_2 CGAs, from the best polymer-surfactant pair in terms of rheology and stability.

5.1. Rheology Comparison

5.1.1. LSRV Comparison

Figure 5-1 (a) shows the LSRV of base fluid, CO_2 CGAs and air CGAs; figure 5-1 (b) shows the change in LSRV for CO_2 CGAs and air CGAs, all being produced from the same four polymer-surfactant pairs.
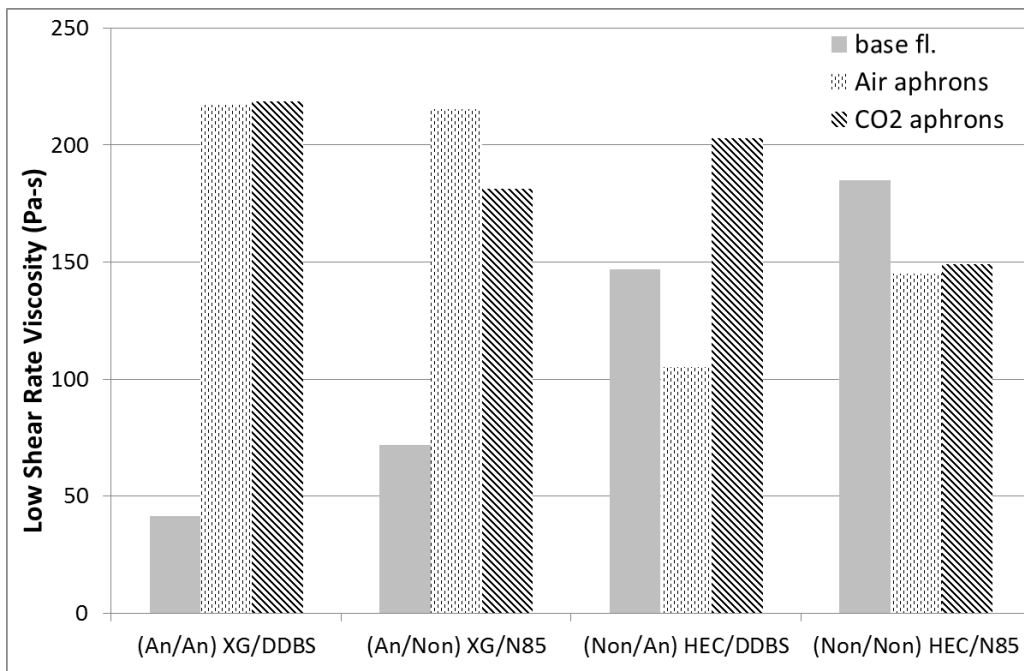

Figure 5-1 (a): LSRV of four Base fluid solutions and their corresponding CO_2 CGAs and Air CGAs
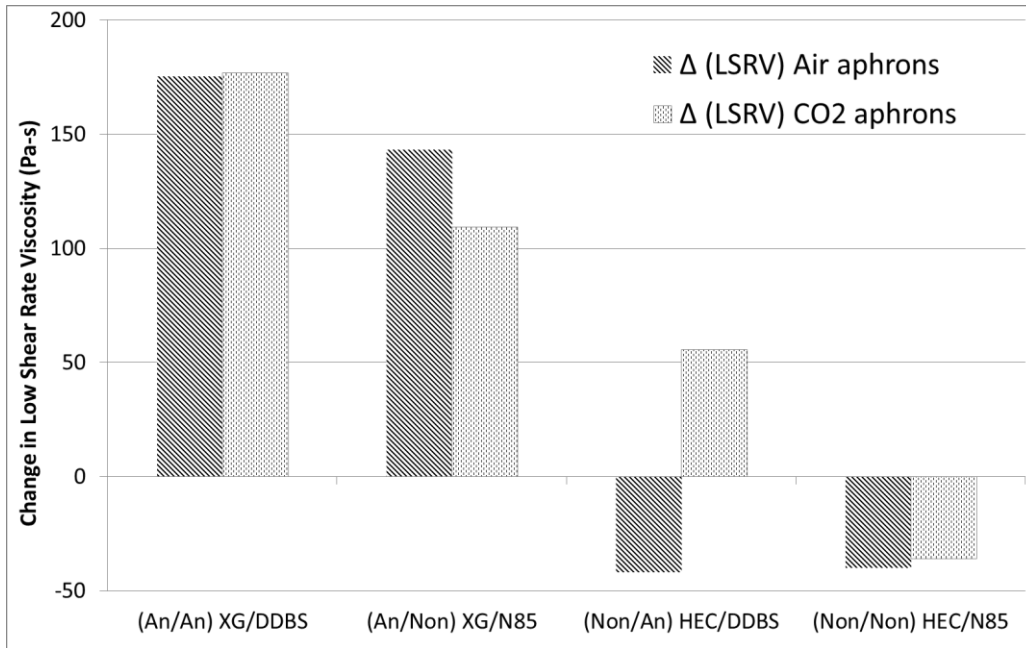
Figure 5-1 (b): Change in LSRV for CO_2 CGAs and Air CGAs, generated from four Polymer-Surfactant pairs

From figure 5-1 (b), it is seen that in case of both CO_2 CGAs and air CGAs, using HEC as polymer, after aphronizing, retards the LSRV of CGAs. On the other hand, with XG, there was significant net increase in LSRV for both CO_2 and air CGAs. For XG/DDBS pair, the increase in LSRV is about the same for both CO_2 and air CGAs. With XG/N85 pair, the increase in LSRV is higher for air aphrons than for CO_2 aphrons.

5.1.2. Viscosity Profile Comparison

Figures 5-2 (a) to (d) display the viscosity profile of the base fluid, CO_2 CGAs, and air CGAs.
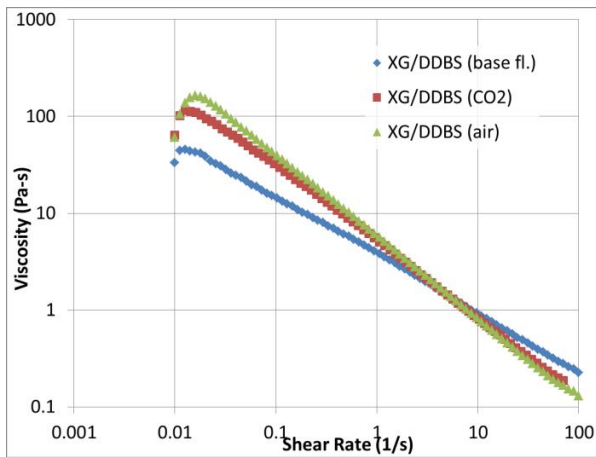
(a)
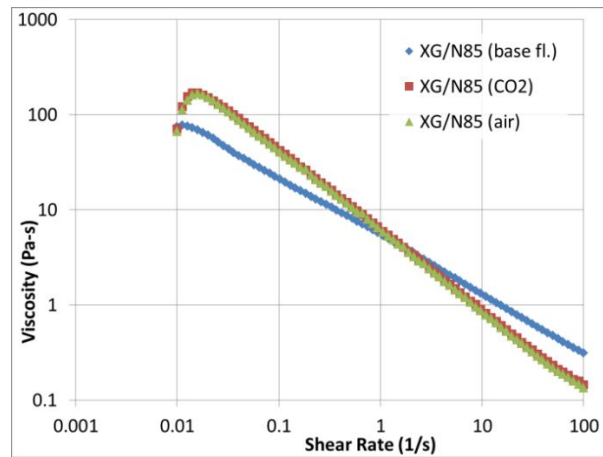
(b)
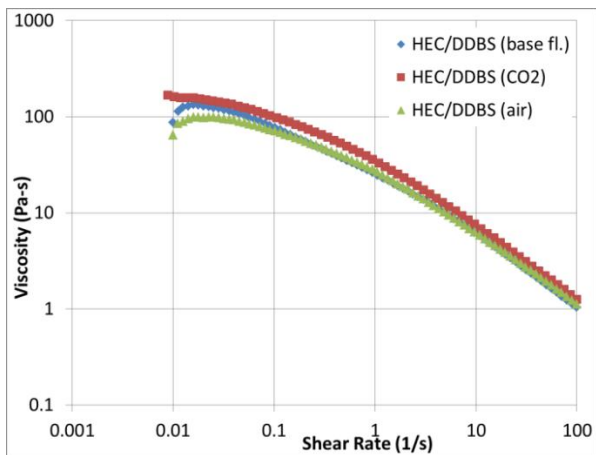
(c)
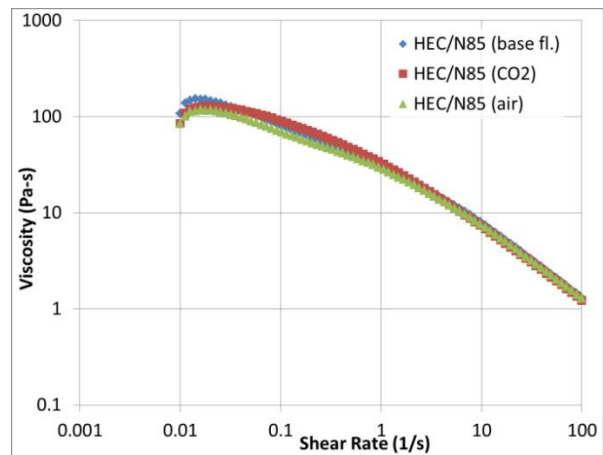
(d)

Figure 5-2: Viscosity profile of Base fluid (♦), CO_2 CGAs (■), and Air CGAs (▲) from (a) XG/DDBS (An-An) solution, (b) XG/N85 (An-Non) solution, (c) HEC/DDBS (Non-An) solution, (d) HEC/N85 (Non-Non) solution

As seen before, in figures 5-2 (c) & (d), HEC does not provide any additional viscosity to either air CGAs or CO_2 CGAs throughout the entire range of shear rate values. In figures 5-2 (a) & (b), upto the shear rate value of $5s^{-1}$, on adding XG, the viscosity of both air and CO_2 CGAs is higher than that of the base fluid. At shear rates values greater than $5s^{-1}$, the viscosity of both air and CO_2 CGAs drops below that of base fluid.

Regardless of the composition of the trapped gas, rheological behavior of both air and CO_2 CGAs is identical for all four fluid pairs.

5.2. Stability Comparison

5.2.1. Time-Stability Comparison

Figures 5-3 (a) to (d) show the time-stability plot comparison of air CGAs and CO_2 CGAs, for all four pairs of polymer-surfactant.
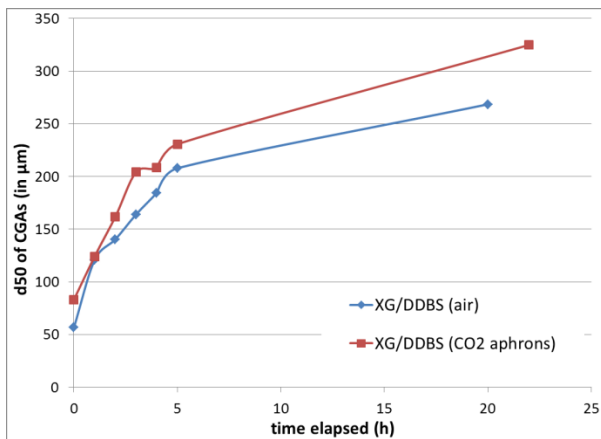

(a)
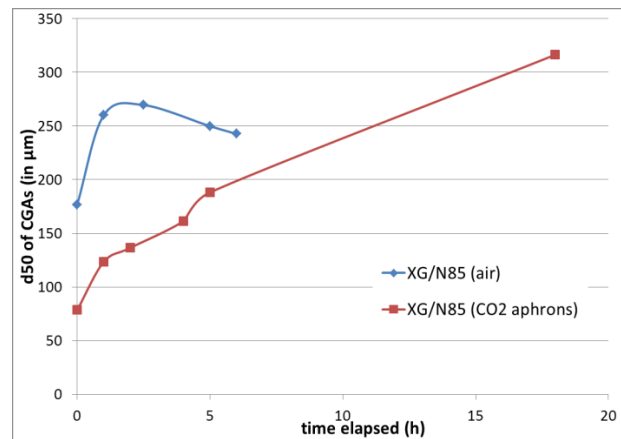
(b)
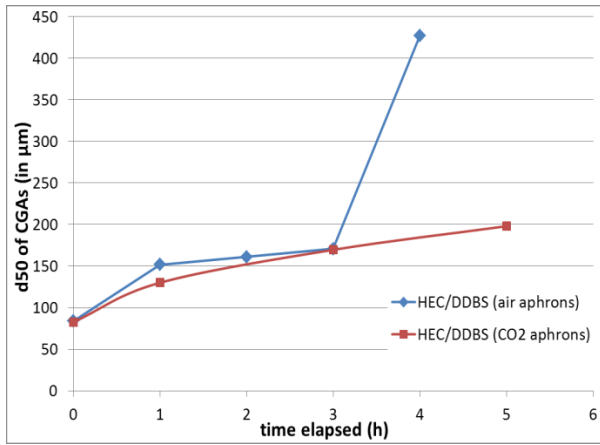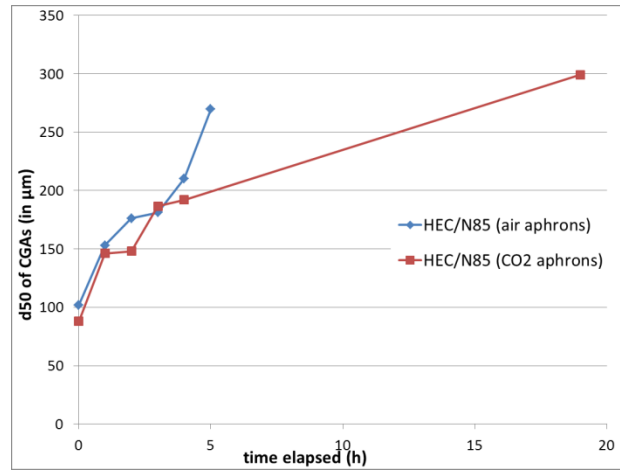
(c)   (d)

Figure 5-3: Time-Stability comparison plot of CO_2 CGAs and Air CGAs for (a) XG/DDBS (An-An) pair; (b) XG/N85 (An-Non) pair; (c) HEC/DDBS (Non-An) pair; (d) HEC/N85 (Non-Non) pair

Figure 5-3 (a) show that XG/DDBS pair provides stable air and CO_2 CGAs, with air CGAs having smaller d50, at all times, than CO_2 CGAs. Growcock et. al (2005) observed some shrinkage in air CGAs and the difficulty in detecting dissolved oxygen in the aphron solution due to the cellulose material being used for generating the air CGAs. He reported that the cellulose reacted with dissolved oxygen rapidly, leaving the core of the air CGAs filled mostly with inert nitrogen gas, and due to this rapid reaction, they observed that the air CGAs shrink slightly. This phenomenon of shrinkage in air CGAs could be the reason for lower d50 (than the CO_2 CGAs counterpart) at all times.

From figure 5-3 (b), the effect of XG/N85 pair is very different on both CO_2 and air CGAs. Recalling from figure 4-4, XG/N85 pair turned out to be the best pair in providing most stable CO_2 CGAs. Figure 5-3 (b) shows highly unstable air CGAs, generated from XG/N85 pair, that does not last past 5 hours. The peculiar shape of the stability plot of air CGAs, from XG/N85, indicates that the remaining big bubbles, after around 2 to 2.5 hours, start to shrink. As per figure 5-3 (d), the air CGAs, from HEC/N85, are highly

unstable as well, compared to CO_2 CGAs generated from the same HEC/N85, just like in case of XG/N85. At around the fourth hour, the d50 of air CGAs is seen to rise rapidly.

While the presence of CO_2-phillic nonlyphenol tail units enable N85 to encapsulate CO_2 gas effectively for longer duration, it has been stated in the literature (Scott and Jones (2000); Wang et al (2011)) that nonylphenol ethoxylates go under aerobic degradation, rendering the surfactant useless. Thus, both pairs, XG/N85 and HEC/N85, did not generate stable air CGAs.

In figure 5-3 (c), with HEC/DDBS, both air and CO_2 CGAs did not last past 5 hours. The stability of air aphrons and CO_2 aphrons are around the same until 3 hours, and then beyond that, the d50 of air CGAs increases drastically making them highly unstable. The reason for this instability is not clear.

5.2.2. Frequency-Distribution Comparison

XG/DDBS (An-An) solution: Figures 5-4 (a) to (c) provide the frequency distribution plots of both CO_2 and air CGAs at three different time intervals for XG/DDBS pair. Initially, as per figure 5-4 (a), for XG/DDBS pair, diameter of air aphrons fall mostly in the ranges of 0-50μm and 50-100μm range, as opposed to diameter of CO_2 aphrons which fall mostly in the range of 50-100μm. Looking at 1 hour and 5 hour intervals, the air aphrons have higher yield in the 100-150μm and 150-200μm categories than the CO_2 aphrons, respectively, thus indicating lower d50 for air CGAs than CO_2 CGAs.

XG/N85 (An-Non) solution: Figures 5-5 (a) to (c) provide the frequency distribution plots of both CO_2 and air CGAs at three different time intervals for XG/N85 pair. It is seen in these figures that the yield of CO_2 CGAs of smaller median diameter (in the ranges of 0-50μm and 50-100μm) is consistently higher than that of air CGAs of similar range of smaller median diameter. The position of the maximum point in the distribution plot of the air aphrons, at all the time intervals, is more towards right than that of CO_2 aphrons which suggests larger average size of the air aphrons at all times. This is supported by the time-

stability plot comparison (figure 5-3 (b)) as well. The right hand side skewed peak of air CGAs is attributed to aerobic biodegradation of N85 surfactant, as explained in the previous section (section 5.2.1).

HEC/DDBS (Non-An) solution: Figures 5-6 (a) to (c) provide the frequency distribution plots of both CO_2 and air CGAs at three different time intervals for HEC/DDBS pair. In figure 5-6 (a), for HEC/DDBS pair, initially, air aphrons have higher yield in the 50-100μm range than CO_2 aphrons. Around 5 hour interval, the position of the maximum point of distribution plot of air CGAs shifts to far right compared to the wide distribution of CO_2 CGAs spread over three d50 intervals of 100-150μm, 150-200μm and 200-250μm, as indicated by the rapid rise in d50 of air CGAs shown in the time stability comparison plot (figure 5-3 (c)).

HEC/N85 (Non-Non) solution: Figures 5-7 (a) to (c) provide the frequency distribution plots of both CO_2 and air CGAs at three different time intervals for HEC/N85 pair. Initially, as per figure 5-7 (a), the yield of CO_2 aphrons, from HEC/N85 pair, is higher than that of air aphrons; more CO_2 aphrons fall in the 50-100μm range than air aphrons. At 1 hour interval, the yields of both aphrons in all categories are around the same. After 5 hours (figure 5-7 (c)), the maximum point in the distribution plot is skewed to the right in case of air CGAs, whereas the maximum point for CO_2 CGAs is widely distributed over the three size intervals of 100-150μm, 150-200μm, and 200-250μm.
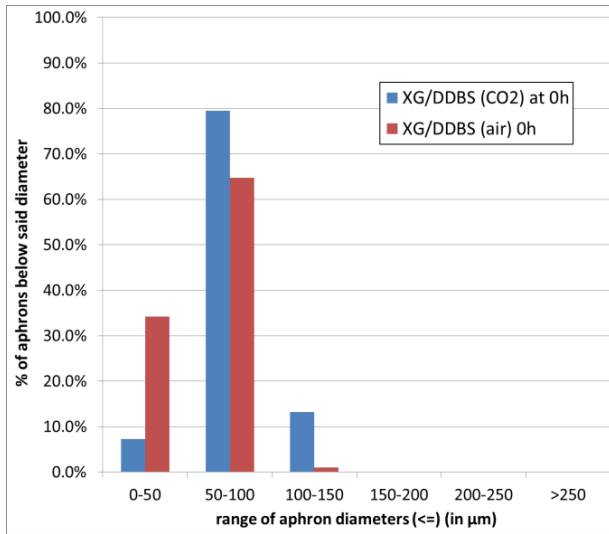
(a)
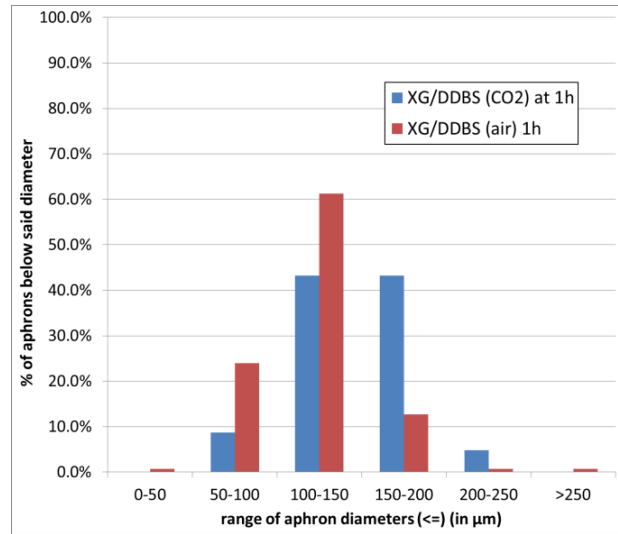
(b)
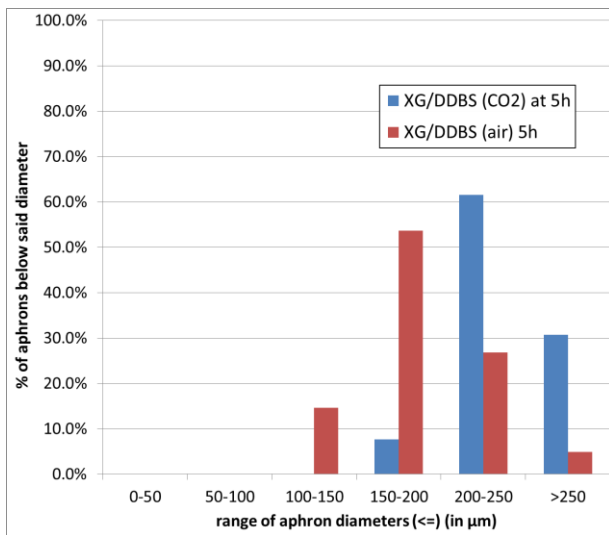
(c)

Figure 5-4: Frequency distribution comparison plot of CO_2 CGAs and Air CGAs, for XG/DDBS (An-An) pair at time intervals of (a) initially; (b) after 1 hour; (c) after 5 hours
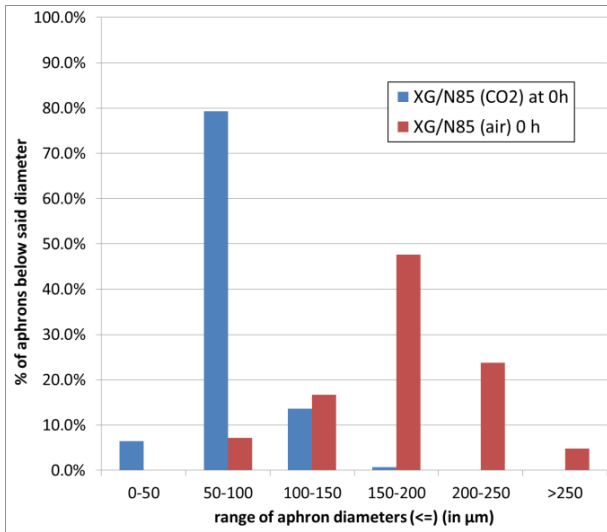
(a)
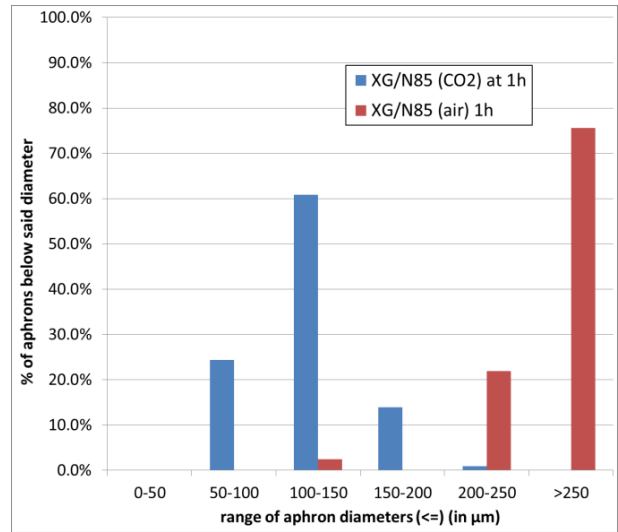
(b)
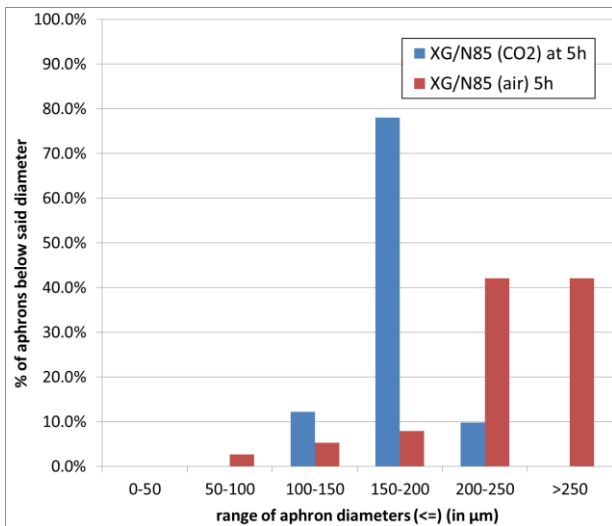
(c)

Figure 5-5: Frequency distribution comparison plot of CO_2 CGAs and Air CGAs, for XG/N85 (An-Non) pair at time intervals of (a) initially; (b) after 1 hour; (c) after 5 hours
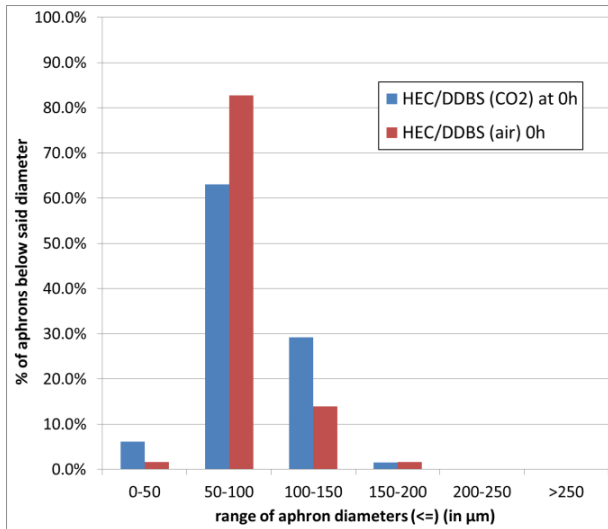
(a)
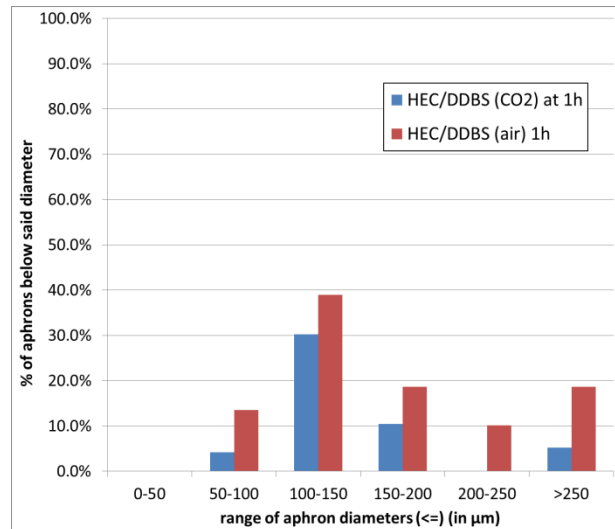
(b)
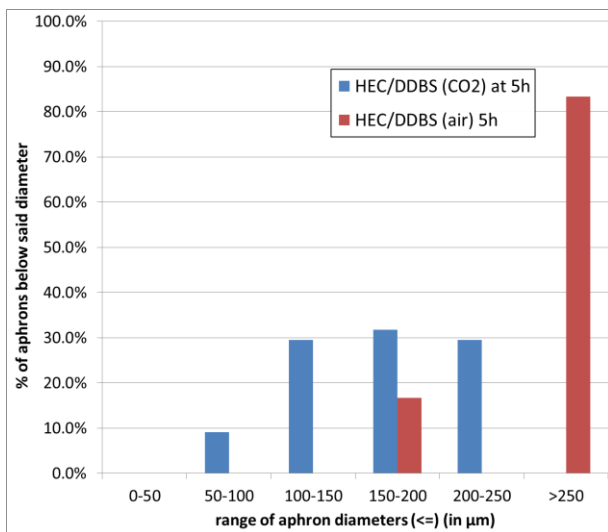
(c)

Figure 5-6: Frequency distribution comparison plot of CO_2 CGAs and Air CGAs, for HEC/DDBS (Non-An) pair at time intervals of (a) initially; (b) after 1 hour; (c) after 5 hours
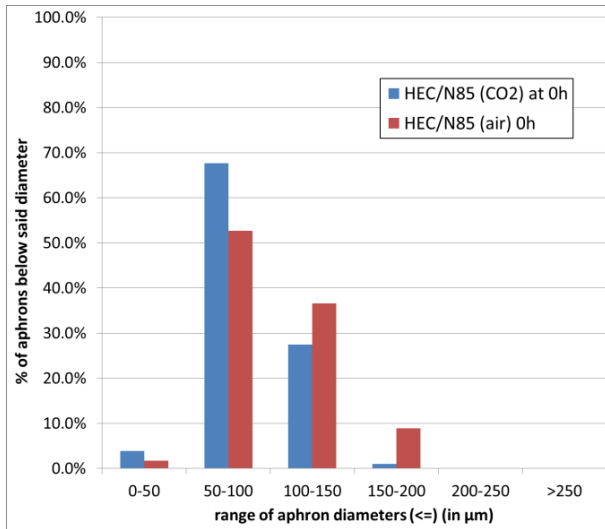
(a)
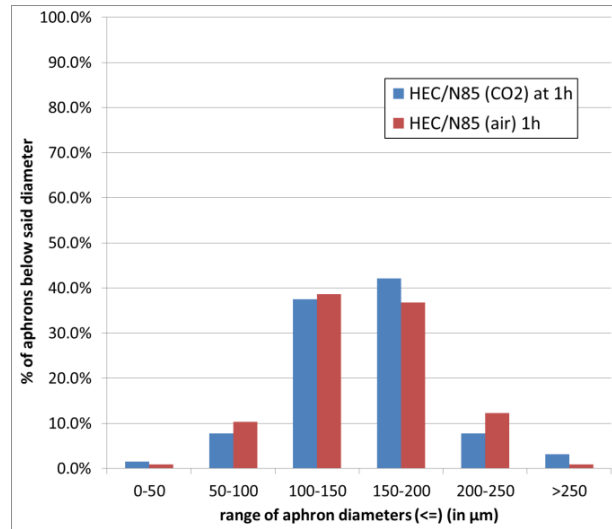
(b)
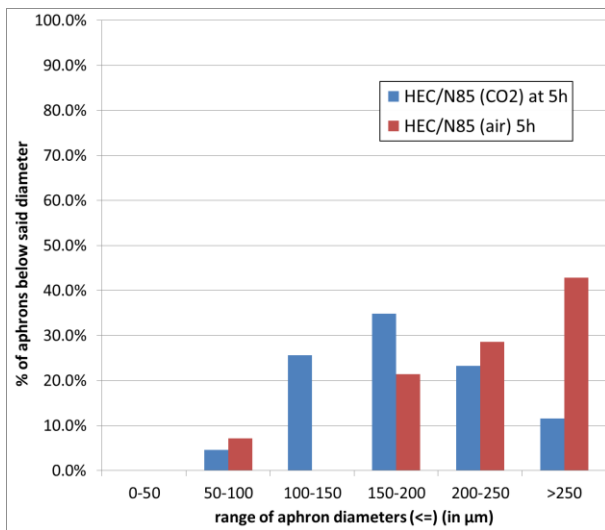
(c)

Figure 5-7: Frequency distribution comparison plot of CO_2 CGAs and Air CGAs, for HEC/N85 (Non-Non) pair at time intervals of (a) initially; (b) after 1 hour; (c) after 5 hours

5.2.3. CGA Picture Comparison:

Figures 5-8 to 5-11 below display microscopic images of both CO_2 CGAs and air CGAs, generated from four pairs of polymer-surfactant base fluid solutions, at three different time intervals of initial time, after 1 hour, and after 5 hours.

XG/DDBS (An-An) solution: Initially, the number of CGAs per unit area, for both CO_2 and air, is abundant; as time passes by, that number decreases. On average, the diameter of air CGAs, at any time, is smaller than the diameter of CO_2 CGAs. The time stability plot (figure 5-3 (a)) and the frequency-distribution comparison plot (figure 5-4) support this observation.

XG/N85 (An-Non) solution: On the right hand side of figure 5-9, it is seen that initially the bulk of CO_2 CGAs is much higher than that of air CGAs. With time, though the number of CGAs per unit area, for both CO_2 and air, goes down, the average diameter of air CGAs remain higher than that of CO_2 CGAs. This difference in diameter, for both air CGAs and CO_2 CGAs, is seen in both the time stability plot (figure 5-3 (b)) and the frequency-distribution comparison plot (figure 5-5).

HEC/DDBS (Non-An) solution: Figure 5-10 shows that initially both the population density and the average diameter of CGAs (CO_2 and air) are about the same. After 5 hours, it is seen that the average diameter of air CGAs is much higher than that of CO_2 CGAs, and the bulk of air CGAs is also seen to be lower than that of CO_2 CGAs. This observation is illustrated in the time stability plot (figure 5-3 (c)) and the frequency-distribution comparison plot (figure 5-6).

HEC/N85 (Non-Non) solution: In figure 5-11, the average diameter of air CGAs look similar to the average diameter of CO_2 CGAs. There seems to be not much difference in the density and the average diameter for air CGAs and CO_2 CGAs with time. The time stability plot (figure 5-3 (d)) and the frequency-distribution comparison plot (figure 5-7), on the other hand, display the CO_2 CGAs being more stable than the air CGAs.
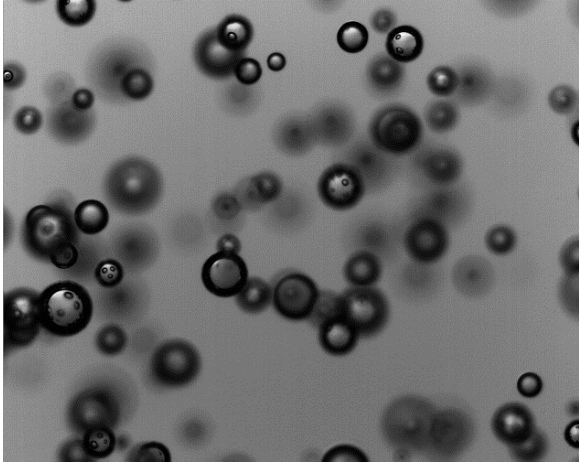
Picture of CO₂ aphron at 0h
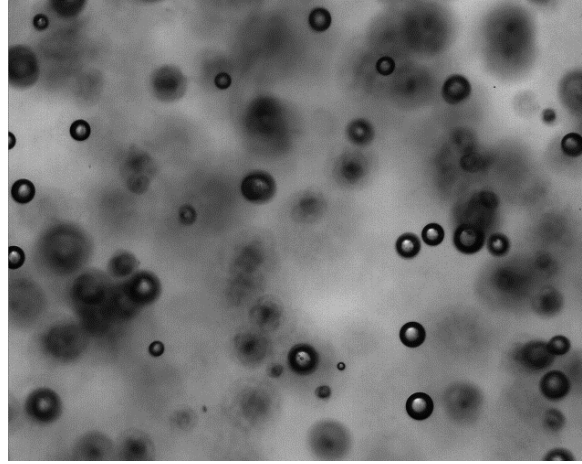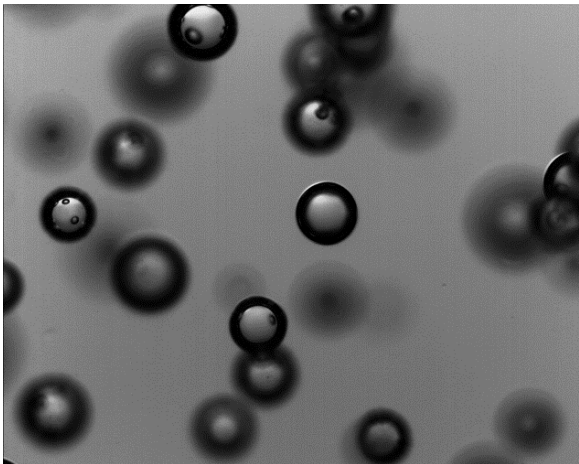
Picture of air aphron at 0h

Picture of CO₂ aphron at 1h
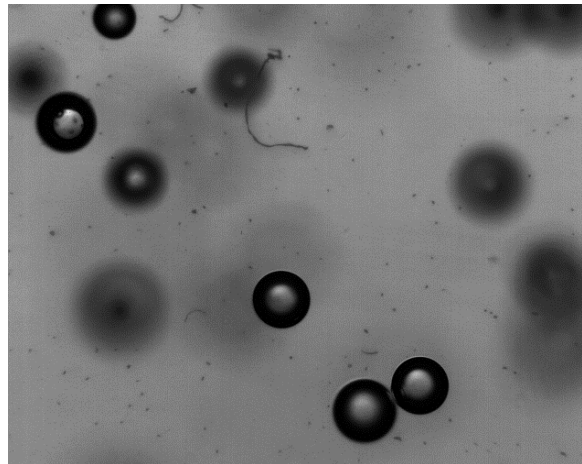
Picture of air aphron at 1h
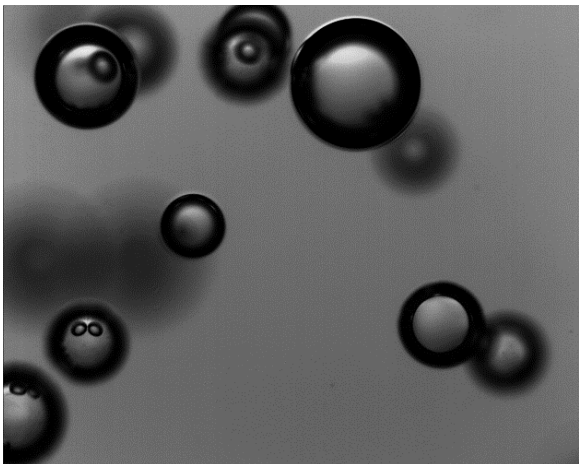
Picture of CO₂ aphron at 5h
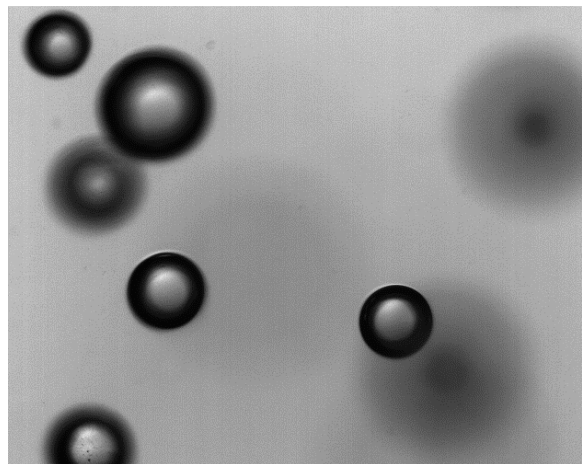
Picture of air aphron at 5h

Figure 5-8: CGA picture comparison initially, after 1 hour, and after 5 hours, of CO_2 and Air, for XG/DDBS (An-An) pair
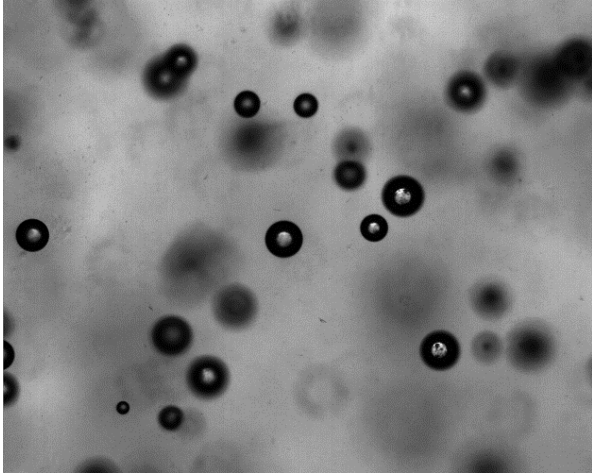
Picture of CO₂ aphron at 0h
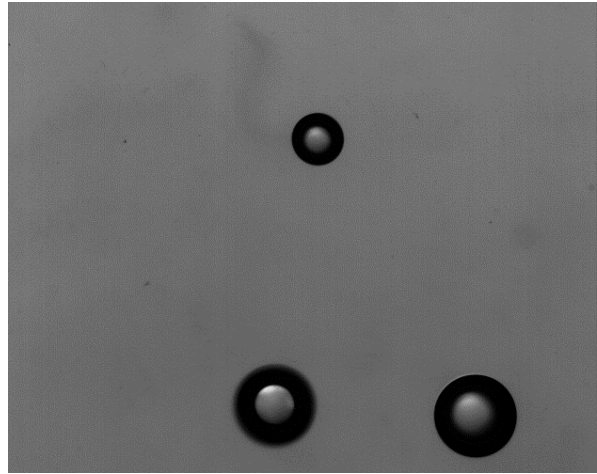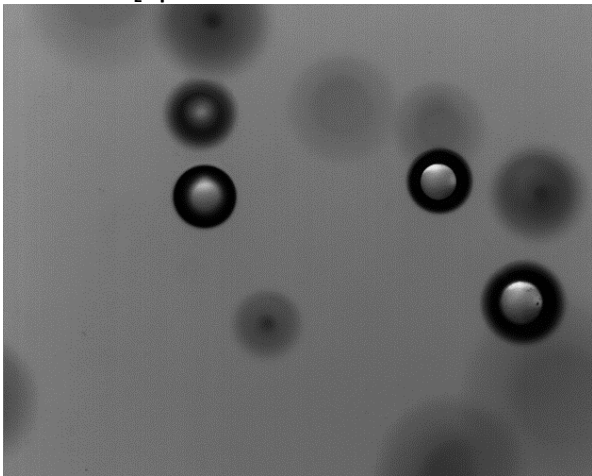
Picture of air aphron at 0h

Picture of CO₂ aphron at 1h
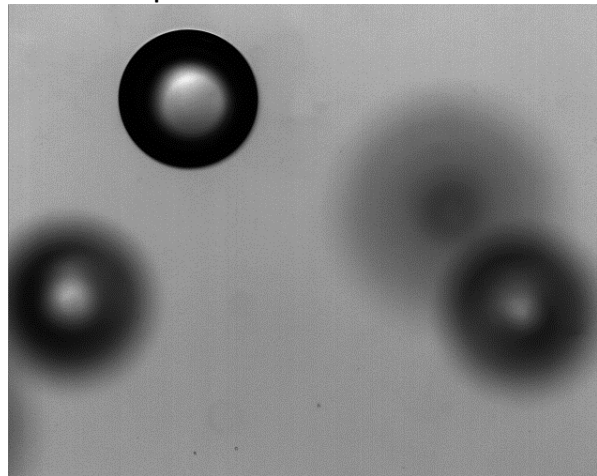
Picture of air aphron at 1h
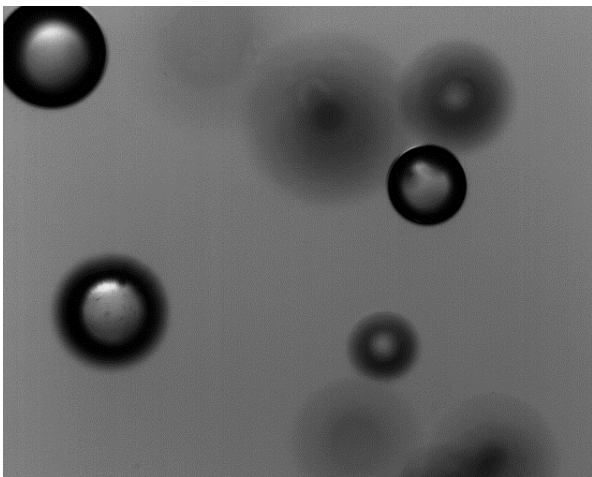
Picture of CO₂ aphron at 5h
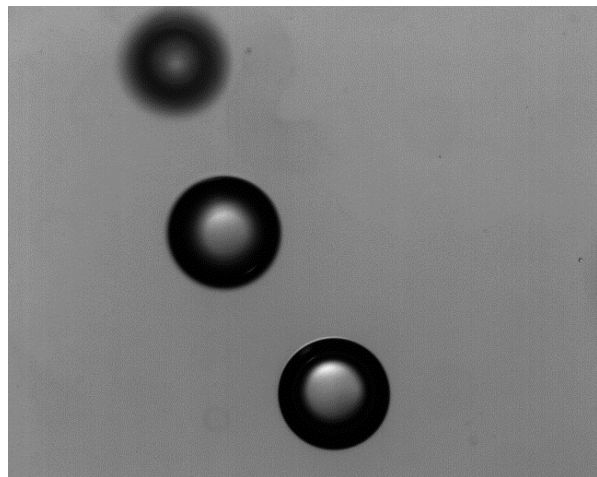
Picture of air aphron at 5h

Figure 5-9: CGA picture comparison initially, after 1 hour, and after 5 hours, of CO_2 and Air, for XG/N85 (An-Non) pair
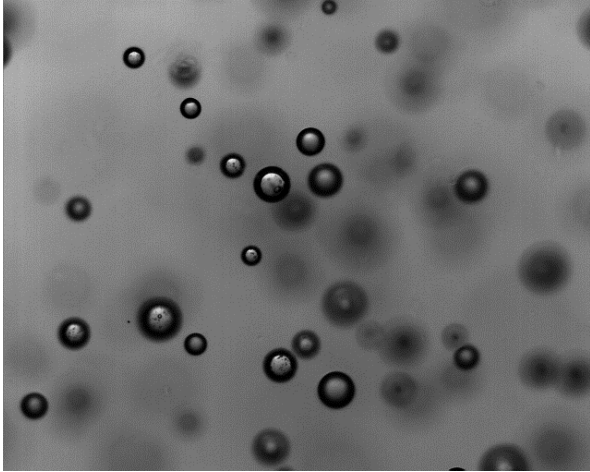
Picture of CO$_2$ aphron at 0h
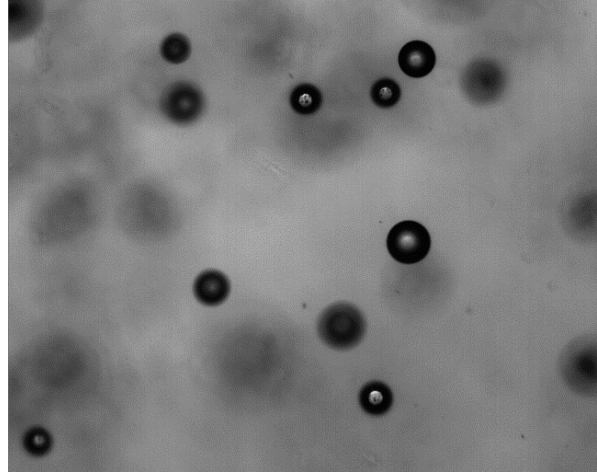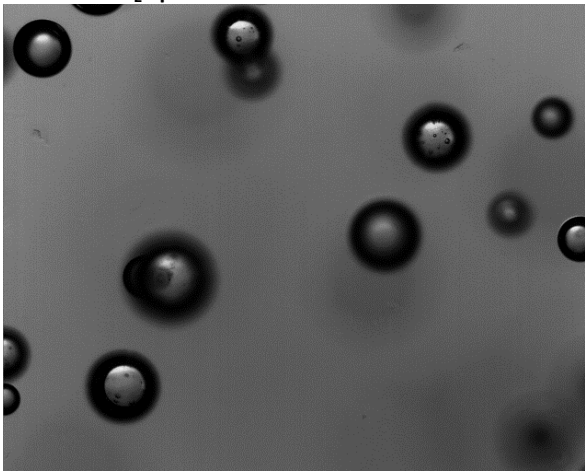
Picture of air aphron at 0h

Picture of CO$_2$ aphron at 1h
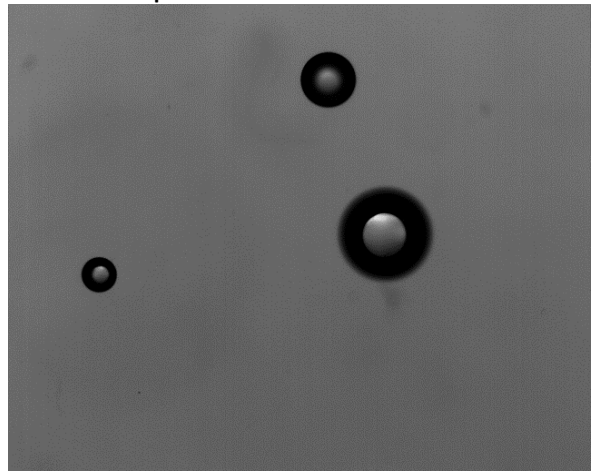
Picture of air aphron at 1h
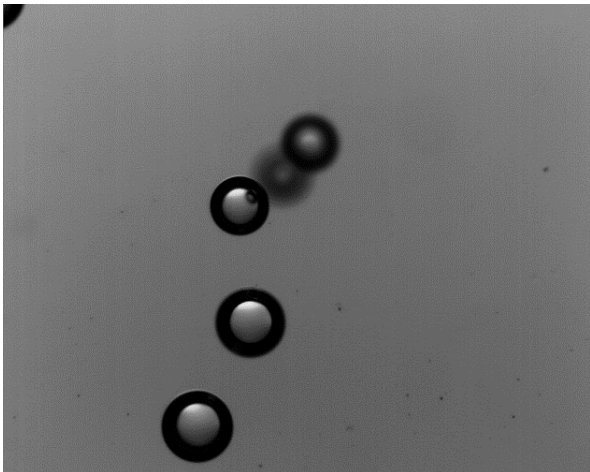
Picture of CO$_2$ aphron at 5h
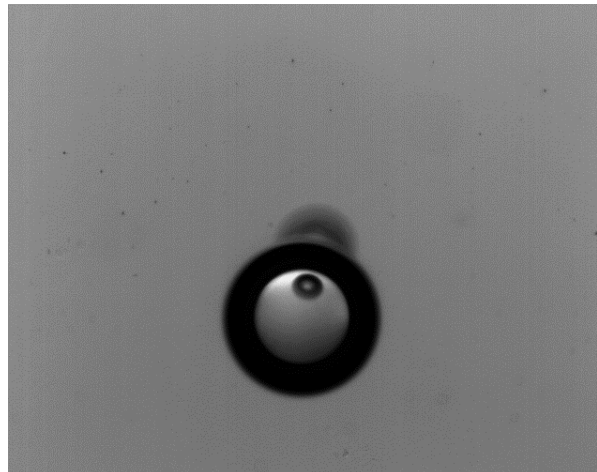
Picture of air aphron at 5h

Figure 5-10: CGA picture comparison initially, after 1 hour, and after 5 hours, of CO$_2$ and Air, for HEC/DDBS (Non-An) pair
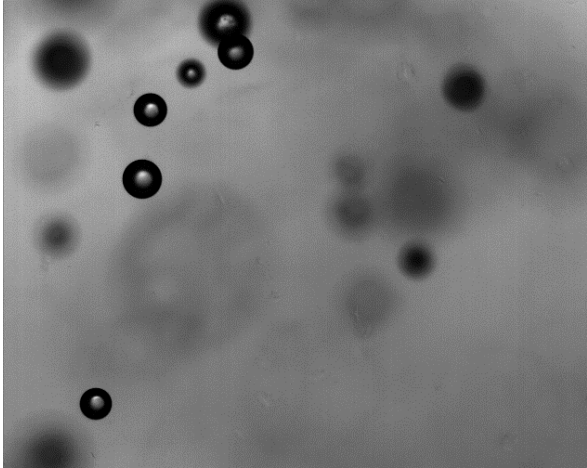
Picture of CO₂ aphron at 0h
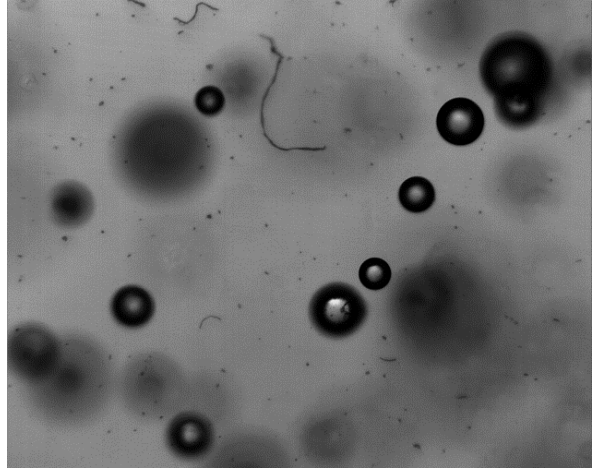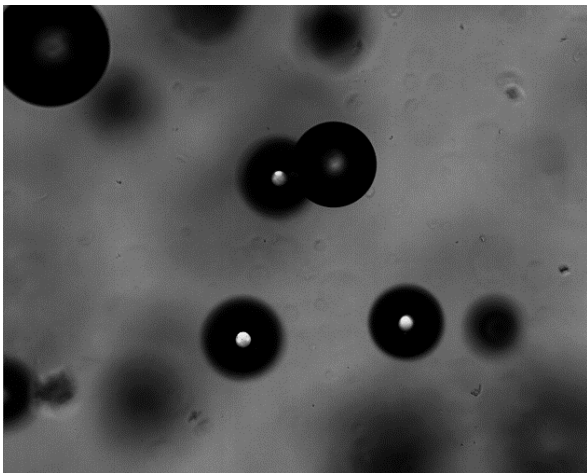

Picture of air aphron at 0h

**Picture of CO₂ aphron at 1h**
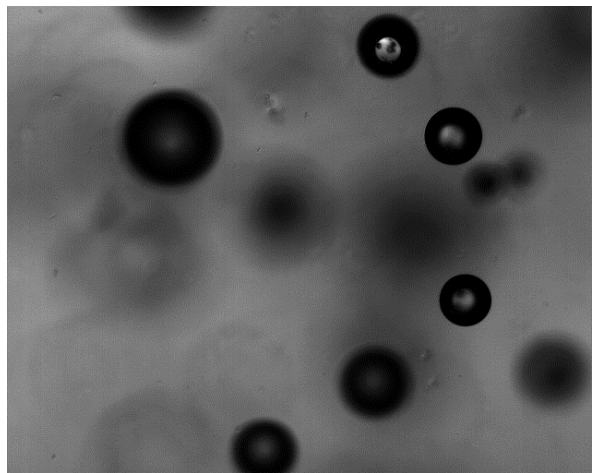
**Picture of air aphron at 1h**
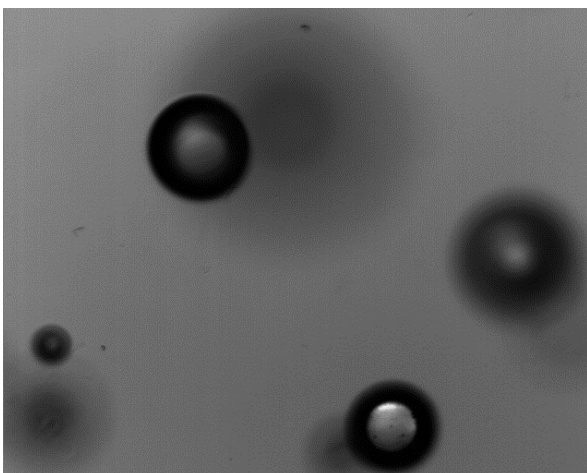
**Picture of CO₂ aphron at 5h**
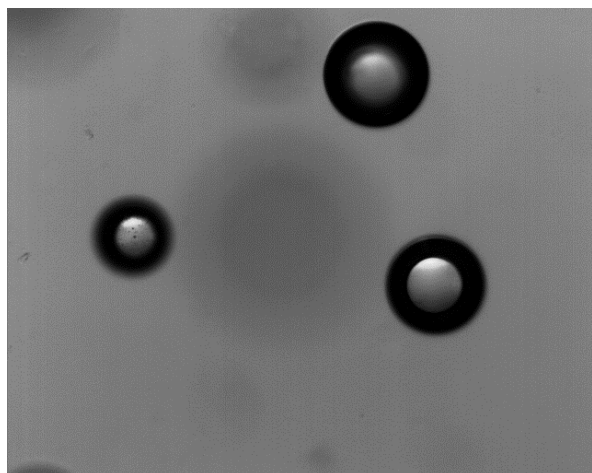
Picture of air aphron at 5h

Figure 5-11: CGA picture comparison initially, after 1 hour, and after 5 hours, of CO_2 and Air, for HEC/N85 (Non-Non) pair

5.3. Summary - Best Polymer-Surfactant Pair for CO_2 CGAs and Air CGAs

The best polymer-surfactant pairs providing most stable CO_2 and air CGAs, based on the selected criteria used in this thesis, are tabulated below in Table 5-1:

Table 5-1: Best Polymer-Surfactant pair that produce viscous, stable CO_2 CGAs and Air CGAs:

Criteria	CO_2 CGAs	Air CGAs
• Rheology (change in LSRV)	XG/DDBS (An-An)	XG/DDBS (An-An)
• Rheology (viscosity profile)	XG/DDBS (An-An)	XG/DDBS (An-An)
• Time stability	XG/N85 (An-Non)	XG/DDBS (An-An)
• Frequency-time distribution	XG/N85 (An-Non)	XG/DDBS (An-An)

From the comparison plots of time stability and frequency distribution, it is concluded that N85 provides stable CO_2 CGAs, with both polymer, but does not impart any stability to air CGAs.

5.4. Best Case of CO_2 CGAs to Best Case of Air CGAs Comparison

Based on rheology and stability characteristics, it seems that XG/N85 (An-Non) solution works best in providing stable CO_2 CGAs. Whereas, the only solution that seems to work for air CGAs at all is XG/DDBS pair.

The best cases of CO_2 CGAs were compared to the best cases of air CGAs by using the four criteria: low shear rate viscosity, viscosity profile at various shear rates, time stability, and frequency-time distribution initially, after 1 hour, and after 5 hours.

5.4.1. Rheology

As per figure 5-1 (b), change is LSRV is about the same for both CO_2 and air CGAs, both being generated from XG/DDBS pair. Looking closely at figure 5-2 (a) (the viscosity profile comparison plot), the viscosity of air CGAs, at around low shear rates of 0.01 to 0.09 s^{-1}, is slightly higher than that of CO_2 CGAs.

5.4.2. Stability

Figures 5-12 and 5-13 show the time stability comparison and frequency distribution comparison plots of CO_2 CGAs and air CGAs, respectively.
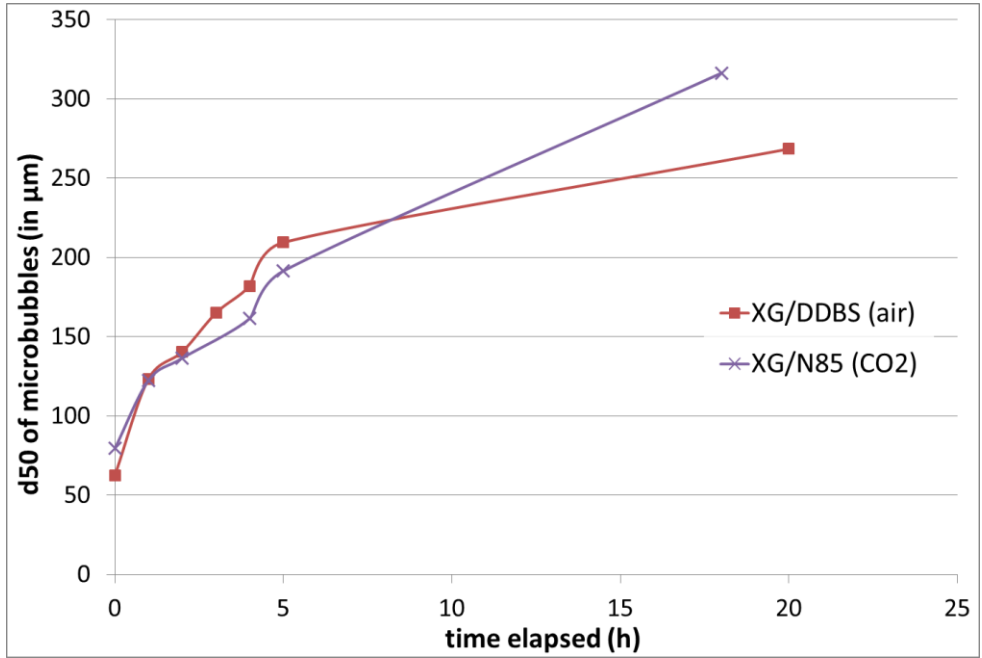
Figure 5-12: Time Stability plot: comparing the best cases of Air CGAs and CO_2 CGAs
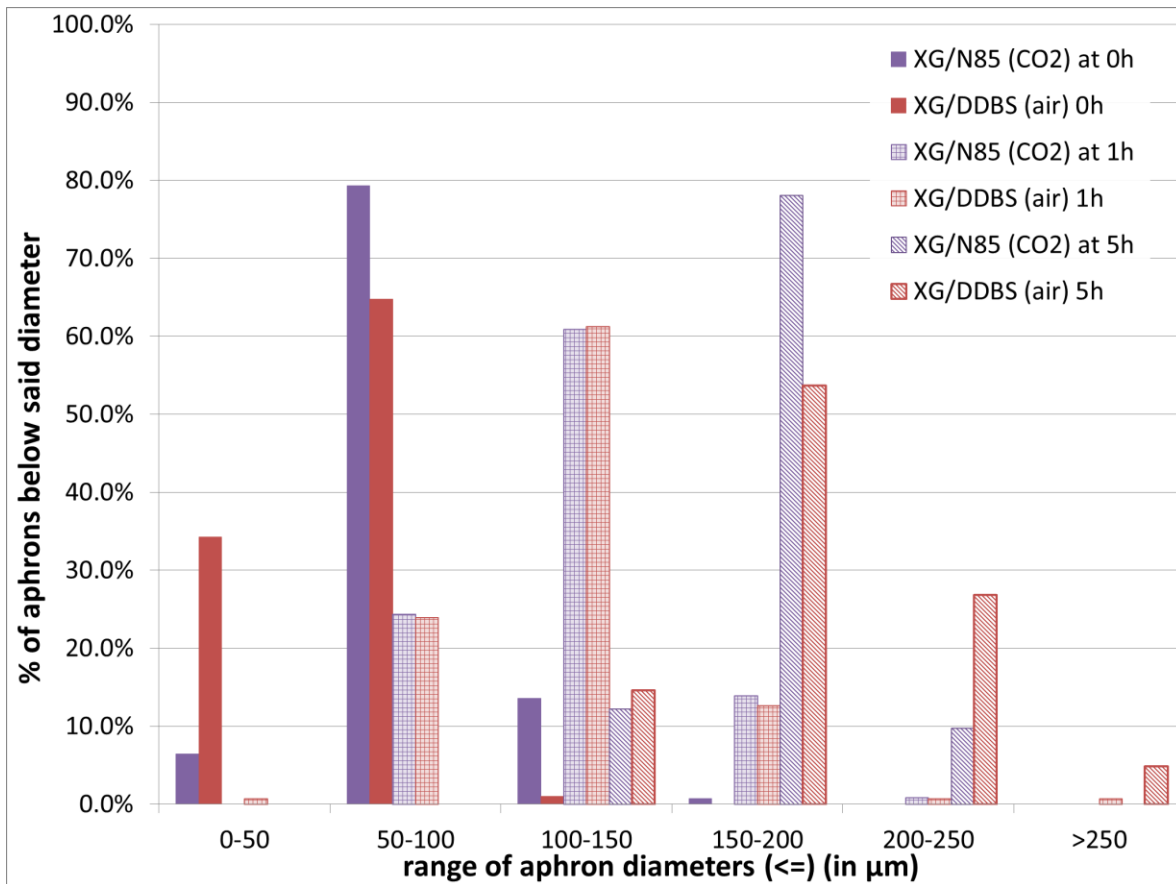
Figure 5-13: Frequency-time Distribution comparison plot: comparing the best cases of Air CGAs and CO_2 CGAs

From stability point of view, from table 5-1, the best pair providing stable CO_2 CGAs was XG/N85 (An-Non), whereas XG/DDBS (An-An) solution generated the most stable air CGAs. As per the time stability comparison plot (figure 5-12) above, the d50 of CO_2 CGAs, from XG/N85 pair, is lower than that of air CGAs, from XG/DDBS within first 6 hours, but later on, the air CGAs, from XG/DDBS (An-An) solution, outperformed the CO_2 CGAs, from XG/N85 (An-Non) solution.

Referring to frequency-time distribution comparison plot (figure 5-13), initially, it was seen that the maximum point on the distribution plot for CO_2 CGAs, from XG/N85 (An-Non) solution was higher than that of air CGAs, from XG/DDBS (An-An) solution indicating the initial yield of CO_2 CGAs was higher than

that of air CGAs. At 1 hour time interval, the positions of the maximum point, for both air and CO_2 CGAs, are located in the 100-150 micron bin, as well as the height of the maximum points, for both CO_2 and air CGAs, are the same. After 5 hours, the maximum point for both CO_2 and air CGAs fall in the 150-200 micron bin; however, the fraction of CO_2 CGAs, with d50 lower than or equal to 200µm, is higher than that of air CGAs. This indicates that the XG/N85 (An-Non) solution provided more stable and consistently high yield CO_2 CGAs than the XG/DDBS (An-An) solution does for air CGAs.

6. Experimental Results & Discussions of CO_2 CGAs Characteristics at High Pressure and Temperature

As it is mentioned in chapters 4 and 5, the best polymer-surfactant pair to generate stable CO_2 CGAs was found to be the XG/N85 (An-Non) pair at room conditions. In order to determine the rheology and stability of CO_2 CGAs generated from XG/N85 (An-Non) pair, viscometry and oscillation tests were conducted under elevated pressures and temperatures to simulate surroundings identical to oil reservoirs.

6.1. HP-HT Viscometry Test Results:

6.1.1. Low Shear Rate Viscosity

The Low Shear Rate Viscosity (LSRV) values of the base fluid (from XG/N85 polymer-surfactant pair) and the corresponding CO_2 CGAs were determined at a constant shear rate of 0.01 s^{-1}, under elevated pressures (100 psi, 500 psi, and 800 psi) and temperatures (25°C and 75°C).

Figure 6-1 shows the LSRV values of the base fluid at elevated temperature and pressure. Figure 6-2 shows the LSRV values of CO_2 CGAs, under elevated pressures and elevated temperatures.
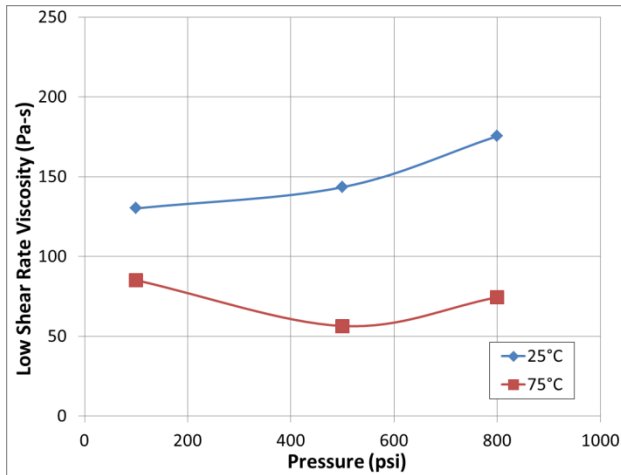
Figure 6-1: LSRV of XG/N85 Base fluid at varying Pressures and Temperatures
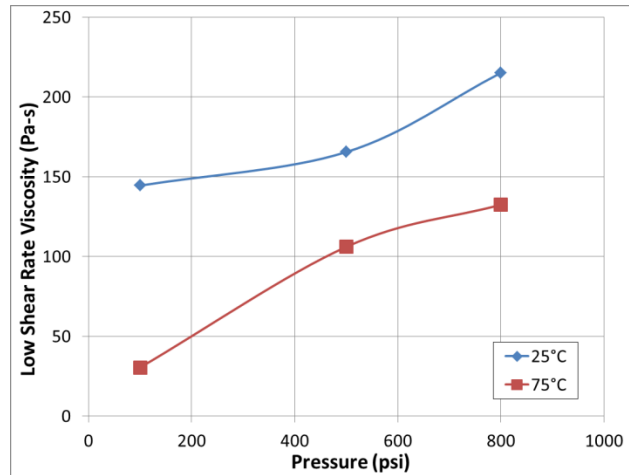
Figure 6-2: LSRV of XG/N85 - CO_2 CGAs at varying Pressures and Temperatures

From figures 6-1 and 6-2, it is seen that LSRV values of the base fluid and CO_2 CGAs drop significantly as temperature increases from 25°C to 75°C, at all pressures. At both low (25°C) and high (75°C) temperatures, the LSRV value of the base fluid and CO_2 CGAs, increases as pressure is increased from 100psi to 800psi, with one exception where the LSRV value of the base fluid at 75°C decreased as pressure was increased from 100psi to 500psi. The reason for this deviation was unclear. With increase in pressure, the gap in between two consecutive CO_2 micro-bubbles decreases, thus providing higher density of CO_2 micro-bubbles per unit volume of CO_2 CGA solution. This, in turn, increases the bulk viscosity of CO_2 CGA sample as more pressure is applied on the test sample.

The y-axis scale, for both figure 6-1 (base fluid) and figure 6-2 (CO_2 CGAs), is same for easier visual comparison of LSRV values between base fluid and CO_2 CGAs at various pressures and temperatures. The LSRV values of CO_2 CGAs remain higher than the LSRV values of base fluid at all other temperature and pressure conditions, with the exception at 75°C/ 100psi where the LSRV of the base fluid exceeds that of CO_2 CGAs.

6.1.2. Comparison of Viscosity Profile- Base fluid vs.CO_2 CGAs

The viscosity profiles of the base fluid (from XG/N85 polymer-surfactant pair) and corresponding CO_2 CGAs were measured, under varying pressures and temperatures, within shear rate ranges of 0.01 s^{-1} to 100 s^{-1}.

Figures 6-3 (a) to (f) show the viscosity profile of the base fluid, consisting of XG/N85 (An-Non) pair, and the corresponding CO_2 CGAs, at varying pressures and temperatures.
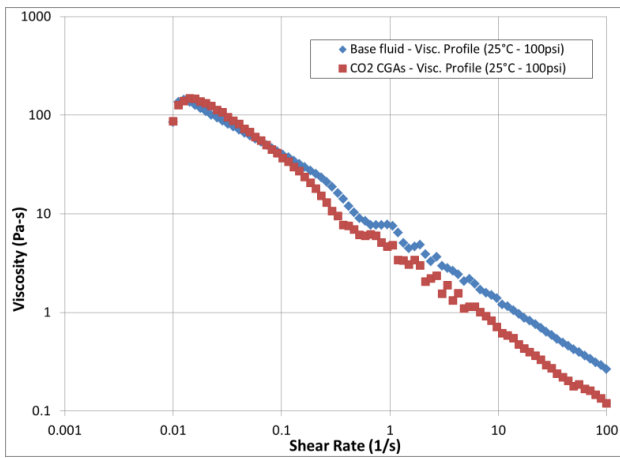
(a) 25°C / 100psi
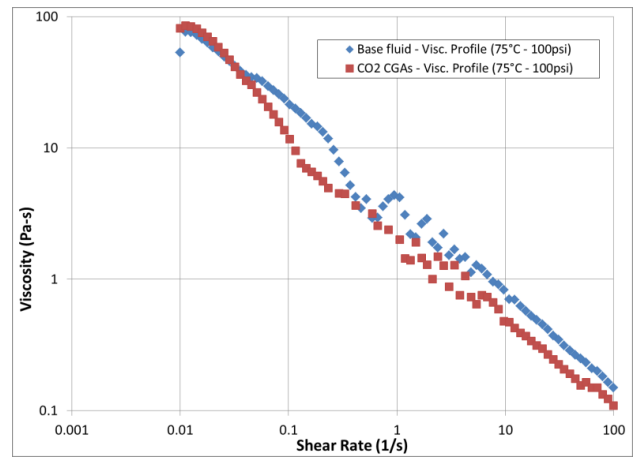
(b) 75°C / 100psi
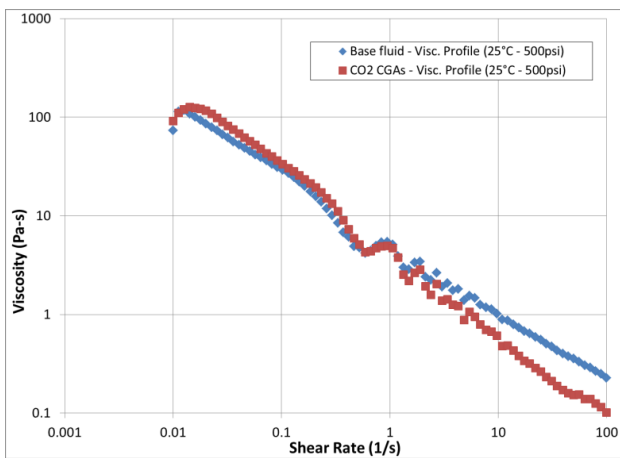
(c) 25°C / 500psi
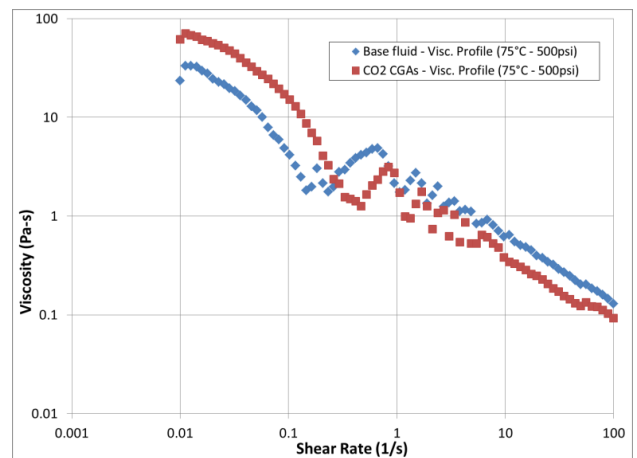
(d) 75°C / 500psi
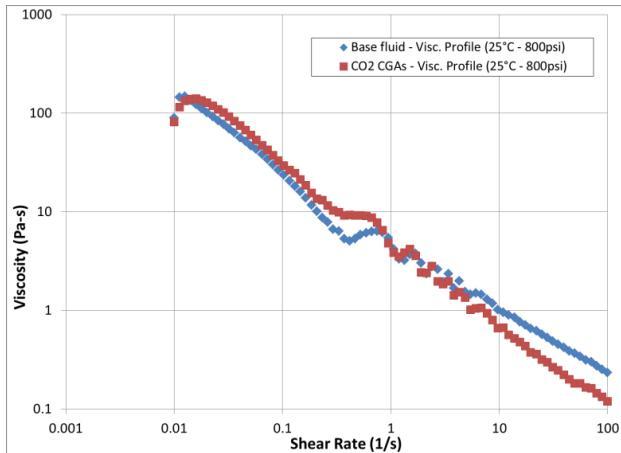
(e) 25°C / 800psi
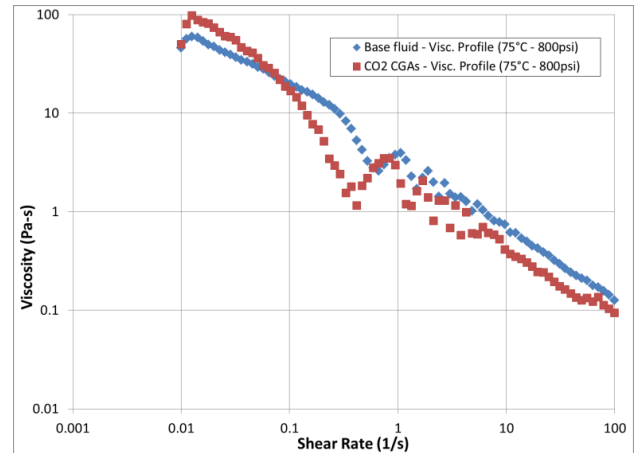
(f) 75°C / 800psi

Figure 6-3: The Viscosity Profile comparison between Base fluid and CO_2 CGAs at varying Pressures and Temperatures

Figures 6-3 (a) to (f) show the rheology of both base fluid and CO_2 CGAs to follow shear thinning, non-Newtonian rheology model, for all pressures and temperatures. Similar to rheological behaviour at ambient conditions, under high pressure-high temperature environment, at very low shear rates (at around 0.01 s^{-1} to 0.04 s^{-1}), the viscosity of CO_2 CGAs is slightly higher than that of base fluid. As shear rate is increased, the viscosity of base fluid overrides the viscosity of CGAs. Thus, at high shear rates, the structure of CO_2 CGAs seem to breakdown and low yield, unstable CGAs remain behind lowering the viscosity of the whole CGA fluid (Chàvez-Montes et al (2007), Herzhaft et al (2005)).

6.1.3. Effect of Temperature and Pressure on the Viscosity of the Base Fluid and CO_2 CGAs

The viscosity profiles of the base fluid and CO_2 CGAs were re-plotted to show the effect of temperature and/or pressure on the rheology, keeping the other parameters constant. Figures 6-4 & 6-5 show the effect of temperature on the rheology of base fluid (from XG/N85 polymer-surfactant pair) and CO_2 CGAs, keeping the pressure constant, respectively.
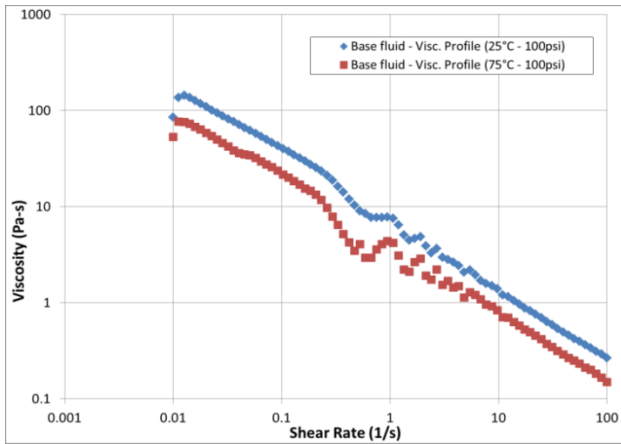
(a) constant pressure of 100psi
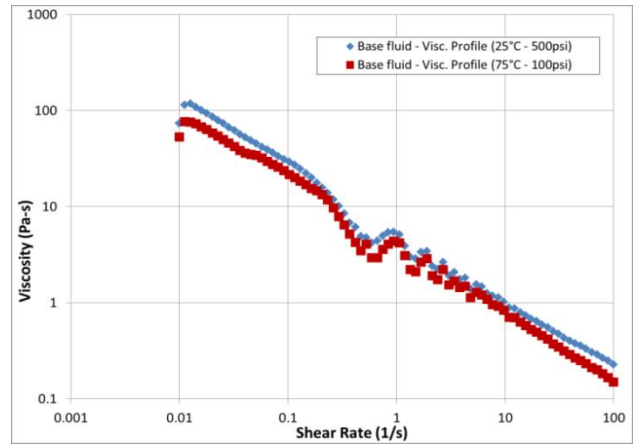
(b) constant pressure of 500psi
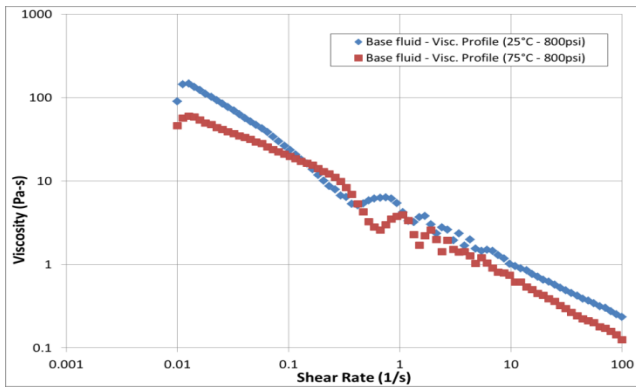
(c) constant pressure of 800psi

Figure 6-4: Effect of Temperature on Rheology of Base fluid
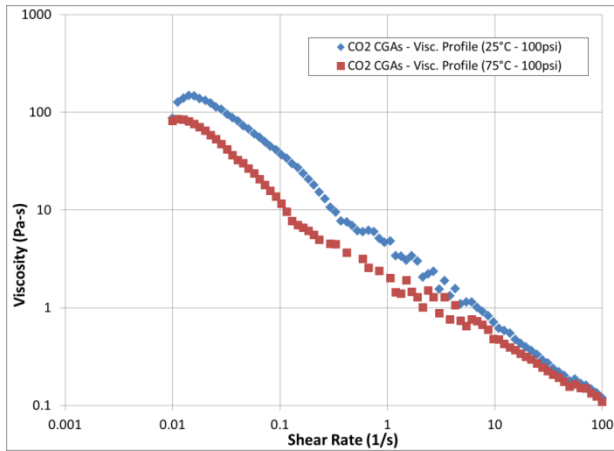
(a) constant pressure of 100psi
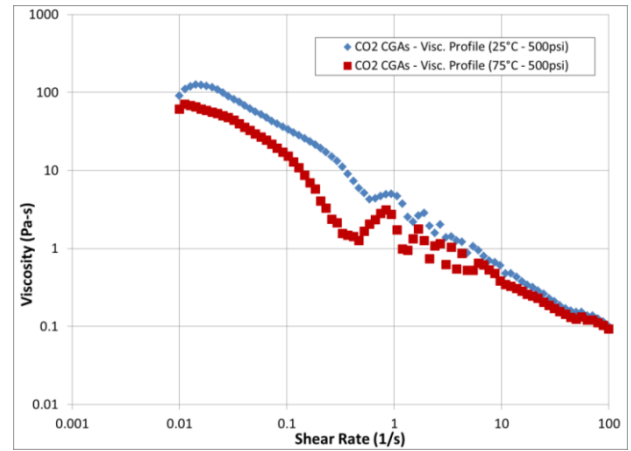
(b) constant pressure of 500psi
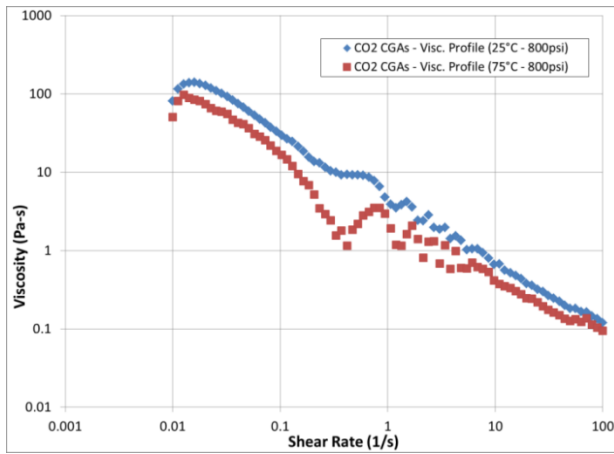
(c) constant pressure of 800psi

Figure 6-5: Effect of Temperature on the Rheology of CO_2 CGAs

Figure 6-4 shows that increasing the temperature causes a significant decrease in the base fluid viscosity at all shear rates. Taking a closer look at figures 6-4 (b) and (c), it is observed that with increase in pressure from 100psi to 500psi (and later on, 800psi), the decline in viscosity, with respect to increase in temperature, decreases.

As shown in figure 6-5, the viscosity of the CO_2 CGAs shifts downward with increasing temperature. This makes sense as increasing the temperature, most likely, causes the aphron structure to break down, and the CO_2 CGA solution becomes more of low viscosity polymer – surfactant solution.

Figures 6-6 & 6-7 show the effect of pressure on the rheology of the base fluid and CO_2 CGAs, respectively, at constant temperatures.
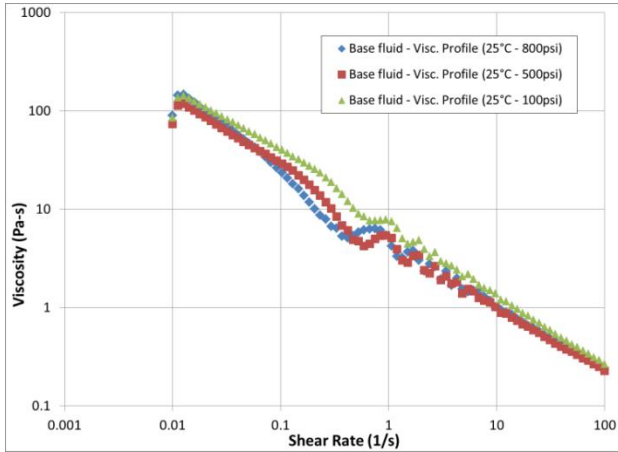
(a) constant temperature of 25°C
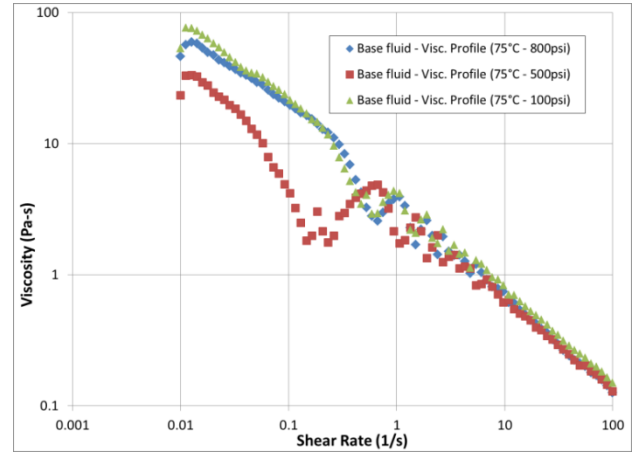
(b) constant temperature of 75°C

Figure 6-6: Effect of Pressure on Rheology of Base fluid
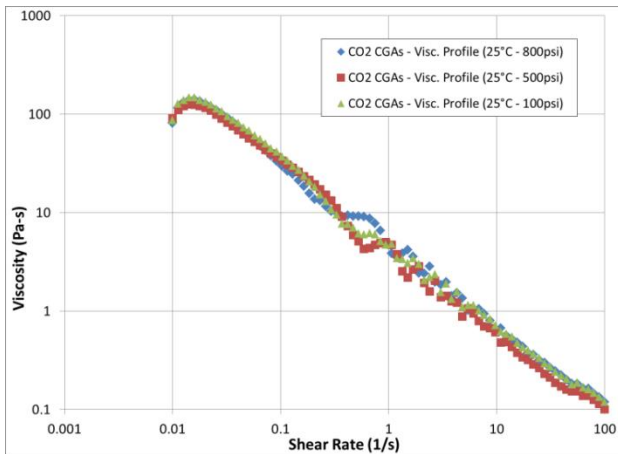
(a) constant temperature of 25°C
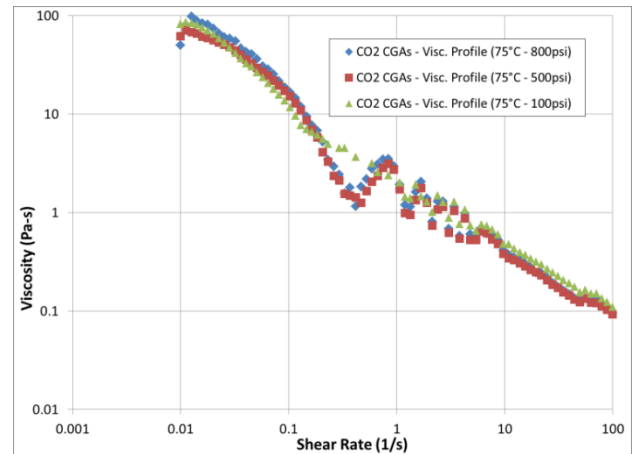
(b) constant temperature of 75°C

Figure 6-7: Effect of Pressure on the Rheology of CO_2 CGAs

In figure 6-6 (a), while maintaining a constant temperature of 25°C, pressure has virtually no effect on the viscosity profile of the base fluid solution; however, in figure 6-6 (b), it is seen that at 500psi, within

the shear rate range of 0.01 s^{-1} to 1.0 s^{-1}, the viscosity of base fluid solution is lowered to a great extent. The reason for this phenomenon is unknown.

As shown in figure 6-7, pressure seems to have no significant effect on the viscosity profile of the CO_2 CGAs, indicating the CO_2 CGAs to be slightly compressible fluid.

Overall, temperature is seen to have a greater effect on the rheological properties than pressure does for both base fluid and CO_2 CGAs.

In all high pressure/high temperature plots shown above (Figures 6-4 to 6-7), a clear distinctive distortion is seen in the viscosity profile within the approximate shear rate range of 0.2 s^{-1} to 1 s^{-1}. This distortion is only noticed when the rheological measurements, for both base fluid and CO_2 CGA samples, are carried out at high pressure/high temperature conditions using concentric cylinder geometry mode of the rheometer. Referring to figures 4-3, and 5-2, it is seen that this deviation is absent in the viscosity profile plot, when the rheology of base fluid and CGAs were being measured using the cone-plate system at ambient conditions.

Furthermore, the distorted data in the viscosity profile is not due to changes in temperature. This can be ascertained from the figure 6-8, where it can be seen that when measurements were taken at elevated temperature using cone-plate low pressure system, the distorted data is replaced by smooth straight line within the shear rate zone of interest (which is in between 0.2 s^{-1} to 1 s^{-1}). Thus, the distortion in the viscosity profile plots (figures 6-3 to 6-7) is attributed to the methodology of rheology measurement at high pressure-high temperature conditions. Additionally, it is observed that at higher temperatures of 75°C, the amplitude of the distortion is higher at all pressures for both base fluid and CO_2 CGAs.
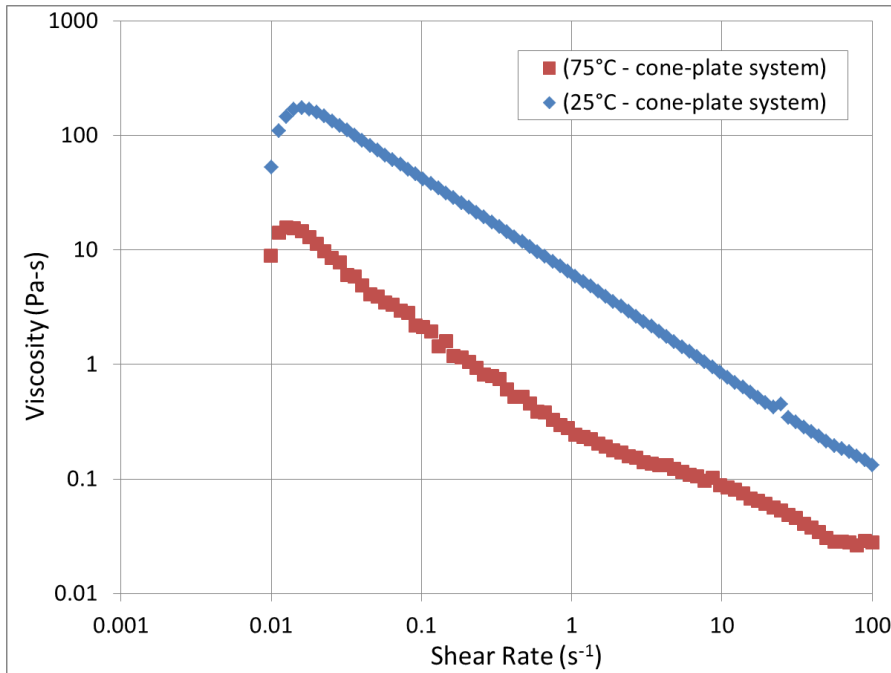
Figure 6-8: Viscosity Profile of CO_2 CGAs measures with slightly truncated cone-plate low pressure system at elevated temperatures

6.2.   HP-HT Dynamic Oscillation Test Results:

Oscillation tests were conducted using Couette flow method, under varying high pressures and high temperatures, to determine the structure stability and mobility of CO_2 CGAs, being generated from XG/N85 (An-Non) polymer-surfactant pair, and compare the structural characteristics to the original base fluid under similar conditions.

6.2.1.   Amplitude Sweep Test Results

Amplitude sweep tests were conducted to determine the viscoelastic properties of the base fluid and CO_2 CGAs at elevated temperature and pressure conditions.

6.2.1.1. Effect of Temperature on Amplitude Sweep Test Results

Figures 6-9, 6-10, and 6-11 display the effect of temperature on the stress-dependant viscoelastic characteristics of the base fluid and CO_2 CGAs, while keeping the frequency constant at 0.1Hz, at constant pressures of 100psi, 500psi, and 800psi, respectively.
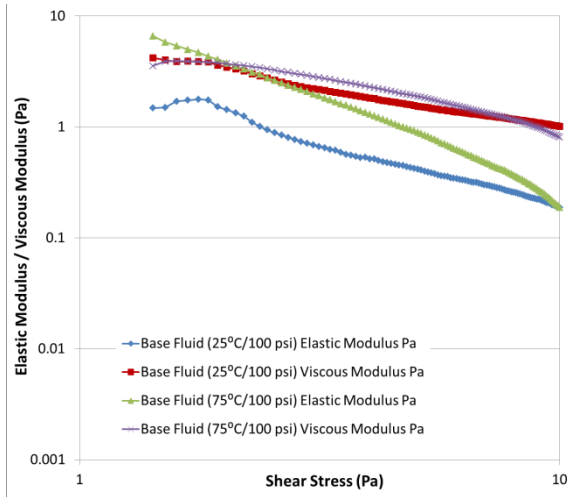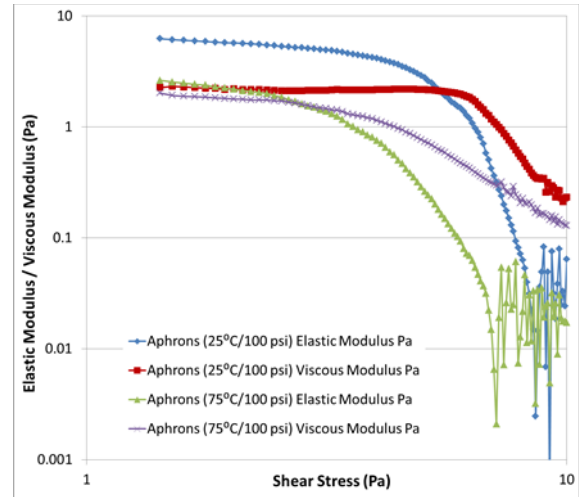
(a) Base Fluid – constant pressure of 100psi   (b) CO_2 CGAs – constant pressure of 100psi

Figure 6-9: Amplitude Sweep at 100psi
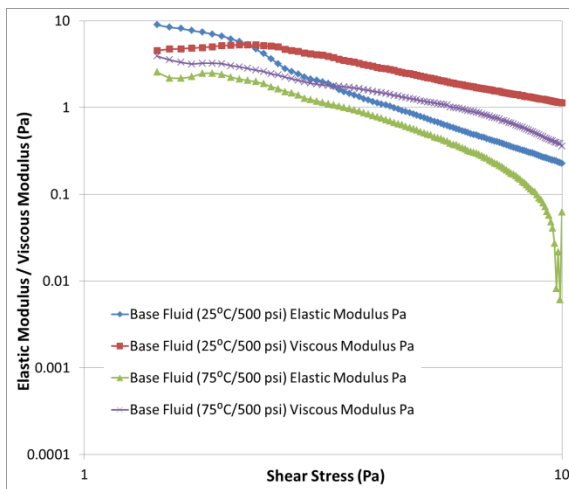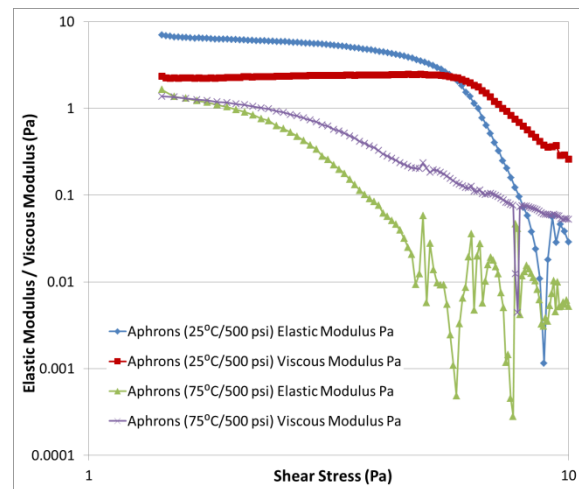
(a) Base Fluid – constant pressure of 500psi   (b) CO_2 CGAs – constant pressure of 500psi

Figure 6-10: Amplitude Sweep at 500psi
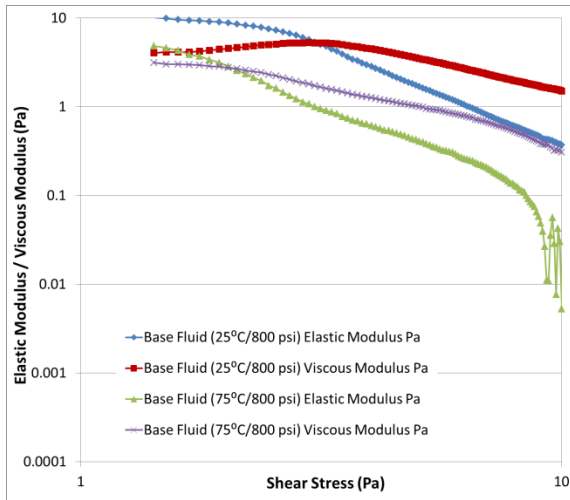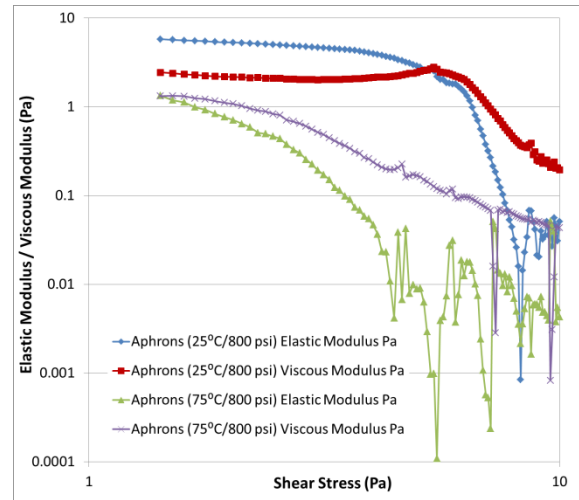
(a) Base Fluid – constant pressure of 800psi   (b) CO_2 CGAs – constant pressure of 800psi

Figure 6-11: Amplitude Sweep at 800psi

As shown in figure 6-9 (a), increasing the temperature from 25°C to 75°C causes significant increase in the bas fluid elastic modulus(G′) values and slight increase in the base fluid viscous modulus (G″) values. This anomalous decrease in ratio of G″ to G′, with increasing temperature, suggests that the base fluid is gaining more rigidity and solid-like behaviour with increase in temperature. As pressure is further increased to 500psi (figure 6-10 (a)) and 800psi (figure 6-11 (a)), crossover between the G′ plot and the G″ plot is observed at low temperatures of 25°C. The G′ curve dominates over the G″ curve within shear stress values of 2.2Pa and 3.0Pa, while pressure is being maintained at 500psi and 800psi, respectively. As the shear stress applied to the base fluid is increased beyond these values, the viscous behaviour dominates the elastic behaviour.

As shown in figures 6-9 (b), 6-10 (b), and 6-11 (b), the viscoelastic behaviour of CO_2 CGAs follow the same trend regardless of pressure applied. Both G′ and G″ curves show constant plateau values of approximately 6.5Pa and 2.0Pa, respectively, which denotes the LVE (linear viscoelastic) region. The

elastic behaviour dominates the viscous behaviour for CO_2 CGAs, indicating structural stability of CO_2 CGAs.

As the temperature is increased to 75°C, both G' and G'' plots decrease rapidly with applied shear stress. Increasing the temperature to 75°C takes away the LVE region from the moduli plots of CO_2 CGAs. Keeping the pressures constant, as the temperature is increased to 75°C, the viscous behaviour dominates (in case of 500psi) or starts to dominate (in case of 100psi and 800psi) the elastic behaviour at lower values of applied shear stress. The CO_2 CGAs, with increase in temperature, resemble closer to mobile, liquid-like viscous fluid with increasing shear stress, as the temperature is increased from 25°C to 75°C, at any given pressure.

Another effect of increasing the temperature is the appearance of distortion in the stress-dependant moduli data. This is particularly prevalent in the amplitude sweep plots for CO_2 CGAs, at 75°C (figures 6-9 (b), 6-10 (b), and 6-11 (b)), where both the elastic and the viscous modulus data get more distorted as the applied shear stress is increased beyond approximately 5Pa. In comparison, at any given pressure, moduli plots for the base fluid (figures 6-9 (a), 6-10 (a), and 6-11 (a)) is smoother than its CO_2 CGA counterpart, at 75°C, throughout the entire range of applied shear stress. This indicates that the presence of added distortion in the CO_2 CGAs modulus data is somehow connected to the presence of CO_2 micro-bubble dispersions in the solution.

6.2.1.2. Effect of Pressure on Amplitude Sweep Test Results

Figures 6-12 a&b show the pressure effect (while keeping the temperature at 25°C) on the viscous and elastic moduli of the base fluid and CO_2 CGAs, respectively. Figures 6-13 a&b show the effect of pressure on the same while keeping the temperature constant at 75°C. Data in both Figs. 6.12 and 6.13 were obtained at constant frequency of 0.1Hz.
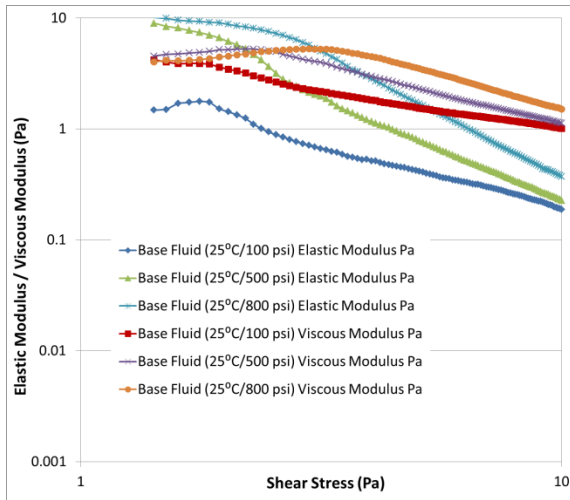
(a) Base Fluid – constant temperature of 25°C
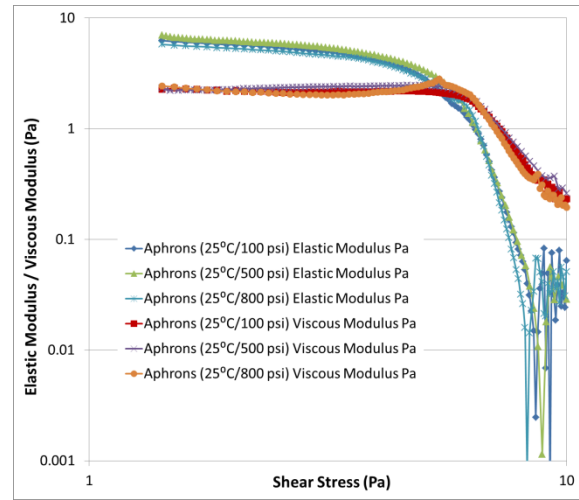
(b) CO_2 CGAs – constant temperature of 25°C

Figure 6-12: Amplitude Sweep at 25°C
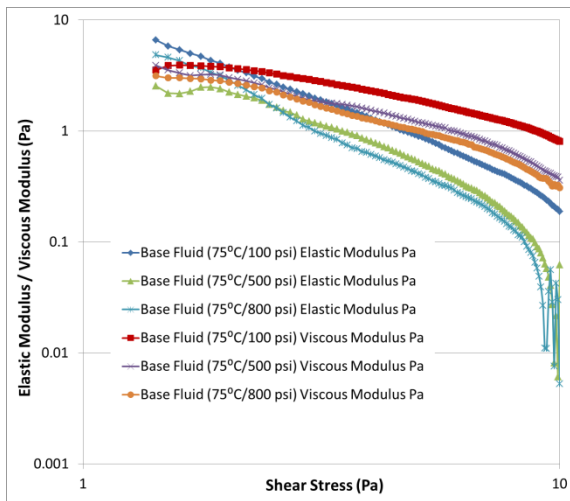
(a) Base Fluid – constant temperature of 75°C
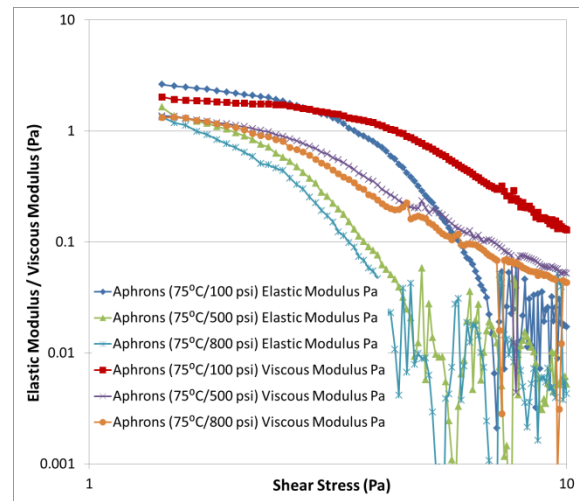
(b) CO_2 CGAs – constant temperature of 75°C

Figure 6-13: Amplitude Sweep at 75°C

For the base fluid, there seems to be no LVE region at all in all three amplitude sweep plots (in figures 6-12 (a) and 6-13 (a)), indicating non-linear viscoelastic behaviour throughout the entire range of pressure and temperature examined. In figure 6-12 (a), while temperature is maintained at 25°C, it is observed that increase in pressure causes the lower range of shear stress, where the G' values dominates the G"

values, to widen. At 100psi, the base fluid exhibits viscous, liquid-like viscoelastic behaviour throughout the entire range of applied shear stress. A crossover is observed between the G' plot and G" plot at 2.0Pa when the pressure is increased to 500psi. On further increasing the pressure to 800psi, the crossover shifts towards right at shear stress value of 3.0Pa.

When the temperature is kept constant at 75°C (figure 6-13 (a)), at 100psi, the G' curve falls rapidly below the G" curve past 2.0Pa. When the pressure is increased to 500psi, the G" plot dominates over the G' plot. Further increasing the pressure to 800psi causes the base fluid to act in a similar way as observed at 100psi; the crossover point, at 800psi, is located at 2.0Pa. Over the range of pressure and temperature examined in this study, the base fluid shows dominant viscous behaviour over the entire range of applied shear stress.

For CO_2 CGAs, referring to figure 6-12 (b), it is seen that increasing the pressure has no visible effect on the moduli plots, when low temperature of 25°C is maintained. The LVE region is clearly seen, which seems to end at around shear stress value of 2.5Pa. In the LVE range with constant temperature of 25°C, the G' plot, at all pressures, is higher than the G" plot, which exhibits structural stability for CO_2 CGAs within the shear rate range of 2.5Pa. Distortions appear particularly in the elastic modulus graph at lower shear stress values of approximately 8.0Pa.

The LVE region, for CO_2 CGAs, disappears in figure 6-13 (b), as the temperature is increased to 75°C. With increase in pressure applied, the CO_2 CGAs lose the elastic, gel-like characteristics at lower values of applied shear stress. At 100 psi, the G' plot falls below G" plot at 2.6Pa. Increasing the pressure to 500psi causes the CO_2 CGAs to lose the elastic behaviour at 1.5Pa; on further increasing the pressure to 800psi, the G" plot completely dominates over the G' plot throughout the entire range of applied shear stress.

6.2.2. Frequency Sweep Results

Frequency sweep tests were conducted to determine the viscoelastic properties of the base fluid and CO_2 CGA fluid at elevated temperature and pressure conditions.

6.2.2.1. Effect of Temperature on the Frequency Sweep Test Results

Figures 6-14, 6-15, and 6-16 show the temperature effect on the frequency-dependant viscoelastic properties of the base fluid and CO_2 CGAs, maintaining the pressures at 100psi, 500psi, and 800psi, respectively. Since the LVE region is only visible for CO_2 CGAs at 25°C, a common range of shear stress, where both base fluid and CO_2 CGAs within the range of pressures and temperatures show linear deformation behaviour, could not be determined. Therefore, the lowest value of shear stress, 1.42Pa, was chosen.
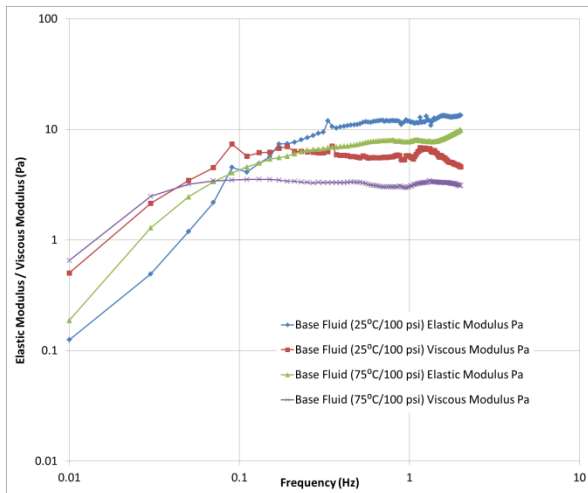
(a) Base Fluid – constant pressure of 100psi
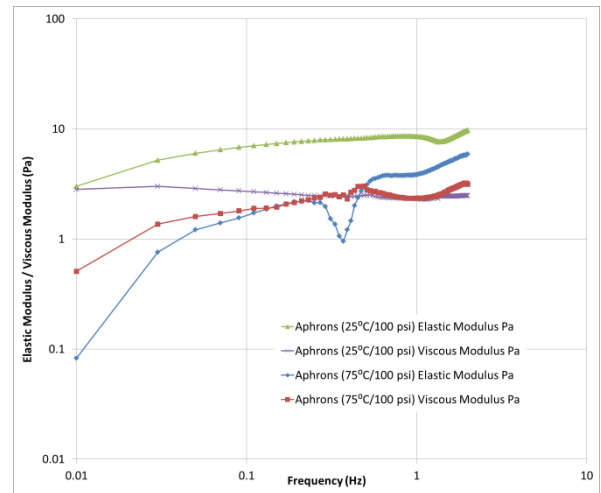
(b) CO_2 CGAs – constant pressure of 100psi

Figure 6-14: Frequency Sweep at 100psi
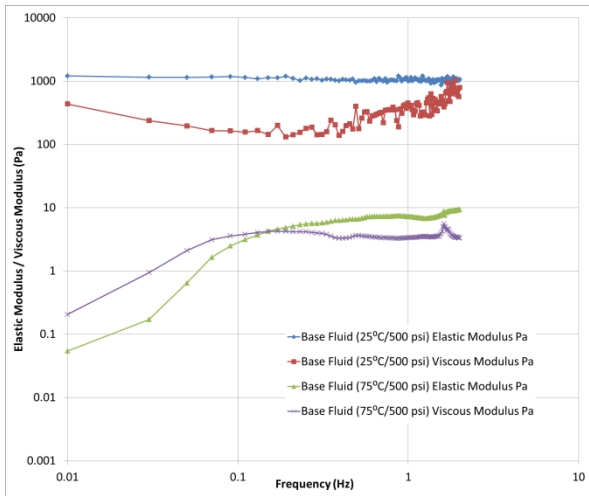
(a) Base Fluid – constant pressure of 500psi
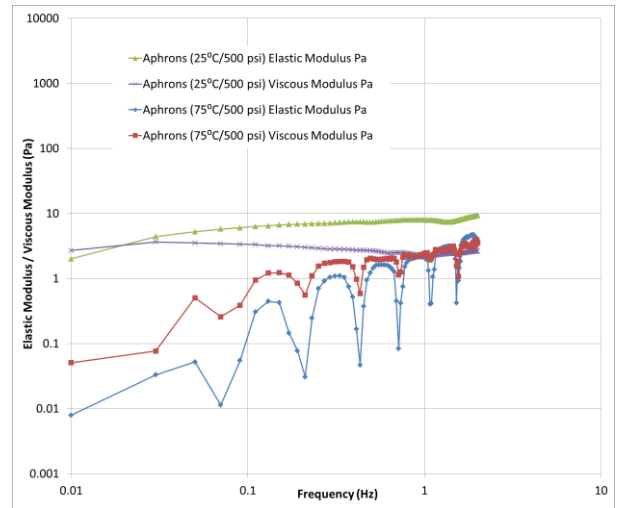
(b) CO$_2$ CGAs – constant pressure of 500psi

Figure 6-15: Frequency Sweep at 500psi
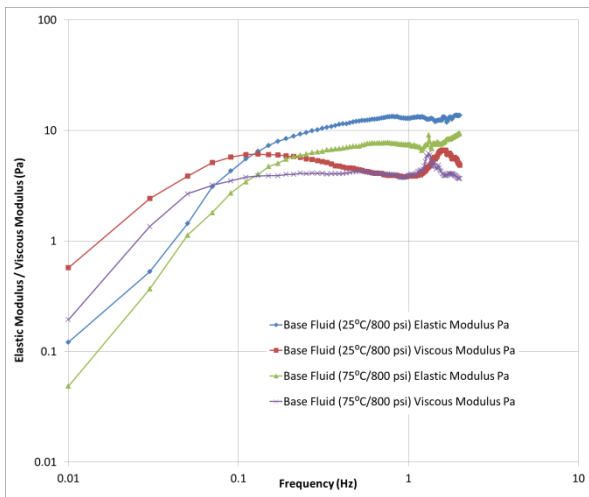
(a) Base Fluid – constant pressure of 800psi
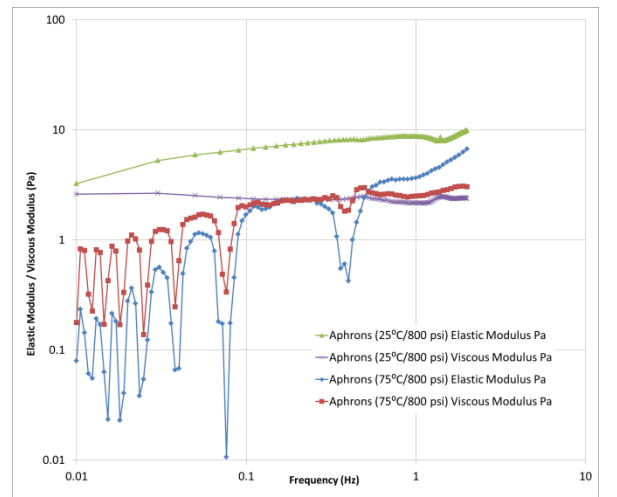
(b) CO$_2$ CGAs – constant pressure of 800psi

Figure 6-16: Frequency Sweep at 800psi

In the range of pressure and temperature examined in this study, the base fluid show transformation from viscous, mobile liquid-like character to elastic, gel-like character as frequency is increased. Referring to figure 6-14 (a), it is seen that at lower range of frequencies, imitating long-term behaviour, the base fluid has higher viscous modulus (G'') than elastic modulus (G'). The overtake of G' plot over G'' plot occurs at around 0.15Hz, at 25°C. This domination shifts toward left at lower frequency value of

approximately 0.04Hz as temperature is increased to 75°C. Overall, pressure being constant at 100psi, the base fluid, at both 25°C and 75°C, transforms from more viscous liquid (in low frequency range) to gel-like, rigid fluid (in high frequency range, imitating short-term behaviour) as frequency is increased.

At 75°C and 500psi (figure 6-15 (a)), the G' plot starts to dominate the G" plot at around 0.15Hz. In figure 6-16 (a) (constant pressure of 800psi), the takeover of G' curve over G" curve, at both temperatures of 25°C and 75°C, happens around the same value of 0.13 Hz.

From figures 6-14 (b), 6-15 (b), and 6-16 (b), it is observed that at 25°C, in any given pressure, the elastic behaviour dominates the viscous behaviour over the entire range of frequency. Thus, the viscoelastic property of the CO_2 CGAs shows more rigid, gel-state viscoelastic behaviour throughout the entire frequency range of 0.01Hz to 2.0Hz. At 25°C, while the G" plot is almost constant with frequency, there exists a gentle incline in the G' plot with increasing frequency.

As the temperature is increased to 75°C, transformation in viscoelastic behaviour is observed in the CO_2 CGAs at all three pressures. Both G' and G" curves increase steeper with increasing frequency. At constant pressure of 100psi (figure 6-14 (b)), the G" plot, for CO_2 CGAs, is higher than the G' plot till about 0.47Hz; at high frequency range, higher than 0.47Hz, the G' plot overtakes the G" plot. In figure 6-15 (b) (500psi constant pressure), the CO_2 CGAs exhibit mobile, liquid-like behaviour, throughout the entire frequency range at 75°C. Similar behaviour is observed at elevated temperatures of 75°C (figure 6-16 (b)) when the pressure is increased and maintained at 800psi till about 0.6Hz; past this point, the G' curve overtakes the G" curve, denoting rigid, solid-state viscoelastic behaviour.

Furthermore, unique "humps"-like distortion is observed in both moduli plots of CO_2 CGAs (figures 6-15 (b) and 6-16 (b)), which is absent for the moduli plots, measured at 25°C.

6.2.2.2.   Effect of Pressure on the Frequency Sweep Test Results

Figures 6-17 and 6-18 show the effect of pressure on the viscoelastic behaviour of base fluid and CO_2

CGAs with changing frequency, while keeping temperature constant at 25°C and 75°C, respectively. The

applied shear stress was kept steady at 1.42Pa.
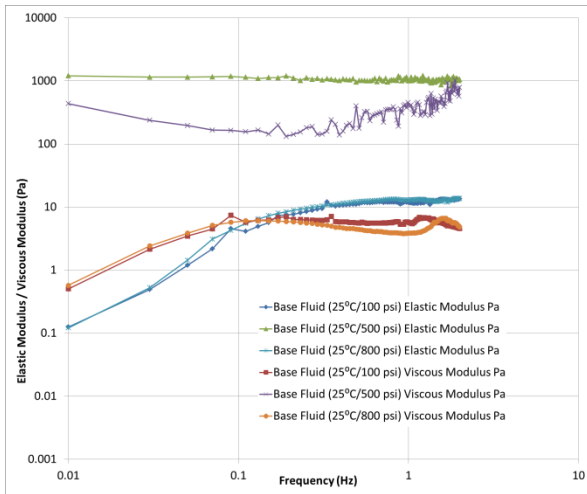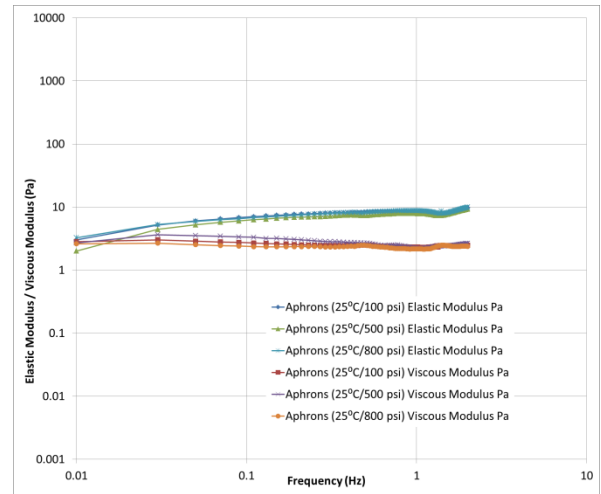
(a) Base Fluid – constant temperature of 25°C   (b) CO_2 CGAs – constant temperature of 25°C

Figure 6-17: Frequency Sweep at 25°C
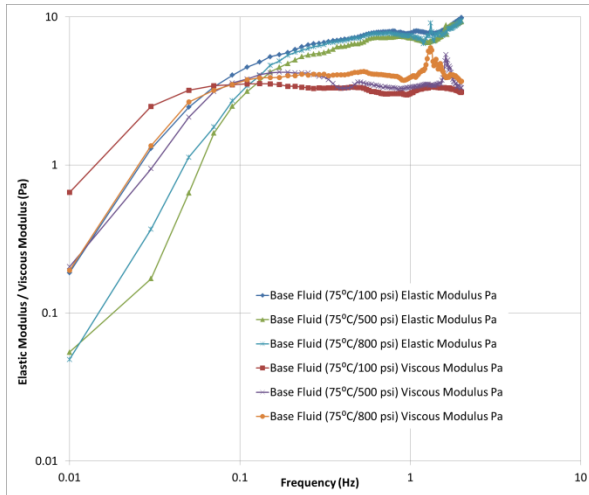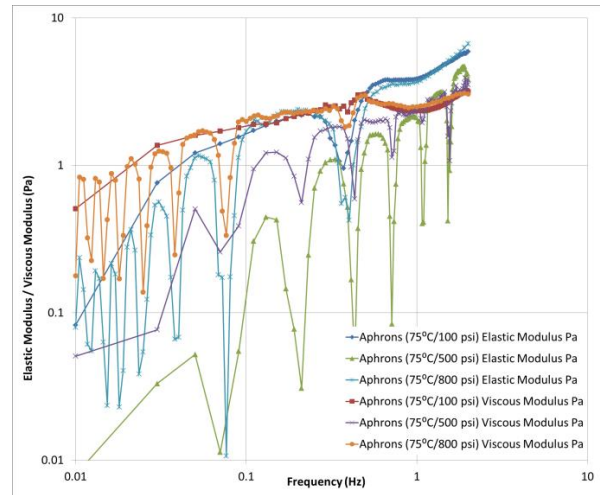
(a) Base Fluid – constant temperature of 75°C   (b) CO_2 CGAs – constant temperature of 75°C

Figure 6-18: Frequency Sweep at 75°C

In figure 6-17 (a), with the exception of modulus values being unusually high and constant throughout the entire frequency range for base fluid at 25°C and 500psi, negligible effect of pressure is seen on both G' and G" curves. The crossover, where G' values exceed G" values, occurs at the same frequency value of 0.15Hz, regardless of the pressure. Beyond 0.15Hz, it is seen that the G" plots (at 100psi and 800psi) become constant with increasing frequency, as opposed to the G' plots which has a slight increasing trend.

Figure 6-18 (a) shows that at higher range of frequencies (0.2Hz to 2.0Hz), pressure has no significant effect on the G' and G" values, as the three G' plots and the three G" plots almost blend together; the G" plot, measured at 800psi and 75°C, is located slightly higher than the other two G" plots. As the frequency is lowered past 0.1Hz, significant effect of pressure on the moduli plots of base fluid is observed. The rise in the G' and G" plots, at 500psi and 800psi, is steeper than the G' and G" plot at 100psi, in the lower range of frequency.

Furthermore, the crossover at which G' plot overtakes the G" plot occurs at 0.07Hz at 100psi. As pressure is increased further to 500psi and 800psi, the crossover shifts right side to higher frequency values of 0.15Hz and 0.2Hz, respectively.

Figure 6-17 (b) show that increasing the pressure has negligible effect on the moduli values for CO_2 CGAs at low temperature values of 25°C. Throughout the entire frequency range of interest, the G' plot dominates over the G" plot, and the moduli values are almost frequency independent.

At elevated temperature of 75°C, the effect of varying the pressure has significant effect on the moduli values of CO_2 CGAs (figure 6-18 (b)). At 100psi, in the lower range of frequency (0.01Hz to 0.15Hz), the G" plot is higher than the G' plot; as the frequency is increased beyond 0.47Hz, the G' plot overtakes the G" plot, indicating transformation in viscoelastic properties from mobile, liquid-state to elastic, solid-state. Increasing the pressure further to 500psi and 800psi introduces distortion in the moduli plots in the form of unique "humps". For the larger part of the frequency range, the G" curve is located above the G' curve. When the frequency values exceed 1.5Hz (for 500psi) and 0.5Hz (for 800psi), the G' curves overtake the G" curves.

6.2.3. Discussions of the HP-HT Oscillation Test Results:

Keeping the temperature constant at 25°C, in both amplitude sweep and frequency sweep tests, pressure had no effect on the viscoelastic behaviour of CO_2 CGAs. Elastic behaviour dominated over viscous behaviour, and both moduli plots were independent of frequency. Similar viscoelastic behaviour have been found in frequency sweep test results of foams and highly concentrated emulsions (Khan et. al (1988), Mason et. al (1995), Mason and Weitz (1995)). Sollich et. al (1997) states in his paper that the viscoelastic response of soft materials arises from their main properties: structural disorder and metastability. As stress is applied to foams and other concentrated dispersed systems, the increase in

strain in the droplets induces local topological rearrangement, and the dispersed system has a new disordered metastable configuration (Höhler and Cohen-Addad (2005), Gopal and Durian (1995)).

Furthermore, the elastic response of the dispersed systems is strongly dependent on the droplet volume fraction (Mason (1999)). For a given applied stress, concentrated emulsions, where the droplets are tightly packed, will exhibit more solid-like elasticity (higher G') than the dilute emulsions will.

Additionally, it has been found that for concentrated XG solutions the elastic modulus is always greater than the viscous modulus over an entire range of frequencies; both these moduli values happen to be weakly dependent upon frequency, indicating gel-like structure is present (Song et al (2006), Navarini el al (1992)). The dominant elastic behaviour of CO_2 CGAs might initiate from the presence of XG polymer in their structure.

Increasing the temperature to 75°C, the viscoelastic response of CO_2 CGAs changed dramatically, regardless of the applied pressure. Viscous behaviour dominated over elastic behaviour, and both moduli plots were frequency-dependent.

No LVE range was detected in the amplitude sweep plots with increase in temperature for CO_2 CGAs, indicating irreversible deformation in the structure of the CGAs. The non-linear viscoelastic behaviour of wet foams, arising from continuous deformations in foam structure and droplet rearrangements is attributed to dynamic dilatancy in wet foams (Rioual et al (2005)). As the shear stress applied to wet foams rises above the yield stress of the foam, continuous local rearrangements of the gas droplets take place and the droplets go under continuous deformation. Mason (1999) states in his paper that for concentrated emulsions, if the applied shear stress is greater than the yield stress of emulsions (which is a function of the interfacial tension of the film layer), droplets can deform, stretch and rupture continuously. He also mentions that dilute emulsions or semi-dilute emulsions, where the droplets are farther apart, will display dominant viscous behaviour even in the range of small applied shear stress.

Low values of the G' (< 10.0Pa) in both amplitude and frequency sweep plots suggests dispersion destabilization (Mezger (2006)). On the whole, figures 6-13 (b) and 6-18 (b), show that increasing the pressure on the CGAs does not compensate for the irreversible deformation caused in the aphron structure by increasing the temperature.

With the exception in figure 6-17 (a) where the G' and G" values are exceptionally high and constant with frequency, the moduli values of the base fluid, at both low and high temperatures, are not very high. It has been mentioned in the literature (Aubry and Moan (1996)) that non-ionic surfactants can strongly influence the rheological properties of hydrophobically modified water soluble polymer solutions when the surfactant concentration falls within critical micelle concentration or a little above it; the interactions lead to a thickening effect. Going above the critical micelle concentration of the surfactant causes disruption in the temporary associating network, leading to weakening of the overall gel network. Figure 4-3 (b) show that adding N85 does not significantly enhance the viscosity of the XG/N85 (An-Non) base fluid solution. XG has ordered helical network but, unlike HEC, does not contain any hydrophobic moieties. Adding N85, well above its critical micelle concentration, to the XG solution could lead to weakening of the gel structure, leading to liquid-like viscoelastic behaviour where G" values dominate.

7. Conclusions and Recommendations:

7.1. Conclusions:

The objective of this research was to develop a formulation for generating stable, viscous CO_2 CGAs that could potentially be used as EOR displacing fluid for recovering hydrocarbons and conduct CO_2 sequestration. Summary of the research results are provided below:

1. In-depth literature review was conducted on various types of polymers and surfactants in order to devise screening criteria for polymers and surfactants that will provide stable, viscous CO_2 CGAs.

2. The following criteria were used for optimum formulation of CO_2 CGAs:

Rheology	Low Shear Rate Viscosity (LSRV) at 0.01 s^{-1} shear rate
	Viscosity Profile (vs. shear rate)
Stability	Time-stability: change in median diameter (d50) with time
	Frequency distribution: reflect the total yield of CO_2 CGAs

3. The polymers chosen in this study, based on the low diffusivity of CO_2 gas through the aqueous polymer solutions, were:

    − Xanthan Gum (XG) (0.55 wt.%)

    − Hydroxyethyl Cellulose (HEC) (0.55 wt.%, 1.0 wt.%, 1.5 wt.%)

    − Carboxymethyl Cellulose (CMC) (0.55 wt.%, 1.0 wt.%, 1.5 wt.%)

    The LSRV of aqueous solution of CMC, within the polymer concentration range studied here, was too low to be considered as a suitable polymer choice for stable CO_2 CGA generation. Thus, XG (0.55 wt.%) and HEC (1.5 wt.%) were the chosen polymers for generating CO_2 CGAs.

4. The surfactants chosen in this study, based on molecular composition (such as, the ethylene oxide units) and type (anionic or non-ionic), were:

   − Dodecyl Benzene Sulfonate (DDBS) (0.29 wt.%)

   − Surfonic N85 (N85) (0.29 wt.%, 0.55 wt.%)

   Increasing the concentration of N85 did not cause any significant change in d50 of CO_2 CGAs over time. Thus, the lower concentration of N85 was used which is 0.29 wt. %.

5. In order to figure out the best polymer-surfactant duo for stable CO_2 CGAs, rheology and stability tests were conducted on CO_2 CGAs, generated from four pair of polymer-surfactant base fluid solutions that are listed below:

   − XG (0.55 wt.%) and DDBS (0.29 wt.%)

   − XG (0.55 wt.%) and N85 (0.29 wt.%)

   − HEC (1.5 wt.%) and DDBS (0.29 wt.%)

   − HEC (1.5 wt.%) and N85 (0.29 wt.%)

6. Ultimately, the ideal polymer and surfactant pair chosen was XG (0.55 wt.%) and N85 (0.29 wt.%); while the increase in viscosity of CO_2 CGAs, from XG/N85 (An-Non) base fluid, was not the highest, over the time the change in d50 of CO_2 CGAs was lowest in case of XG/N85 (An-Non) pair.

7. CO_2 CGAs, from XG/N85 (An-Non), were compared to air CGAs, from XG/DDBS (An-An), in terms of rheology and stability. The results are tabulated below:

Criteria	Best Polymer-Surfactant pair
• Rheology (change in LSRV)	same
• Rheology (viscosity profile)	Air CGAs [XG/DDBS (An-An)]
• Time stability	CO_2 CGAs [XG/N85 (An-Non)]
• Frequency-time distribution	CO_2 CGAs [XG/N85 (An-Non)]

8. After figuring out the optimum formulation for generating CO_2 CGAs using XG/N85 (An-Non) pair as the ideal base fluid solution, following tests were conducted under elevated pressures and temperatures:

Viscometry tests	Low Shear Rate Viscosity (LSRV) at 0.01 s^{-1} shear rate
	Viscosity Profile (vs. shear rate)
Oscillation tests	Amplitude Sweep tests at constant frequency of 0.1Hz
	Frequency Sweep tests at constant shear stress of 1.42Pa

Temperatures used in this study were 25°C and 75°C; pressures used were 100psi, 500psi, and 800psi.

9. Both CO_2 CGAs and the associated base fluid exhibit shear-thinning, non-Newtonian rheological properties within the range of pressure and temperature studied here. At very low shear rates, the viscosity of CO_2 CGAs exceed that of base fluid; however, at high shear rates, the base fluid viscosity exceeds the CO_2 CGA viscosity.

10. At low temperatures of 25°C, CO_2 CGAs demonstrate gel character (G' > G"), indicating the micro-bubble dispersions being stable. The LVE region is clearly visible in the amplitude sweep plots of CO_2 CGAs. CO_2 CGAs show non-linear deformational behaviour as the temperature is increased to 75°C.

11. Frequency sweep plots show that elevated pressures has insignificant effect on the viscoelastic behaviour of CO_2 CGAs, at low temperature of 25°C. CO_2 CGAs display "weak-gel" viscoelastic behaviour. Both G' and G" are almost frequency independent. After the temperature is increased to 75°C, change in viscoelastic properties in CO_2 CGAs is observed within the range studied here. Both G' and G" are frequency dependent. In the lower range of frequencies,

viscous behaviour dominates, and in the higher range of frequencies, elastic behaviour starts to take over.

7.2. Recommendations:

The following recommendations are suggested for future research studies on CO_2 CGAs:

1. Oil recovery experiments could be conducted using CO_2 CGAs to see the effectiveness of CO_2 CGAs as recovery fluid.

2. It was seen in this study that temperature had a huge negative effect on rheological and viscoelastic properties of CO_2 CGAs. The use of thermal stabilizers to enhance the stability of CO_2 CGAs should be further investigated.

3. Detailed research on the effect of salinity on the rheology and stability of CO_2 CGAs should be conducted.

4. Further on, research on the optimum formulation of generating CGAs encapsulating flue gases should be considered.

8. References

Adkins S. S., Chen X., Chan I., Torino E., Nguyen Q. P., Sanders A. W., Johnston K. P. (2010) "Morphology and Stability of CO_2-in Water Foams with Nonionic Hydrocarbon Surfactants" – *Langmuir*, Vol. 26, Issue 8, pages 5335-5348

Aiba S., Someya J. (1965) "Molecular diffusivity of carbon dioxide in highly viscous Newtonian and non-Newtonian liquids" – *Hakko Kogaku Zasshi*, Vol. 43, pages 603-608

Amiri M. C., Woodburn E. T. (1990) "A Method for the Characterisation of Colloidal Gas Aphron Dispersions" – *Trans. Inst. Chem. Eng.*, Vol. 68, pages 154-160

Astarita G., Marrucci G., Palumbo G. (1964) "Non-Newtonian Gravity Flow Along Inclined Plane Surfaces" – *Industrial and Engineering Chemistry Fundamentals*, Vol. 3, Issue 4, pages 333-339

Aubry T., Moan M. (1996) "Influence of non-ionic surfactant on the rheology of a hydrophobically associating water soluble polymer" – *Journal of Rheology*, Vol. 40, Issue 3, pages 441-448

Berg J. C. (2010) "*An Introduction to Interfaces and Colloids – The Bridge to Nanoscience*" – World Scientific, Singapore

Bjorndalen N., Alvarez J. M., Jossy W. E., Kuru E. (2011) "A Study of the Effects of Colloidal Gas Aphron Composition on Pore Blocking" – *SPE Drilling and Completions*, SPE 121417, presented at the SPE International Symposium on Oilfield Chemistry, The Woodlands, Texas, April 20-22

Bjorndalen N., Kuru E. (2008) "Physico-Chemical Characterization of Aphron Based Drilling Fluids" – *Journal of Canadian Petroleum Technology*, Vol. 47, No. 11, presented at the Petroleum Society's 6th Canadian International Petroleum Conference (56th Annual Technical Meeting), Calgary, AB, June 7-9, doi: 10.2118/08-11-15-CS

Bjorndalen N., Kuru E. (2008) "Stability of Microbubble-Based Drilling Fluids Under Downhole Conditions" – *Journal of Canadian Petroleum Technology*, Vol. 47, No. 6, pages 40-47

Bredwell M. D., Worden R. M. (1998) "Mass-Transfer Properties of Microbubbles. 1. Experimental Studies" – *Biotechnology Progress*, Vol. 14, Issue 1, pages 31-38

Bredwell M.D., Telgenhoff M. D., Worden R. M. (1995) "Formation and Coalescence Properties of Microbubbles" – *Applied Biochemistry and Biotechnology*, Vol. 51-52, Issue 1, pages 501-509

Brookey T. (1998) "Microbubbles: New Aphron Drill-In Fluid Technique Reduces Formation Damage in Horizontal Wells" – *Society of Petroleum Engineers*, SPE 39589, presented at the SPE International Symposium on Formation Damage Control, February 18 – 19

Caballero M., Cela R., Perez-Bustamante J. A. (1989) "Studies on the Use of Colloidal Gas Aphrons in Coflotation and Solvent Sublation Processes: A Comparison with the Conventional Technique" – *Separation Science Technology*, Vol. 24, Issues 9-10, pages 629-640

Cardoso J. J. F., Spinelli L. S., Monteiro V., Lomba R., Lucas E. F. (2010) "Influence of polymer and surfactant on the aphrons characteristics: Evaluation of fluid invasion controlling" – *eXPRESS Polymer Letters*, Vol. 4, No. 8, pages 474-479

Chang S., Grigg R. B. (1999) "Effects of Foam Quality and Flow Rate on CO2-Foam Behavior at Reservoir Temperature and Pressure" – *Society of Petroleum Engineers Reservoir Evaluation & Engineering*, SPE 56856, Vol. 2, No. 3, pages 248-254

Chaphalkar P.G., Valsaraj K.T., Roy D. (1993) "A Study of the Size Distribution and Stability of Colloidal Gas Aphrons Using a Particle Size Analyzer" – *Separation Science Technology*, Vol. 28, Issue 6, pages 1287-1302

Chàvez-Montes B. E., Choplin L., Schaer E. (2007) "`Rheological Characteristics of Wet Food Foams" – *Journal of Texture Studies*, Vol. 38, Issue 2, pages 236-252

Ciriello S., Barnett S. M., Deluise F. J. (1982) "Removal of Heavy Metals from Aqueous Solutions Using Microgas Dispersions"- *Separation Science Technology*, Vol. 17, Issue 4, pages 521-534

Clunie J. S., Goodman J. F., Symons P. C. (1967) "Solvation Forces in Soap Films" – *Nature*, Vol. 216, No. 5121, pages 1203-1204

Cohen-Addad S., Hoballah H., Höhler R. (1998) "Viscoelastic response of a coarsening foam" – *Phys. Rev. E*, Vol. 57, Issue 6, pages 6897-6901

Dai Y., Deng T. (2003) "Stabilization and Characterization of Colloidal Gas Aphron Dispersions" – *Journal of Colloid and Interface Science*, Vol. 261, Issue 2, pages 360-365

Derkach S. R. (2010) "Rheology on the Way from Dilute to Concentrated Emulsions" – *International Review of Chemical Engineering*, Vol. 2, No. 3, pages 465-472

Dim A., Gardner G. R., Ponter A. B., Wood T. (1971) "Diffusion of Carbon Dioxide into Primary Alcohols and Methyl Cellulose Ether Solutions" – *Journal of Chemical Engineering of Japan*, Vol. 4, Issue 1, pages 92-95

Enick R. M., Olsen D. K. (2012) "Mobility and Conformance Control for Carbon Dioxide Enhanced Oil Recovery (CO_2-EOR) via Thickeners, Foams, and Gels – A Detailed Literature Review of 40 Years of Research" – National Energy Technology Laboratory, DOE/NETL-2012/1540

Exerowa D., Kruglyakov P. M. (1998) "*Foam and Foam Films: Theory, Experiment, Application*" - Elsevier, Amsterdam

Feng W., Singhal N., Swift S. (2009) "Drainage mechanism of microbubble dispersion and factors influencing its stability" – *Journal of Colloid and Interface Science*, Vol. 337, Issue 2, pages 548-554

Gopal A. D., Durian D. J. (1995) "Nonlinear Bubble Dynamics in a Slowly Driven Foam" – *Phys. Rev. Lett.*, Vol. 75, Issue 13, pages 2610-2613

Growcock F. (2005) "Enhanced Wellbore Stabilization and Reservoir Productivity with Aphron Drilling Fluid Technology - Final Report" - MASI Technologies *LLC*, DOE Award Number DE-FC26-03NT42000

Harris P. C., Haynes R. J., Egger J. P. (1984) "The Use of CO_2-Based Fracturing Fluids in the Red Fork Formation in the Anadarko Basin, Oklahoma" – *Journal of Petroleum Technology*, Vol. 36, No. 6, pages 1003-1008

Heller J. P. (1994) "CO_2 Foams in Enhanced Oil Recovery," in *Foams: Fundamentals and Applications in the Petroleum Industry*, Schramm L. L. (ed.), *Advances in Chemistry*, Vol. 242, pages 201-234

Herzhaft B., Kakadjian S., Moan M. (2005) "Measurement and modeling of the flow behavior of aqueous foams using a recirculating pipe rheometer" – *Colloids and Surfaces A: Physicochemical and Engineering Aspects*, Vol. 263, Issues 1-3, pages 153-164

Höhler R., Cohen-Addad S. (2005) "Rheology of liquid foam" – Journal of Physics: Condensed Matter, Vol. 17, No. 41, pages R1041-R1069

Holmberg K., Jonsson B., Kronberg B., Lindman B. (2002) "*Surfactants and Polymers in Aqueous Solutions*" - John Wiley & Sons Ltd., Chichester

Ivan C. D., Growcock F., Friedheim J. E. (2002) "Chemical and Physical Characterization of CGA based Drilling Fluids" – *Society of Petroleum Engineers*, SPE 77445, presented at the SPE Annual Technical Conference and Exhibition held in San Antonio, Texas, USA, September 29 – October 2

Jauregi P., Mitchell G. R., Varley J. (2000) "Colloidal Gas Aphrons (CGA): Dispersion and Structural

Features" – *AIChE Journal*, Vol. 46, Issue 1, pages 24-36

Jauregi P., Varley J. (1998) "Colloidal gas aphrons: A novel approach to protein recovery" –

Biotechnology and Bioengineering, Vol. 59, Issue 4, pages 471-481

Jauregi P., Gilmour S., Varley J. (1997) "Characterization of Colloidal Gas Aphrons for Subsequent use for

Protein Recovery" – *Chemical Engineering Journal*, Vol. 65, Issue 1, pages 1-11

Ju L., Ho C. S. (1986) "The measurement of oxygen diffusion coefficients in polymeric solutions" –

Chemical Engineering Science, Vol. 41, No. 3, pages 579-589

Katiyar A., Sarkar K. (2010) "Stability analysis of an encapsulated microbubble against gas diffusion" –

Journal of Colloid and Interface Science, Vol. 343, Issue 1, pages 42-47

Khan S. A., Schnepper C. A., Armstrong R. C. (1988) "Foam Rheology: III. Measurement of Shear Flow

Properties" – *Journal of Rheology*, Vol. 32, Issue 1, pages 69-92

Koehler S. A., Stone H. A., Brenner M. P., Eggers J. (1998) "Dynamics of foam drainage" – *Phys. Rev. E*,

Vol. 58, Issue 2, pages 2097-2106

Kuehne D. L., Frazier R. H., Cantor J., Horn Jr. W. (1992) "Evaluation of Surfactants for CO2 Mobility

Control in Dolomite Reservoirs" – *Society of Petroleum Engineers*, SPE 24177, presented at the SPE/DOE

Enhanced Oil Recovery Symposium, 22-24 April 1992, Tulsa, Oklahoma

Kunjappu J. T., Somasundaran P. (1996) "Recent trends in bilayer formation of synthetic amphiphiles" –

Colloids and Surfaces A: Physicochemical and Engineering Aspects, Vol. 117, Issues 1-2, pages 1-5

Larmignat S., Vanderpool D., Lai H. K., and Pilon L. (2008) "Rheology of Colloidal Gas Aphrons (Microfoams)" – *Colloids and Surfaces A: Physicochemical and Engineering Aspects*, Vol. 322, Issues 1-3, pages 199-210

Lescure B. M., Claridge E. L. (1986) "CO2 Foam Flooding Performance vs. Rock Wettability" – *Society of Petroleum Engineers*, SPE 15445, presented at the SPE Annual Technical Conference and Exhibition, 5-8 October 1986, New Orleans, Louisiana

Longe T.A. (1989) "Colloidal Gas Aphrons: Generation, Flow Characterization and Application in Soil and Groundwater Decontamination" – PhD Thesis, Virginia Polytechnic Institute and State University

MacPhail W. F., Cooper R. C., Brookey T., Paradis J. (2008) "Adopting Aphron Fluid Technology for Completion and Workover" – *Society of Petroleum Engineers*, SPE 112439, presented at the SPE International Symposium and Exhibition on Formation Damage Control held in Lafayette, Louisiana, February 13 – 15

Mashelkar R. A., Soylu M. A. (1982) "Gas diffusion in polymer solutions: a double-cone flow technique" – *Journal of Applied Polymer Science*, Vol. 27, Issue 2, pages 697-708

Mashelkar R. A., Soylu M. A. (1974) "Diffusion in flowing films of dilute polymeric solutions" – *Chemical Engineering Science*, Vol. 29, No. 5, pages 1089-1099

Manzello S., Yang J. C. (2002) "The Effect of an Alcohol Resistant Aqueous Film Forming Foam (AR-AFFF) on the Evaporation, Boiling, and Collision Dynamics of a Water Droplet on a Heated Solid Surface" – *Journal of Colloid and Interface Science*, Vol. 256, Issue 2, pages 418-427

Marze S. P. L., Saint-Jalmes A., Langevin D. (2005) "Proteins and surfactant foams: linear rheology and dilatancy effect" – *Colloids and Surfaces A: Physicochemical and Engineering Aspects*, Vol. 263, Issues 1-3, pages 121-128

Mason T. G. (1999) "New fundamental concepts in emulsion rheology" – *Current Opinion in Colloid & Interface Science*, Vol. 4, Issue 3, pages 231-238

Mason T. G., Bibette J., Weitz D. A. (1995) "Elasticity of Compressed Emulsions" – *Phys. Rev. Lett.*, Vol. 75, Issue 10, pages 2051-2054

Mason T. G., Weitz D. A. (1995) "Optical Measurements of Frequency-Dependent Linear Viscoelastic Moduli of Complex Fluids" – *Phys. Rev. Lett.*, Vol. 74, Issue 7, pages 1250-1253

Mezger T. G. (2006) "*The Rheology Handbook: For users of rotational and oscillatory rheometers*" – Vincentz Network, Hannover

Nagarajan R. (2002) "Molecular Packing Parameter and Surfactant Self-Assembly: The Neglected Role of the Surfactant Tail" – *Langmuir*, Vol. 18, Issue 1, pages 31-38

Navarini L., Cesàro A., Ross-Murphy S. B. (1992) "Viscoelastic properties of aqueous solutions of an exocellular polysaccharide from cyanobacteria" – *Carbohydrate Polymers*, Vol. 18, Issue 4, pages 265-272

Perez J. F., Sandall O. C. (1973) "Diffusivity measurements for gases in power law non-Newtonian liquids" – *AIChE Journal*, Vol. 19, Issue 5, pages 1073-1075

Phillips A. M., Couchman D. D., Wilke J. G. (1987) "Successful Field Application of High-Temperature Rheology of CO_2 Foam Fracturing Fluids" – *Society of Petroleum Engineers*, SPE 16416, presented at the 1987 SPE/DOE Low Permeability Reservoirs Symposium held in Denver, Colorado, USA, May 18-19, 1987

Polymer Handbook; John Wiley & Sons Inc.: New York, 1999, Fourth Edition, Chapter 7, Tables of Viscosity – Molecular Weight Relationships

Quinn J. A., Blair L. M. (1967) "Diffusion in Gels and Polymeric Solutions" – *Nature*, Vol. 214, page 907, doi:10.1038/214907a0

Rioual F., Hutzler S., Weaire D. (2005) "Elastic dilatancy in wet foams: A simple model" – *Colloids and Surfaces A: Physicochemical and Engineering Aspects*, Vol. 263, Issues 1-3, pages 117-120

Rocha S. R. P., Psathas P. A., Klien E., Johnston K. P. (2001) "Concentrated CO_2-in-Water Emulsions with Nonionic Polymeric Surfactants" – *Journal of Colloid and Interface Science*, Vol. 239, Issue 1, pages 241-253

Saint-Jalmes A., Durian D. J. (1999) "Vanishing elasticity for wet foams: Equivalence with emulsions and role of polydispersity" – *Journal of Rheology*, Vol. 43, Issue 6, pages 1411-1422

Samuel S. (2012) "A Laboratory Study of Aqueous Colloidal Gas Aphrons for Enhanced Oil Recovery Applications" – MSc Thesis, University of Alberta

Save S. V., Pangarkar V. G. (1994) "Characterisation of Colloidal Gas Aphrons" – *Chemical Engineering Communications*, Vol. 127, No. 1, pages 35-54

Save S. V., Pangarkar V. G., Kumar S. V. (1993) "Intensification of mass transfer in aqueous 2-phase systems" - *Biotechnology and Bioengineering*, Vol. 41, Issue 1, pages 72-78

Scott M. J., Jones M. N. (2000) "The biodegradation of surfactants in the environment" – *Biochimica et biophysica acta.*, Vol. 1508, Issues 1-2, pages 235-251

Sebba F. (1987) "*Foams and Biliquid Foams*" - John Wiley & Sons, Chichester

Shivhare S. (2011) "A Study of the Rheology, Stability and Pore Blocking Ability of Non Aqueous Colloidal Gas Aphron Drilling Fluids" – MSc Thesis, University of Alberta

Sollich P., Lequeux F., Hébraud P., Cates M. E. (1997) "Rheology of Soft Glassy Materials" – *Phys. Rev. Lett.*, Vol. 78, Issue 10, pages 2020-2023

Song Ki-Won, Kuk Hoa-Youn, Chang Gap-Shik (2006) "Rheology of concentrated xanthan gum solutions: Oscillatory shear flow behavior" – *Korea-Australia Rheology Journal*, Vol. 18, No. 2, pages 67-81

Spinelli L.S., Neto G.R., Freire L.F.A., Monteiro V., Lomba R., Michel R. and Lucas E. (2010) "Synthetic Based Aphrons: Correlation between Properties and Filtrate Reduction Performance" – *Colloids and Surfaces A: Physicochemical and Engineering Aspects*, Vol. 353, Issue 1, pages 57-63

Srinivasan N. (1967) – MS Thesis, Illinois Institute of Technology

Stevenson P. (2011) "Foam Separations" – *Comprehensive Biotechnology (2nd Edition)*, Academic Press, Vol. 2, pages 715-726

Talu E., Hettiarachchi K., Nguyen H., Lee A. P., Powell R. L., Longo M. L., Dayton P. A. (2006) "Lipid-stabilized Monodisperse Microbubbles Produced by Flow Focusing for Use as Ultrasound Contrast Agents" – *IEEEXplore*, presented at the 2006 IEEE Ultrasonics Symposium in Vancouver, Canada, October 3-6, 2006

Tseng H., Pilon L., Warrier G. R. (2006) "Rheology and convective heat transfer of colloidal gas aphrons in horizontal mini-channels" – *International Journal of Heat and Fluid Flow*, Vol. 27, Issue 2, pages 298-310

Vincent-Bonnieu S., Höhler R., Cohen-Addad S. (2006) "Slow viscoelastic relaxation and aging in aqueous foam" – *Europhys. Lett.*, Vol. 74, No. 3, pages 533-539

Wallis D. A., Michelson D. F., Sebba F., Carpenter J. K., Houle D. (1985) "Applications of aphron technology to biological separations" - *Biotechnology and Bioengineering Symposium*, Vol. 15, pages 399-408

Wang P., Nong X. H., Ge J. H. (2011) "Aerobic biodegradation of nonylphenol ethoxylates in shaking flask test" – *Journal of Biotechnology*, Vol. 14, Issue 4, page 1

Weaire D. L., Hutzler S. (2001) "*The Physics of Foams*" – Oxford University Press, London

Xing D., Wei B., Trickett K., Mohamed A., Eastoe J., Soong Y., Enick R. (2010) "CO_2-Soluble Surfactants for Improved Mobility Control" – *Society of Petroleum Engineers*, SPE 129907, presented at the 2010 SPE Improved Oil Recovery Symposium in Tulsa, Oklahoma, USA, April 24-28 2010

Xu Q. Y., Nakajima M., Ichikawa S., Nakamura N., Shiina T. (2009) "A comparative study of microbubble generation by mechanical agitation and sonication" – *Journal of Colloid and Interface Science*, Vol. 332, Issue 1, pages 208-214

Yaghoobi H., Heller J. P. (1994) "Laboratory Investigation of Parameters Affecting CO_2-Foam Mobility in Sandstone at Reservoir Conditions" – *Society of Petroleum Engineers*, SPE 29168, presented at SPE Eastern Regional Meeting, 8-10 November 1994, Charleston, West Virginia

Yang L., Wang K., Tan J., Lu Y. (2012) "Experimental study of microbubble coalescence in a T-junction microfluidic device" – *Microfluidics and Nanofluidics*, Vol. 12, Issue 5, pages 715-722

Zhao J., Pillai S., Pilon L. (2009) "Rheology of Colloidal Gas Aphrons (Microfoams) made from Different surfactants" – *Colloids and Surfaces A: Physicochemical and Engineering Aspects*, Vol. 348, Issues 1-3, pages 93-99

Zeng Z., Grigg R. B., Bai B. (2006) "Experimental Development of Adsorption and Desorption Kinetics of a

CO_2-Foaming Surfactant Onto Berea Sandstone" – *Society of Petroleum Engineers*, SPE 103117,

presented at the SPE Annual Technical Conference and Exhibition, 24-27 September 2006, San Antonio,

Texas, USA

Zheng Li-Hui, He Xiao-qing, Fu Li-xia, Wang Xiang-chun (2009) "The Multiphase Flow System Used in

Exploiting Depleted Reservoirs: Water-based Micro-bubble Drilling Fluid" – *Journal of Physics:*

Conference Series, Vol. 147, No. 1, doi:10.1088/1742-6596/147/1/012022